DISSERTATION

DEVELOPMENT OF BIOINSPIRED HYALURONAN ENHANCED SYNTHETIC POLYMERS FOR MEDICAL APPLICATIONS

Submitted by

Justin Phillip Gangwish

School of Advanced Materials Discovery

In partial fulfillment of the requirements

For the Degree of Doctor of Philosophy

Colorado State University

Fort Collins, Colorado

Summer 2023

Doctoral Committee:

Advisor: Susan P. James
Co-Advisor: Travis S. Bailey

Lakshmi Prasad Dasi
Ketul Popat
Eric Monnet

ABSTRACT

DEVELOPMENT OF BIOINSPIRED HYALURONAN ENHANCED SYNTHETIC POLYMERS FOR MEDICAL APPLICATIONS

The first transcatheter aortic valve replacement (TAVR) was performed in 2002, and over the past two decades has become as prevalent as surgical aortic valve replacements in America. TAVR's have significant potential to provide relief for patients with aortic valve disease, but due to their high cost remain accessible primarily in wealthy nations. Furthermore, TAVR's have limited lifespans and are radiotransparent so they can only be evaluated for function through echocardiography. Thus, an expensive medical implant with limited durability is only replaced after it has begun to fail and cause the patient further stress on their heart.

To address these issues this dissertation reviews the research performed in generating a novel heart valve leaflet material that is radiopaque, made primarily out of linear low-density polyethylene (LLDPE), and incorporates the biological polymer hyaluronan (HA). These leaflets could significantly reduce the cost of TAVR's potentially allowing for global adoption of the technology. They are radiopaque and easily imaged using x-ray fluoroscopy allowing changes in leaflet shape or movement to be identified prior to when the echocardiography would have shown a deleterious effect to function. They incorporate HA which is found in the interior lumen of blood vessels and has been shown to decrease calcification and thrombosis, both of which have caused polymeric leaflets to fail in previous research. Finally, they can be easily shaped and reinforced allowing for a potentially far greater device lifespan.

The leaflets are made by melt pressing in radiopaque powders of either tungsten or bismuth trioxide into sheets of LLDPE followed by treatment with HA to form an interpenetrating

polymer network. The material properties of the leaflets were evaluated for their tensile mechanical properties, their hydrophilicity, their radio transparency (or lack thereof), and their hemodynamics. The biocompatibility of the leaflets was evaluated through a cytotoxicity assay, whole blood clotting on the surface of the material, and the ability for platelets to adhere and activate on the material surface. The results demonstrate the material has significant potential to function as a heart valve leaflet in a TAVR.

Beyond evaluating this novel material, the process by which HA is incorporated into LLDPE was examined and optimized for commercial scale up. First, the need for solvent distillation and nitrogen blankets during treatment were determined to be unnecessary to produce an HA IPN with LLDPE. Then the rate at which the LLDPE is drawn from the HA solution as well as the vacuum pressure and temperature during this process was found to affect the amount of active HA at the surface of the material. Finally initial evidence was found that shows that HA IPN does not form through the bulk of the material, but rather in the first few microns of the LLDPE.

Unrelated to TAVR's a study was performed to enhance the non-woven polypropylene used in surgical masks and N-95 masks against COVID-19 using HA and polyethylene glycol (PEG). HA was used to form a microcomposite on the surface of the non-woven polypropylene while PEG was grafted to the surface with oxygen plasma. The resulting materials were evaluated for their tensile mechanical properties, breathability, chemical composition, hydrophilicity, cytotoxicity, and ability to adsorb COVID-19 spike protein. The results indicate the material has notable potential to make masks more effective at preventing the transfer of COVID-19, however further studies using live SARS-CoV-2 virus beyond the capabilities of this laboratory are necessary before that potential can be fully confirmed.

ACKNOWLEDGMENTS

Edward Abbey once said, “May your trails be crooked, winding, lonesome, dangerous, leading to the most amazing view. May your mountains rise into and above the clouds. May your rivers flow without end.” Working towards a PhD often feels like a river without an end that is dangerous and lonesome, however each experiment serves a small false summit in the clouds. Only as I approached the defense did I begin to see the mountain top and only after was I able to look down and appreciate how each step whether easy or painful served to propel me just a little further up the mountain. However, the beauty of this journey was that with each step upwards there were amazing people giving me strength and supporting me.

First, I would like to acknowledge my advisors, Dr. Susan James and Dr. Travis Bailey. Though it may have been an insignificant day in a sophomore chemical engineering class, it was Travis’s presentation on his research that sparked me into pursuing research for the first time. While Travis started my journey and would be integral to its completion, Sue gave me my first opportunity to start working in a research lab, a lab that would be where I completed my doctoral research. Beyond giving me this first opportunity, she supported and encouraged me throughout a moderately tumultuous graduate journey. While words cannot express the gratitude I feel there are two further points to be made. First is that Sue can see the future, and predicted my return to graduate school, and second is that Sue’s guidance and kindness has shaped me into a better person.

To my committee, thank you for all your support and answering my endless questions over the past several years.

To my lab mates and predecessors, Alyssa Bailey, Nipa Khair, Jules Kindsfater, Ethan Harrell, Srujana Joshi, Christian Steinmetz, Steve Rosa, Roberta Sabino, Vignesh Manivasagam, Abhishek Bhattacharjee, Nelson Isaacson, Harvinder S. Virk, James Michael II, Aniruddha

Savargaonkar, Liszt Coutinho-Madruga, Boston Morris, Allee Klug, Zack Umstead, Boston Morris, Cara Leone, Hieu Bui, Casey Dean, and so many more thank you for all the work, lessons, and time that made this research possible.

I would be remiss if I did not thank Mr. Hanley, Mr. Huitt, Mrs. Libbey, and Mr. Suding. Mr. Suding, thank you for lighting the fire in me to love science. Mrs. Libbey, thank you for showing me that reading and writing can be the best way through understanding difficult emotions and challenges. Mt. Huitt, thank you for sharing a love of baseball to last a lifetime. Mr. Hanley, thank you for teaching me to love the outdoors, for without this escape from society I do not think I would have made it through this work.

To my friends (including those listed above), Karl Nelson, Stuart Schwanitz, Daniel Silverstein, Ryan Arey, Alec Richardson, Royce Quintana, Jamie Quintana, Evon Patek, Doran and Megan, Colton Feller, Tom Horensky, Gary Migliaccio, and so many more thank you for bringing joy to my life!

To my family. Mom and Dad, there are no words, no amount of time, and no gesture that could possibly encompass what you and your endless support and love have meant to me. No matter how challenging I was you always were there. David, you may have taught me many lessons the hard way, but your love and your immense dedication to your career has always inspired me. Saim, we may have met as friends but I am beyond lucky that you are my brother. Your kindness and love are something I look to emulate. Mikey, I might be your older brother, but in so many ways I look up to you. Your work ethic, compassion, and ability to look inwards at a challenge and keep going is amazing. To all of you, thank you and I love you.

To Jaqueline, I cannot imagine what my life would be like without you, nor do I want to. From across the country and back again (twice just in grad school) you have been my life partner. You listened to my presentations, you saw every high and low, you drew my blood, and you were always there. You are truly the kindest person I have ever met. I love you and I would have never made it here without you.

DEDICATION

I dedicate this work to my family. Mom, Dad, David, Saim, Mikey, and Jacqueline.

TABLE OF CONTENTS

CHAPTER 1: INTRODUCTION

1.1 Research Overview

Synthetic and biological polymers have been the focus of an incalculable amount of scientific and engineering research for over a century. From understanding the extraordinary chemistry coding and translating our genetics to the mundane enhancement of food storage, polymers play a vital role everyday life across the globe. Despite the widespread use of polymers in biomedical implants, to this day no flexible polymeric heart valve leaflet has been commercialized and widely implanted despite the need for hundreds of thousands of valve replacements globally. This dissertation describes the incorporation of a biological polymer, hyaluronan, into two synthetic polymers, polyethylene and polypropylene, to generate novel biomaterials. Hyaluronan (HA) is a naturally occurring polymer found in the human cell membranes throughout the body. Most relevant to this work hyaluronan is found in the inner lumen of blood vessels known as the endothelial glycocalyx where it prevents thrombosis.

The first novel biomaterial developed and evaluated in this dissertation is a radiopaque linear low-density polyethylene (LLDPE) with an interpenetrating polymer network (IPN) with HA for use as artificial heart valve leaflets. There are three key aspects that the radiopaque LLDPE-HA valve leaflet offers when compared to current bioprosthetic leaflets. First, LLDPE is a thermoplastic material that can be shaped into optimal geometries that mimic natural leaflets and generate optimal flow through the artificial valve. Second, HA acts as a façade for the LLDPE in the body giving it a molecular composition at the surface similar to natural blood vessels and leaflets thus preventing an immune response and implant rejection. Finally, while LLDPE is radiotransparent, tungsten or bismuth trioxide are not and can be embedded into the LLDPE in the melt rendering the material radiopaque. By introducing radiopacity to the heart valve leaflets the leaflets can be imaged in the human body using conventional techniques such as x-ray

fluoroscopy. Should this development be commercialized it would allow physicians and engineers to see valve leaflets function directly post implantation. With the ability to image and analyze valve leaflet movement engineers and physicians can finally incorporate real time information to drive valve redesign. Currently, the in-vivo hemodynamics of valve leaflets cannot be correlated with leaflet movement and shape due to the inability to image the leaflets in-situ. While the main focus of this research was creating and evaluating the material properties of the novel radiopaque LLDPE-HA material, the processes by which HA is incorporated was simplified and optimized for commercial scale up.

The second biomaterial developed was a non-woven polypropylene textile coated with a hyaluronic acid microcomposite. Non-woven polypropylene is a common material used in medical personal protective equipment (PPE), specifically surgical masks and N-95 masks. As the COVID-19 pandemic spread, it became apparent that any enhancement to masks could be helpful in dampening the spread of the disease. Thus, an effort was made to adhere HA and polyethylene glycol (PEG) to non-woven polypropylene to increase the molecular affinity of external COVID-19 spike proteins to the non-woven polypropylene in the hope that it could prevent disease transfer. Beyond developing the materials, the methodology used presents a blueprint for researchers to follow when looking for a process to evaluate a novel biomaterial with instruments available at most R1 universities.

1.2 Background

Heart valve disease is prevalent both globally and in the United States with an estimated 2.5% of adults having some type of heart valve disease in the US[1–3]. Over 80,000 heart valve replacements were performed in the United States in 2014 and the global need is expected to exceed 850,000 by 2050[4,5]. Currently available replacements fall into two categories, mechanical valves and bioprosthetic valves. While both mechanical and bioprosthetic valves improve patient's lives they also pose significant risks to patient health.

Mechanical valves are preferred for younger patients due to the valve's expected lifespan of 50-70 years[6]. The implantation of a mechanical valve is extremely invasive requiring open-heart surgery and cardiopulmonary bypass. The patient pool which can tolerate mechanical valve implantation is limited due to the high surgical risks associated with the procedure, the limited availability of surgeons capable of performing the complex procedure, and the intensive resources required[6,7]. Furthermore, patients who undergo successful valve replacement are required to take vitamin K antagonists for life-long anticoagulation therapy. Vitamin K antagonists have significant risks and side effects. First and foremost, they prevent coagulation causing even minor bleeding to be life threatening. Thus, patients are tied to the medical system because they need immediate medical care for otherwise insignificant injuries such as minor cuts and bruising. Furthering this tie to hospitals, their drug regimen must be monitored closely by physicians. Other notable side effects include but are not limited to: significant fetal loss for pregnant women, dietary restrictions around vitamin k intake, limited alcohol consumption, and the loss of opportunity due to the restricted lifestyle[8,9].

Bioprosthetic aortic valves have become far more prevalent over the last decade because a new approach has been developed in which the device can be delivered via a catheter. This relatively new medical device is known as a transcatheter aortic valve replacement or TAVR. The TAVR is placed transapically or transfemorally preventing the need for open heart surgery[10,11]. It should be noted bioprosthetic valves are implanted via open heart surgery as well. However, valves delivered via catheter have more stringent design requirements as they must be able to be compressed and passed through a catheter. This requires the valve to be made with thin leaflets placed on either a nitinol or cobalt chrome stent that can be crimped to about 5 mm in diameter. The transfemoral approach is greatly preferred to the transapical approach, however both significantly reduce the surgical risks when compared to open heart surgery[12]. Less invasive valve implantation has led to a significant increase in the use of bioprosthetic valves to treat valvular disease. Though heart valve replacement is not limited to the aortic valve it is the most

commonly replaced valve[13], and due to this aortic valve replacements are ideal to analyze for trends in valve replacement.

In the United States from 2012 to 2016 treatment of aortic stenosis (AS) and regurgitation (AR) with surgical aortic valve replacement (SAVR) decreased from 21.9% of patients to 18.5% of patients while treatment of AS and AR with transcatheter aortic valve replacement (TAVR) increased from 2.6% to 12.5%[14]. All other patients were treated medically rather than surgically. While this shift in treatment indicates a promising new technology, surgically placed bioprosthetic valves have significant reoperation rates ranging up to 20% within 10 years of implantation[15]. A small study of TAVR's, which have thinner leaflets due to the need for a low profile when implanting through a catheter, reported 50% structural valve deterioration within 7 years of implantation[16]. It has been estimated that over 80% of TAVR's have irregular deployment that may result in poor hemodynamics which may cause rapid valve deterioration and blood clotting[17]. The recent advent of valve in valve transcatheter replacements where a second artificial valve is placed in the first artificial valve replacement gives slight reprieve to the short lifetimes, but this is a limited technique and does not address irregular deployment which can lead to failure. In fact, valve in valve deployment is likely to significantly increase the potential for irregular deployment. Beyond irregular deployment, valve in valve deployments increase the risk of prothesis-patient mismatch, can cause coronary artery overlap, and have only a 38% survival rate after 8 years[18–20]. It should be noted that the data on valve in valve implants is limited due to the recency of the procedure and that the procedure is mostly performed in high-risk individuals. Outside of surgical and medical complications TAVR's cost approximately $30,000 for the valve alone significantly limiting global access[21,22].

A paradigm shift is needed to address the growing need for artificial heart valves. Ideally a valve can be developed that has the longevity seen from mechanical valves, operates in a non-thrombogenic manner preventing the need for anticoagulants, can be placed via catheter preventing the surgical risks associated with open heart procedures, and would be made from

low-cost materials allowing for global use. While many consider tissue engineered heart valves to be the ultimate replacement, the engineering of these constructs has yet to deliver promising and reproducible results[23,24]. Polymeric heart valves are the most promising technologies in development to address the growing need. Designing a radiopacified valve that could help prevent irregular deployment, be monitored for leaflet deterioration, and prevent poor placement leading to coronary artery overlap has the potential to shift the paradigm from waiting on failure to active monitoring of artificial valve function.

While this dissertation focuses on using radiopacified HA-LLDPE as an artificial heart valve leaflet, a radiopaque blood compatibilized polyethylene has significant potential for use in pediatric valved conduits, vascular grafts, catheter delivery systems, and any long term implantable blood contacting medical device used in fluoroscopic procedures.

There are multiple polymeric heart valves in development, utilizing POSS-PCU, xSIBS, silicone, SEBS, and other polymeric materials. None of these valves are radiopaque and cannot be directly monitored in-vivo. No polymeric heart valve has been approved by the FDA, however the Tria™ Valve made by Foldax® has recently been implanted in a human as part of an FDA trial. The next section will briefly review polymeric heart valves currently under development.

1.3 Current Polymeric Heart Valves

1.3.1 Polynova Valve made from xSIBS

The Polynova valve being developed by the Bluestein group out of Stonybrook University uses a novel triblock copolymer xSIBS poly(Styrene-*coblock*-4-vinylbenzocyclobutene)-polyIsoButylene-poly(Styrene-*coblock*-4-vinylbenzocylcobutene). The vinylbenzocylcobutene coblock is able to undergo a Diels-Alder reaction upon the addition of heat crosslinking the nanostructured material into a stiff block copolymer[25]. The valve leaflets are made by compression molding at 220 °C and

at 4 tons of pressure for one hour. After molding the polymeric structure is sutured onto a laser cut nitinol stent with 6-0 black braided silk[26].

1.3.2 Triskele Valve

The Triskele is currently under development at University College London under the direction of Dr. Gaetano Burriesci. The polymeric leaflet material is made from polyhedral oligomeric silsesquioxanes (POSS) nanoparticles which are attached as pendant chain functional groups to the backbone of poly(carbonate urea) urethane (PCU). The POSS-PCU underwent three sterilization techniques submersion in ethanol, autoclaving, and gamma irradiation. Only gamma irradiation caused a decrease in molecular weight (MW) indicating degradation, however the presence of ester bonds in the backbone of the PCU are subject to degradation via hydrolysis. POSS-PCU was developed to prevent PCU degradation though no mechanism was given as to why covalently bound POSS would prevent PCU degradation. The leaflets are dip coated onto a stainless steel mandrel from a POSS-PCU polymer solution (18% w/v). The valve stent is manufactured by crimping nitinol wires with stainless steel sleeves[27–29].

1.3.3 Strait Access Technologies Valve

Strait Access Technologies is startup out of the University of Cape Town lead by Dr. Peter Zilla, which has developed a polymeric valve from photocurable silicone. Neither the company or the associated personal have released the specific chemistry of the silicones describing them as "MedaSil 40, 73, and 80 from Spectroplast, Zürich, Switzerland". The founders of Spectroplast are associated with Strait Access Technologies and the patents describe a range of chemistries for polysiloxane (silicone) based additive manufacturing ink which uses a thiol based crosslinking agent dispersed as an emulsion in polysiloxane bearing "a plurality of alkenyl groups"[30–32]. The valve is manufactured by spraying one form of the silicone onto a mandrel to form leaflets. This

followed by 3d printing a stiffer silicone over the top of the leaflets to form a “stent” that mimics the shape of the aortic valve sinus[31].

1.3.4 PoliValve

The PoliValve is being developed out of the University of Cambridge and the University of Bristol and is lead by Dr. Geoff Moggridge and Dr. Raimondo Ascione. The leaflet material is made from heparin coated Poly(styrene-*block*-ethylene/butylene-*block*-styrene) (SEBS) manufactured by Kraton. The valve is manufactured as follows. SEBS (29% polystyrene) polymer is heated and injection molded into an aluminum alloy mold forming the stent, then a second SEBS (20% Polystyrene) is over-molded on the stent to form the leaflets. Through a slow injection molding and a 10 minute anneal the styrene forms 10 nm cylinders in an ethylene butylene matrix with long range order in the circumferential direction of the valve. Authors claim this nanostructure helps mimic the collagen reinforcement seen in native leaflets though collagen fibers are 2-3 orders of magnitude larger than the styrene nanocylinders. The valve is then coated in heparin (Corline Heparin Conjugate CHC™ (Corline Biomedical AB, Sweden) or Astute® Advanced Heparin Coating (Biointeractions Ltd, UK)). The mechanism by which heparin coating is applied is not described by the authors[33,34].

1.3.5 Tria™ Valve by Foldax®

The Tria™ Valve is being privately developed by Foldax®. Though the patents are opaque, Dr. Pathiraja Gunatillake who is on the scientific advisory board of Foldax® has published several papers on siloxane poly(urea-urethane) or SiPUU’s for use in heart valve applications[35–37]. These SiPUU’s use macrodiols (poly(dimethylsiloxane) or poly(hexamethylene oxide) linked with diisocyanates to form soft segments of the polymer chain and diamines and diisocyanates to form the hard segments. The work describes multiple formulations of these SiPUU’s, but the company has not released the specific formulation they refer to as LifePolymer™ nor do they precisely

describe the dip coating method of manufacture. The patent for the valve is opaque in its but can be summarized as dip coating a frame (PEEK, polyurethane, and/or metals) on a mandrel in a polymer solution to form the leaflets. The frame is then sutured onto a sewing cuff [38].

1.3.6 Summary

Each of these valves is made from a unique polymer representing the breadth of synthetic polymers as potential heart valve materials. However, except for the Polivalve, none are treated for blood compatibilization. Calcification is one known blood compatibility issue with polymeric valves[39]. Due to this the recommended animal model for valve examination uses juvenile sheep as sheep have similar cardiac architecture and cardiovascular implants calcify rapidly in these animals[40]. However, none of these valves have inherent anti-calcific properties highlighting this single aspect of blood compatibilization clearly demonstrates the need to account for human biology when implanting synthetic polymers. Beyond blood compatibilization none of these valves are radiopacified to allow for in-vivo assessment of valve function and deterioration.

1.4 Impetus for Radiopacified Heart Valve Leaflets

When issues arise in patients who have artificial heart valve implants their valvular function is tested using echocardiography, computed tomography (CT) scans, and with aortic root angiography[41]. These methods assess valve function but have no predictive value and cannot assess leaflet movement, shape, or integrity. Leaflet movement, shape, or integrity are all affected by the location of placement in the aortic root and the shape of valve upon deployment. Less than 20% of TAVR deployments are considered circular, despite this being the ideal geometry[17]. Non-circular or irregular deployments results in increased strain in the valve leaflets leading to sub optimal valve function, tearing, and calcification[42,43]. Furthermore, even a circular deployment of a TAVR that is oversized causes pinwheeling resulting in increased valve leaflet strain.

Beyond con-circular deployment, many TAVR valves encounter issues with coronary artery overlap[44,45]. Coronary artery overlap occurs when the commissural posts covers the ostium of the left or right coronary arteries or when the leaflet of the TAVR blocks the ostium preventing access and blood flow[46]. The issues arising from coronary artery overlap are significant enough that several TAVRs have begun adding markers to aid in valve deployment to prevent the overlap from occurring, however these measures do not prevent the leaflet from obstructing the ostium after valve in valve procudures[20,45]. A valve that could be assessed for proper deployment would provide doctors and their patients significant peace of mind while also giving the manufacture vital information on how the valve behaves in preclinical and clinical trials. Beyond characterizing deployment, data on the temporal behavior of leaflets, specifically how the leaflet movement and shape changes over time, allows for information driven redesign. One significant drawback of this approach is that patients would be subject to ionizing radiation. However, radiation exposure from fluoroscopy procedures is much less than that of CT scans. Even before this technology is developed for use in human patients, it can be used in long term animal studies to assess how an HA enhanced LLDPE heart valve leaflet behaves over time. Understanding the temporal behavior of the material in the heart and correlating it to leaflet movement may provide physicians with an understanding of when a valve will fail preventing aortic regurgitation from occurring. Considering chronic aortic regurgitation causes left ventricle pressure and volume overload, and acute aortic regurgitation causes pulmonary edema and is cause for emergency surgery[47], an understood model that enables monitoring of a replacement valve and prevention before failure has inherent value.

1.5 Systematic evaluation of HA-LLDPE Treatment

In 2004 Dr. Min Zhang published her dissertation on the novel HA silylation process and investigation into an ultra-high MW hyaluronan micro-composite[48]. The research explored the novel synthesis of hyaluronan-cetyltrimethylammonium (HACTA) and silylated HACTA

(SHACTA). Dr. Zhang used SHACTA to generate a polyethylene based microcomposite with SHACTA and lightly investigated degradation of SHACTA over time. In 2019 Dr. Hieu Bui completed his dissertation on generating an interpenetrating polymer network (IPN) between SHACTA and LLDPE. The research demonstrated that a robust IPN could be formed between SHACTA and LLDPE through vapor crosslinking with toluene diisocyanate (TDI). While the results of these works are impressive, the many of the processes involved in producing the final materials are onerous, time consuming, inefficient, and have produced irregular results[49]. Though the HA-LLDPE material itself is quite impressive the process by which it is made is not ideal for automated manufacturing, scale up, and product consistency.

The processes by which HA-LLDPE films is described in detail in chapter 2.1.1, “Hyaluronan enhancement of LLDPE”. The process can be divided into three steps.

1. HA is chemically modified into SHACTA so that it can be infused into LLDPE.
2. LLDPE is swollen into a SHACTA/xylene solution allowing the SHACTA to diffuse into the LLDPE, after which it is crosslinked in place.
3. The SHACTA is reverted back to native HA through a multistep hydrolysis process.

The first aspect of the treatment process that posed a challenge to automated manufacturing was swelling HA into LLDPE under a nitrogen blanket. While it is not impossible, treatment under atmospheric conditions would remove the need for gas tight chambers and an extensive nitrogen supply. The second aspect that posed a challenge to scale up was the use of distilled solvents. Though this not inherently problematic for manufacturing, it is energy intensive and dangerous. The final aspects of the process investigated were methods to improve the confluency of the surface layer of the HA-LLDPE IPN to produce a more consistent product. While each of these aspects is not necessarily related, each represents a potential improvement to the HA-LLDPE process allowing for a more seamless transition from the laboratory bench to a commercial manufacturing.

1.6 Hyaluronan and Polyethylene Glycol Enhancement of Polypropylene to Prevent COVID-19 Transfer.

During the COVID-19 pandemic all non-essential research at Colorado State University was paused and then limited to reduce disease transfer. Rather than wait for lab access a project was undertaken to try and generate a novel mask material that could help prevent the transfer of COVID-19. As this section of the dissertation does not align with the general focus of HA-LLDPE materials used for artificial heart valves a detailed background section is presented at the beginning of chapter rather than here in the introduction. Briefly, the Centers for Disease Control and Prevention has reported over a million deaths from the COVID-19 pandemic and strongly recommended the use of N-95 masks to prevent disease transmission especially amongst healthcare personnel[50–52]. Non-woven polypropylene (PP) is commonly used to make the filtration layer of N-95 masks, but it also has been shown to harbor live SARS-CoV-2 virus for much longer than other materials[53–55]. The SARS-CoV-2 virus outwardly presents a spike protein extensively decorate in the n-linked glycan mannose[56,57]. As mannose has five hydrogen bond donors it was hypothesized that introducing hydrogen bond acceptors to polypropylene would allow the material to better trap and retain SARS-CoV-2 virions and prevent disease transfer. To test this hypothesis methods to alter polypropylene with HA polyethylene glycol (PEG) were investigated. Both HA and PEG net hydrogen bond acceptors. The materials generated were shown to adsorb SARS-CoV-2 spike protein a higher rate than unaltered non-woven PP.

1.7 Summary

HA has demonstrated remarkable viability to improve the biocompatibility of synthetic polymers[48,49,49,58], and radiopacifiers have long been used to generate easily imaged materials for long term implantable devices[59–61]. This research aspires to demonstrate that incorporating both HA and radiopacification agents into LLDPE has the potential to generate a low-cost heart valve

leaflet capable of addressing many of the shortcomings of current aortic valve replacements. Beyond HA's use as a blood contacting material, the variety of application methods allow the molecule to be incorporated into other synthetic polymers for uses such as enhancing COVID-19 spike protein adsorption. The specific aims of this dissertation are listed below and represent the focus of each chapter of this dissertation.

1. Characterize material properties of radiopacified HA-LLDPE
2. Assess hemocompatibility of radiopacified HA-LLDPE
3. Evaluate and Optimize the HA treatment of LLDPE
4. Enhancing Non-Woven Polypropylene (PP) against SARS-CoV-2

1.8 References

1. Bartoli-Leonard, F., Zimmer, J. & Aikawa, E. Innate and adaptive immunity: the understudied driving force of heart valve disease. *Cardiovasc. Res.* **117**, 2506–2524 (2021).

2. Coffey, S., Cairns, B. J. & Iung, B. The modern epidemiology of heart valve disease. *Heart* **102**, 75–85 (2016).

3. Nkomo, V. T. *et al.* Burden of valvular heart diseases: a population-based study. *Lancet Lond. Engl.* **368**, 1005–1011 (2006).

4. Kheradvar, A. *et al.* Emerging Trends in Heart Valve Engineering: Part II. Novel and Standard Technologies for Aortic Valve Replacement. *Ann. Biomed. Eng.* **43**, 844–857 (2015).

5. Yacoub, M. H. & Takkenberg, J. J. M. Will heart valve tissue engineering change the world? *Nat. Clin. Pract. Cardiovasc. Med.* **2**, 60–61 (2005).

6. Azari, S. *et al.* A systematic review of the cost-effectiveness of heart valve replacement with a mechanical versus biological prosthesis in patients with heart valvular disease. *Heart Fail. Rev.* **25**, 495–503 (2020).

7. Williams, T. E., Sun, B., Ross, P. & Thomas, A. M. A formidable task: Population analysis predicts a deficit of 2000 cardiothoracic surgeons by 2030. *J. Thorac. Cardiovasc. Surg.* **139**, 835–840 (2010).

8. Caterina, R. *et al.* Vitamin K antagonists in heart disease: Current status and perspectives (Section III): Position Paper of the ESC Working Group on Thrombosis – Task Force on Anticoagulants in Heart Disease. *Thromb. Haemost.* **110**, 1087–1107 (2013).

9. Steinberg Zachary L., Dominguez-Islas Clara P., Otto Catherine M., Stout Karen K., & Krieger Eric V. Maternal and Fetal Outcomes of Anticoagulation in Pregnant Women With Mechanical Heart Valves. *J. Am. Coll. Cardiol.* **69**, 2681–2691 (2017).

10. Walther, T. *et al.* Transapical aortic valve implantation: step by step. *Ann. Thorac. Surg.* **87**, 276–283 (2009).

11. Boone, R. H. *et al.* Transcatheter pulmonary valve implantation using the edwards SAPIEN^{TM} transcatheter heart valve. *Catheter. Cardiovasc. Interv.* **75**, 286–294 (2010).

12. Buzzatti, N., Sala, A. & Alfieri, O. Comparing traditional aortic valve surgery and transapical approach to transcatheter aortic valve implant. *Eur. Heart J. Suppl.* **22**, E7–E12 (2020).

13. Kidane, A. G. *et al.* Current developments and future prospects for heart valve replacement therapy. *J. Biomed. Mater. Res. B Appl. Biomater.* **88B**, 290–303 (2009).

14. Goldsweig, A. M. *et al.* The Evolving Management of Aortic Valve Disease: 5-Year Trends in SAVR, TAVR, and Medical Therapy. *Am. J. Cardiol.* **124**, 763–771 (2019).

15. Padala, M. A heart valve is no stronger than its weakest link: The need to improve durability of pericardial leaflets. *J. Thorac. Cardiovasc. Surg.* **156**, 207–208 (2018).

16. First Look at Long-term Durability of Transcatheter Heart Valves: Assessment of Valve Function up To 10-years After Implantation. *TCTMD.com* https://www.tctmd.com/slide/first-look-long-term-durability-transcatheter-heart-valves-assessment-valve-function-10-years.

17. Gunning, P. S., Saikrishnan, N., Yoganathan, A. P. & McNamara, L. M. Total ellipse of the heart valve: the impact of eccentric stent distortion on the regional dynamic deformation of pericardial tissue leaflets of a transcatheter aortic valve replacement. *J. R. Soc. Interface* **12**, 20150737 (2015).

18. Bleiziffer, S. *et al.* Long-term outcomes after transcatheter aortic valve implantation in failed bioprosthetic valves. *Eur. Heart J.* **41**, 2731–2742 (2020).

19. Sengupta, A., Alexis, S. L., Zaid, S. & Tang, G. H. L. Will valve-in-valve transcatheter aortic valve replacement shift the treatment paradigm for young adults with aortic valve disease? *Ann. Cardiothorac. Surg.* **10**, 509–511 (2021).

20. Alexis, S. L. *et al.* Transcatheter aortic valve replacement aortic root orientation: implications for future coronary access and redo transcatheter aortic valve replacement. *Ann. Cardiothorac. Surg.* **9**, 502–504 (2020).

21. Pollak, P. M., Mack, M. J. & Holmes, D. R. Quality, Economics, and National Guidelines for Transcatheter Aortic Valve Replacement. *Prog. Cardiovasc. Dis.* **56**, 610–618 (2014).

22. Reddy, K. P., Groeneveld, P. W., Giri, J., Fanaroff, A. C. & Nathan, A. S. Economic Considerations in Access to Transcatheter Aortic Valve Replacement. *Circ. Cardiovasc. Interv.* **15**, e011489 (2022).

23. Li, R. L. *et al.* Mechanical considerations for polymeric heart valve development: Biomechanics, materials, design and manufacturing. *Biomaterials* **225**, 119493 (2019).

24. Abdelbasset, W. K. *et al.* Polysaccharides, as biological macromolecule-based scaffolding systems in heart valve tissue engineering: a review. *Cellulose* **29**, 5395–5428 (2022).

25. Sheriff, J. *et al.* Physical Characterization and Platelet Interactions under Shear Flows of a Novel Thermoset Polyisobutylene-Based Co-Polymer. *ACS Appl. Mater. Interfaces* **7**, 22058–22066 (2015).

26. Rotman, O. M. *et al.* Novel Polymeric Valve for Transcatheter Aortic Valve Replacement Applications: In Vitro Hemodynamic Study. *Ann. Biomed. Eng.* **47**, 113–125 (2019).

27. Ahmed, M., Punshon, G., Darbyshire, A. & Seifalian, A. M. Effects of sterilization treatments on bulk and surface properties of nanocomposite biomaterials. *J. Biomed. Mater. Res. B Appl. Biomater.* **101**, 1182–1190 (2013).

28. Rahmani, B. *et al.* In Vitro Hydrodynamic Assessment of a New Transcatheter Heart Valve Concept (the TRISKELE). *J Cardiovasc. Transl. Res.* **10**, 104–115 (2017).

29. Rahmani, B. *et al.* A new transcatheter heart valve concept (the TRISKELE): feasibility in an acute preclinical model. *EuroIntervention* **12**, 901–908 (2016).

30. US Patent Application for Silicone 3D Printing Ink Patent Application (Application #20200216692 issued July 9, 2020) - Justia Patents Search. https://patents.justia.com/patent/20200216692#history.

31. Coulter, F. B. *et al.* Bioinspired Heart Valve Prosthesis Made by Silicone Additive Manufacturing. *Matter* **1**, 266–279 (2019).

32. Frontiers | Thiol-ene cross-linking and functionalisation of Polydimethylsiloxane for biomedical applications. https://www.frontiersin.org/10.3389/conf.FBIOE.2016.01.01724/event_abstract.

33. Stasiak, J. *et al.* A bio-inspired microstructure induced by slow injection moulding of cylindrical block copolymers. *Soft Matter* **10**, 6077–6086 (2014).

34. R. Stasiak, J. *et al.* Design, development, testing at ISO standards and in vivo feasibility study of a novel polymeric heart valve prosthesis. *Biomater. Sci.* (2020) doi:10.1039/D0BM00412J.

35. Dandeniyage, L. S. *et al.* Morphology and surface properties of high strength siloxane poly(urethane-urea)s developed for heart valve application. *J. Biomed. Mater. Res. B Appl. Biomater.* **107**, 112–121 (2019).

36. Dandeniyage, L. S. *et al.* In vitro oxidative stability of high strength siloxane poly(urethane-urea) elastomers based on linked-macrodiol. *J. Biomed. Mater. Res. B Appl. Biomater.* **107**, 2557–2565 (2019).

37. Jenney, C. *et al.* Assessment of a Siloxane Poly(urethane-urea) Elastomer Designed for Implantable Heart Valve Leaflets. *Adv. NanoBiomed Res.* **1**, 2000032 (2021).

38. US Patent for Prosthetic heart valves with elastic support structures and related methods Patent (Patent # 10,231,833 issued March 19, 2019) - Justia Patents Search. https://patents.justia.com/patent/10231833.

39. Bezuidenhout, D., Williams, D. F. & Zilla, P. Polymeric heart valves for surgical implantation, catheter-based technologies and heart assist devices. *Biomaterials* **36**, 6–25 (2015).

40. Flameng, W. *et al.* Factors influencing calcification of cardiac bioprostheses in adolescent sheep. *J. Thorac. Cardiovasc. Surg.* **132**, 89–98 (2006).

41. Pislaru, S. V., Nkomo, V. T. & Sandhu, G. S. Assessment of Prosthetic Valve Function After TAVR. *JACC Cardiovasc. Imaging* **9**, 193–206 (2016).

42. Trowbridge, E. A. & Crofts, C. E. Pericardial heterograft valves: an assessment of leaflet stresses and their implications for heart valve design. *J. Biomed. Eng.* **9**, 345–355 (1987).

43. Schoen, F. J., Fernandez, J., Gonzalez-Lavin, L. & Cernaianu, A. Causes of failure and pathologic findings in surgically removed Ionescu-Shiley standard bovine pericardial heart valve bioprostheses: emphasis on progressive structural deterioration. *Circulation* **76**, 618–627 (1987).

44. Tang, G. H. L., Zaid, S., Ahmad, H., Undemir, C. & Lansman, S. L. Transcatheter Valve Neo-Commissural Overlap With Coronary Orifices After Transcatheter Aortic Valve Replacement. *Circ. Cardiovasc. Interv.* **11**, e007263 (2018).

45. Tang, G. H. L. *et al.* Alignment of Transcatheter Aortic-Valve Neo-Commissures (ALIGN TAVR): Impact on Final Valve Orientation and Coronary Artery Overlap. *JACC Cardiovasc. Interv.* **13**, 1030–1042 (2020).

46. Yudi, M. B., Sharma, S. K., Tang, G. H. L. & Kini, A. Coronary Angiography and Percutaneous Coronary Intervention After Transcatheter Aortic Valve Replacement. *J. Am. Coll. Cardiol.* **71**, 1360–1378 (2018).

47. Bekeredjian, R. & Grayburn, P. A. Valvular Heart Disease. *Circulation* **112**, 125–134 (2005).

48. Zhang, M. Surface Modification of Ultra High Molecular Weight Polyethylene with Hyaluronan for Total Joint Replacement Application. (Colorado State University, 2004).

49. Bui, H. T. Development of hyaluronan enhanced expanded polytetrafluoroethylene and linear low density polyethylene for blood contacting applications, The. (Colorado State University, 2019).

50. CDC. Coronavirus Disease 2019 (COVID-19) PPE. *Centers for Disease Control and Prevention* https://www.cdc.gov/coronavirus/2019-ncov/hcp/using-ppe.html (2020).

51. Reddy, S. C., Valderrama, A. L. & Kuhar, D. T. Improving the Use of Personal Protective Equipment: Applying Lessons Learned. *Clin. Infect. Dis.* **69**, S165–S170 (2019).

52. Fischer, W. A., Weber, D. J. & Wohl, D. A. Personal Protective Equipment: Protecting Health Care Providers in an Ebola Outbreak. *Clin. Ther.* **37**, 2402–2410 (2015).

53. Lam, T.-N. *et al.* Multi-Scale Microstructure Investigation for a PM2.5 Air-Filter Efficiency Study of Non-Woven Polypropylene. *Quantum Beam Sci.* **3**, 20 (2019).

54. Tang, S. *et al.* Aerosol transmission of SARS-CoV-2? Evidence, prevention and control. *Environ. Int.* **144**, 106039 (2020).

55. N95 Masks Explained | Honeywell. https://www.honeywell.com/content/honeywell/us/en/newsroom/news/2020/03/n95-masks-explained.html.

56. Walls, A. C. *et al.* Structure, Function, and Antigenicity of the SARS-CoV-2 Spike Glycoprotein. *Cell* **181**, 281-292.e6 (2020).

57. Walls, A. C. *et al.* Glycan shield and epitope masking of a coronavirus spike protein observed by cryo-electron microscopy. *Nat. Struct. Mol. Biol.* **23**, 899–905 (2016).

58. Bui, H. T., Prawel, D. A., Harris, K. L., Li, E. & James, S. P. Development and Fabrication of Vapor Cross-Linked Hyaluronan–Polyethylene Interpenetrating Polymer Network as a Biomaterial. *ACS Appl. Mater. Interfaces* **11**, 18930–18941 (2019).

59. Abboud, M., Vol, S., Duguet, E. & Fontanille, M. PMMA-based composite materials with reactive ceramic fillers Part III: Radiopacifying particle-reinforced bone cements. *J. Mater. Sci. Mater. Med.* **11**, 295–300 (2000).

60. Bogie, R. *et al.* Novel Radiopaque Ultrahigh Molecular Weight Polyethylene Sublaminar Wires in a Growth-Guidance System for the Treatment of Early-Onset Scoliosis: Feasibility in a Large Animal Study. *Spine* **39**, E1503 (2014).

61. Lewis, G., Towler, M. R., Madigan, S. & German, M. J. Influence of a novel radiopacifier (nano-sized strontia particles) on in vitro properties of a PMMA bone cement for use in total joint replacements. *Int. J. Nano Biomater.* **3**, 78–93 (2010).

CHAPTER 2: MATERIAL CHARACTERIZATION OF RADIOPACIFIED HA ENHANCED LLDPE

2.1 Chapter Introduction

There has been significant investigation into a composite material made from hyaluronic acid (HA) and polyethylene. This composite has significant potential as an implantable biomaterial for orthopedic and cardiovascular applications[1–5]. However, these materials are radio transparent and cannot be easily imaged or identified using common techniques such as x-ray, fluoroscopy, and computed tomography. TAVR leaflet function is assessed using echocardiography however as Seller's et al succinctly explains, "These approaches provide diagnostic but not granular or real-time mechanistic insights to degeneration."[6] Introducing radiopacity to the material would allow physicians to understand how these leaflets change shape or how their movement profile changes over time in the body giving "real-time mechanistic insight". This understanding of how the leaflet behavior changes in time from material fatigue or other factors will allow engineers to pursue information driven redesign of the implant. Beyond these extreme changes ability to directly image the leaflets will ensure they are not blocking the coronary ostium upon placement and show if the leaflets are not moving properly due to placement. Furthermore, it would allow for rapid identification of implant displacement in catastrophic scenarios. This chapter addresses an investigation into whether these polyethylene materials can be radiopacified with barium sulphate, bismuth trioxide, and tungsten, what effects radiopacification has on the material properties of HA enhanced LLDPE and how radiopacification affects the hemodynamics of the valve and aids implantation of the device.

2.1.1 Hyaluronan Enhancement of LLDPE

HA enhancement of LLDPE can be summarized with three steps.

1. HA is chemically modified such that it may be dissolved in non-polar organic solvents. The final polymer, silylated hyaluronic acid complexed with cetyl trimethyl ammonium bromide, is referred to as both the acronym SHACTA and silyl-HA in this dissertation. The process is described below in *Silylation of HA*. Detailed protocols can be found in appendix A.1 and A.2, "Complexation of HA-CTA" and "Silylation of HA-CTA".

2. LLDPE is swollen in a SHACTA/xylene solution allowing SHACTA to diffuse into the LLDPE forming an unbound interpenetrating polymer network (IPN). The SHACTA is crosslinked in place forming covalent bonds that prevent phase separation of SHACTA and LLDPE. Described in *Formation of an IPN between HA and LLDPE.*

3. The SHACTA is reverted to semi-native HA (HA that is in its native state except for the formation of the new covalent bonds bounding the IPN) by removing the cetyltrimethylammonium (CTA) and silyl groups through counter ion replacement and hydrolysis. Described in Hydrolysis of HA. A detailed protocol of "*Hydrolysis of HA*" and the previous step "*Formation of an IPN between HA and LLDPE*" can be found in appendix A.3, "SHACTA Treatment of LLDPE".

Silylation of HA

700 kDa sodium hyaluronate (Lifecore biomedical) is dissolved in deionized water (DI) at 0.3% (w/v) for 12 hours. Cetyltrimethylammonium bromide (CTAB) (Fisher Scientific) is dissolved in deionized water (DI) at 1.0% (w/v) for 15 minutes at 40 °C. An ion exchange occurs in which the cetyltrimethylammonium ion replaces the sodium ion forming a hyaluronan-cetyltrimethylammonium (HACTA, or HA-CTA) precipitate (Figure 2.1). The bromide ion and the sodium ion form a salt which stays in solution. The HACTA is washed with DI, dried under vacuum, and ground into a powder under cryogenic (-196 °C) conditions. Purified HACTA is dissolved in dry dimethyl sulfoxide (DMSO) under a blanket of dry nitrogen at 50 °C for 12 hours.

Dry hexamethyldisilazane (HMDS) is added in excess by cannula maintaining the blanket of nitrogen and the solution is heated to 75 °C for 48 hours allowing the hydroxyl protons of HA to be replaced with silyl groups while off gassing ammonia formed from the protons of HA and the nitrogen of HMDS. After which the upper HMDS layer containing the silyl HA-CTA (SHACTA) is separated from the lower DMSO layer and the HMDS is evaporated off at 60 °C using a rotary evaporator. The SHACTA is washed 5x with xylenes and dried under vacuum for 24-48 hours yielding purified SHATCA, a light-yellow crystalline material (Figure 2.2).

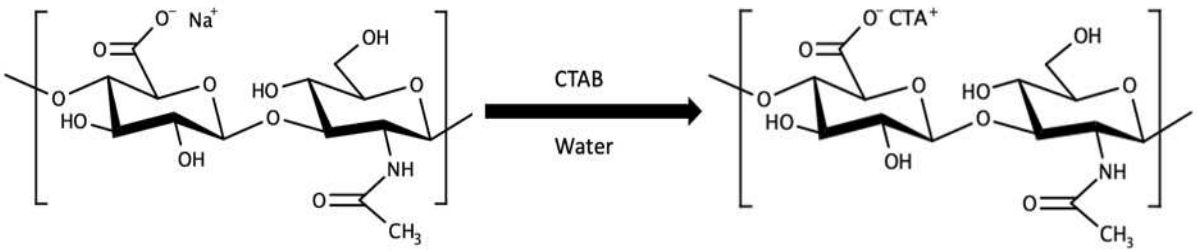

Figure 2.1: Synthesis of HACTA

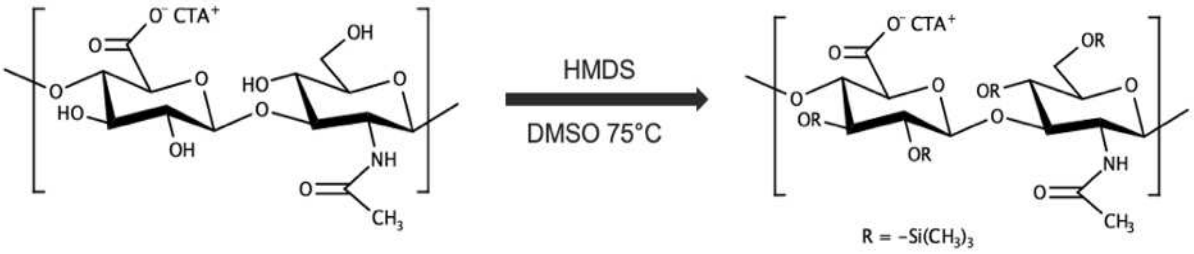

Figure 2.2: Synthesis of SHACTA

Formation of an IPN between HA and LLDPE

Eighty µm thick blown film from Dowlex 2045G resin (Dow Inc.) is immersed in xylenes for 12 hours, rinsed with acetone, and vacuum dried. Xylenes are dried over 3 Å molecular sieves at 10% (w/v) for at least 72 hours prior to use. The clean film is immersed in a 1.0% (w/v) solution of SHACTA in xylenes for 1 hour at 50 °C allowing the silyl HA to penetrate the swollen LLDPE. The xylene solution is slowly drained over one hour under vacuum (-15 inHg). After draining the solution is removed from the vacuum oven and the LLDPE films are dried for at least another 3

hours. Once dry, the films are placed above a 2% (v/v) solution of toluene diisocyanate (TDI) in xylenes at 60 °C in a closed system. The films are crosslinked in the TDI/xylene vapor for 1 hour in which the isocyanate groups react with the silylated oxygen forming crosslinks between the HA and itself. The films are dried under vacuum for three to twelve hours.

Hydrolysis of HA

The silyl HA in the film is reverted to native HA by sonicating in 0.2 M NaCl in DI/ethanol (1:1, v/v) solution for one hour, after the solution is replaced and the sonication repeated twice more for a total of 3x sonications. Samples are rinsed with DI then sonicated in 0.2 M NaCl in DI for one hour. Excess CTA and silyl groups are allowed to leech from the material in a 3:2 solution of DI/ethanol for at least 2 hours. The HA enhanced LLDPE undergoes a final sonication in DI for 30 minutes before being dried overnight under vacuum.

2.1.2 Statistical Analysis

Data sets were evaluated for equal variance using Levene's test and evaluated for normality using the Anderson-Darling test. Once these parameters were established significance was determined using ANOVA with post hoc Tukey's test (p value < 0.05). For data sets that did not have equal variance the Games-Howell test was performed (p value < 0.05). A post hoc power analysis was performed on all data sets to verify sample size with a minimum effect size of 0.8. All statistics were performed using Minitab.

2.2 Embedding radiopaque materials in LLDPE

Though there is not a linear relationship between density or atomic number and radiopacity, a loose association can be made between both density and radiopacity and atomic number and radiopacity. As both density of a material and/or the atomic number of the elements making up a material increases, generally the material will attenuate more of an incident x-ray beam[7–9]. By

embedding high density and biologically inert materials in polyethylene, the low density polymer can be rendered radiopaque for biological use[10].

2.2.1 Methods

Three common powdered radiopaque materials were selected for the radiopacification of LLDPE: barium sulfate, bismuth trioxide, and tungsten. The powders were spread between LLDPE sheets (2 cm x 2 cm) then melt pressed at 150°C for 3 minutes at 50 PSI. Loading weight percent's (w/w) of the radiopaque material were based on high and low industry standards and are summarized in table 2.1 below. These materials have been used as radiopacifiers in rubber, ceramics, and plastics in the loadings seen in table 2.1[10–13]. Barium sulphate and bismuth trioxide have been used extensively in polymethylmethacrylate bone cements, and all three radiopacifiers are recognized for use by the medical device and diagnostic industry[14–17].

Table 2.1: Loading percent (w/w) of different radiopaque materials in LLDPE

	Tungsten	Bismuth Trioxide	Barium Sulfate
High Loading (w/w)	70%	30%	50%
Low Loading (w/w)	40%	10%	10%

Samples were imaged using an EPX-F2800 x ray source and a Universal Imaging MyRad digital radiography machine. The accelerating voltage was 75 kV and there was 0.5 mAs of radiation produced. The samples were first imaged after melt pressing the radiopaque fillers between two LLDPE sheets (figure 2.3 left image). After imaging the samples were trimmed to size and put through the HA enhancement process. The trim was set aside as a control. After the application of HA the samples and the untreated trim were imaged again (figure 2.3 right image). Samples were also imaged at 75 kV and 2.5 mAs, 85 kV and 0.8 mAs, and 95 kV and 0.8 mAs. The images did not vary with the changing parameters.

A detailed protocol for melt pressing can be found in appendix A.4 "Melt Pressing Radiopacifiers into LLDPE".

2.2.2 Results

Figure 2.3 shows X-ray images of the radiopacified samples before and after HA enhancement. It is clear from the images that the control is radiotransparent, and the samples containing tungsten, barium sulfate, and bismuth trioxide are radiopaque.

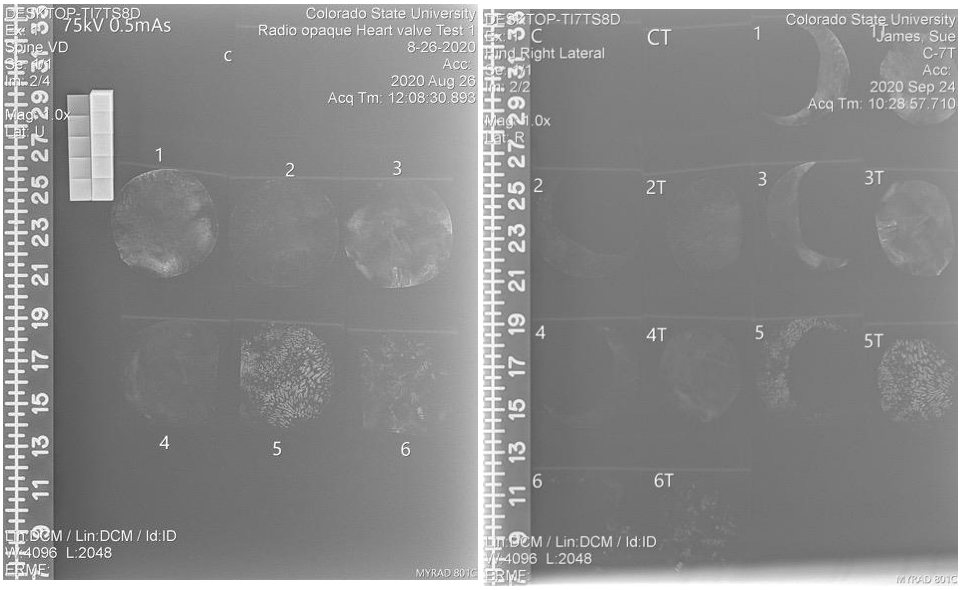

Figure 2.3: Image on the left shows LLDPE samples embedded with radiopaque materials. C. Control (No radiopaque filler) 1. Tungsten 70%. 2. Tungsten 40%. 3. Bismuth Trioxide 30%. 4. Bismuth Trioxide 10%. 5. Barium Sulfate 50%. 6. Barium Sulfate 10%. The image on the right follows the same nomenclature with T indicating the sample had HA treatment while a number alone is the untreated trim from the same sample.

2.2.3 Discussion

LLDPE is radiotransparent before and after HA treatment. Barium sulfate at 50% loading (Sample 5) generated the greatest contrast in the x-ray images but was difficult to distribute evenly through the sample. Tungsten at 70% loading (Sample 1) also generated significant contrast. Low loading percentages generated poor contrast though this is not surprising considering the thinness of film creates an inherently short path length for contrast.

2.3 Toluidine Blue O (TBO) Staining of Hyaluronic Acid

TBO stains carboxyl groups by forming an electrostatic complex at high pH (PH~10) through ion exchange with the acidic proton[18].

2.3.1 Methods

A 0.1% (w/w) solution of toluidine blue O (TBO) was prepared to determine the presence of HA on the radiopacified HA enhanced LLDPE. First an 8 M solution of urea was prepared after which 0.1% (w/w) of TBO was added. LLDPE samples were placed in solution for 30 minutes, removed and agitated in deionized water until all excess dye was leached from the surface. After drying the samples were imaged against a white background. A detailed protocol for melt pressing can be found in appendix A.5, "Toluidine Blue O Staining Assay".

2.3.2 Results

Figure 2.4 shows radiopaque samples with and without HA enhancement after TBO staining. The bottom row of HA treated samples are stained blue indicating the presence of HA. These results indicate that the impregnation of LLDPE with radiopaque materials does not prevent the enhancement of the material with HA.

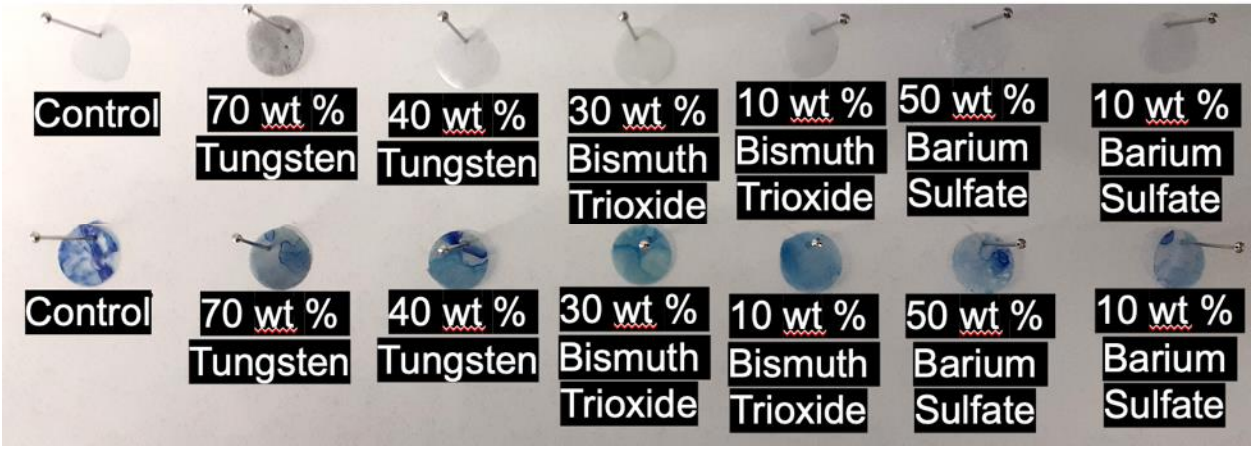

Figure 2.4: TBO stained samples of radiopacified samples. Top row are samples not treated with HA. Bottom row are samples treated by HA.

2.3.3 Discussion

TBO stains carboxyl groups and LLDPE contains no carboxyl groups, while HA has one per repeat unit. The absence of a stain on the control samples indicate no HA is present while the blue stains on the treated samples indicate that the treatment successfully incorporated HA across the surface of the LLDPE samples.

While each HA sample is stained blue there is clear variation in the color and location of the stained samples. First is that LLDPE is semitransparent and TBO stained HA is on both sides of the samples. However, only the control sample retains its visual semi transparency as the materials with radiopaque filler are fairly opaque. Thus, the fact that the radiopaque samples are a lighter blue compared to the control is likely because we are only seeing only one side of the stain as opposed to both. Second is that the TBO stain is not uniform. This is likely because the HA is not uniformly distributed. While this is less than ideal chapter 4 reviews methods to increase the uniformity of HA distribution and the results shown in this chapter and chapter 3 demonstrate that perfect uniformity is not necessary to producing a blood compatibilized radiopaque heart valve leaflet. Finally, as with all photography of samples the imaging conditions are variable (shading, light source and location, background). While all images of TBO stained samples were taken with a white background to attempt to provide some uniformity, the realities of variation due to the photographer, setting, and camera must be acknowledged.

Regardless of the challenges, each HA treated sample clearly stained blue indicating the presence of HA. Neither melt pressing the LLDPE alone nor melt pressing in tungsten or bismuth prevented the HA treatment as indicated by the blue TBO stain on the treated samples.

Though quantitative TBO was not performed on these samples future researchers should consider this assay to determine a numeric evaluation. Along these lines a comprehensive study using thermogravimetric analysis, quantitative TBO, and contact angle are compared may provide insight into the consistency of HA-LLDPE IPN's and HA surface confluency. Thermogravimetric

analysis would prove a clear mass percent of HA in the bulk while quantitative TBO shows the amount of HA at the surface. Contact angle would show the consistency and if any of the three measurements can be correlated it would generate a clearer understanding of the HA-LLDPE IPN treatment process and results.

2.4 Contact Angle Goniometry

Contact angle goniometry is used to determine the two-dimensional surface characteristics pertaining to the interaction between liquids and solids. Static contact angle is the tangent at the liquid-vapor interface and the liquid-solid interface at the triple phase line of a drop of liquid on a solid surface measured through the liquid. This angle is shown in figure 2.5. Measuring contact angle by placing a droplet of liquid on a surface is known as the sessile droplet method. The static contact angle of an atomically smooth and a perfect chemically homogenous surface in contact with a pure liquid can be modeled through Young's equation.

$$Cos\theta = \frac{\gamma_{SV} - \gamma_{SL}}{\gamma_{LV}}$$

θ represents the contact angle, γ_{SV} represents the solid surface energy, γ_{SL} represents the solid-liquid interfacial energy, and γ_{LV} represents the liquid surface tension. In the ideal scenario described above as liquid is added (advancing contact angle) or withdrawn (receding contact angle) the advancing and receding contact angles would approach the static contact angle. Advancing and receding contact angles can be seen in figure 2.5. However, since nearly every surface is both physically and chemically heterogeneous the difference between the advancing and receding contact angles is measured and referred to as the contact angle hysteresis. Contact angle hysteresis is a measure of physical and chemical heterogeneity.

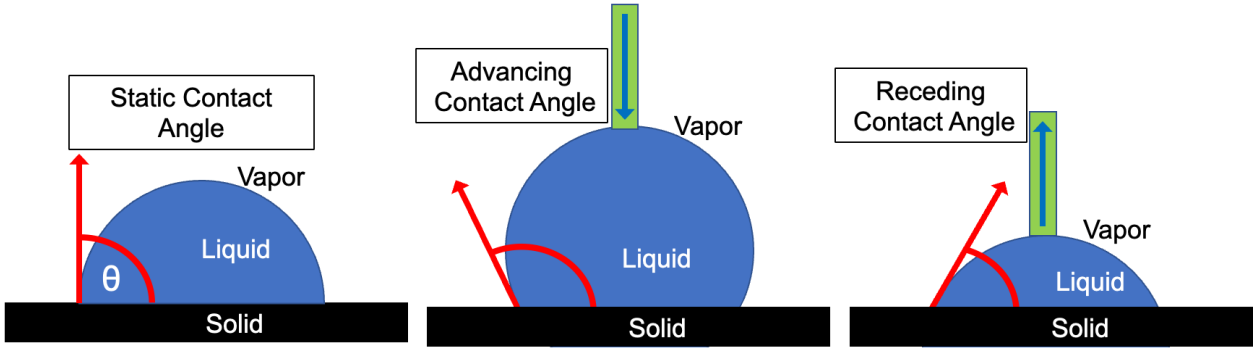

Figure 2.5: Diagram of sessile static, advancing, and receding contact angles. The green rectangle represents a needle adding (advancing) or removing (receding) liquid from the surface droplet.

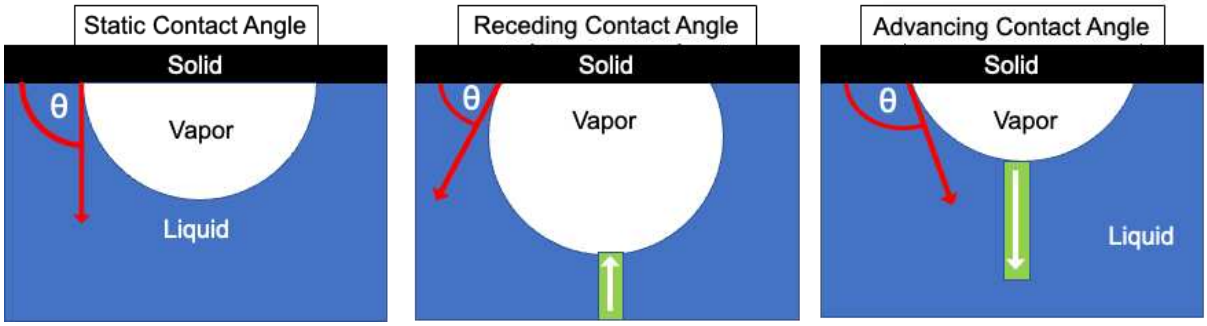

Figure 2.6: Diagram of captive bubble static, advancing, and receding contact angles. The green rectangle represents a needle adding or removing vapor from the captive vapor bubble.

Surfaces that have altered characteristics in dry and hydrated states, such as HA-LLDPE, should have their contact angles measured in the appropriate state. Measuring the hydrated state of a material requires an inversion of the system where a vapor bubble is placed underneath the hydrated solid. This method of determining contact angle is known as the captive bubble method. Figure 2.6 shows a diagram of the captive bubble method.

2.4.1 Methods

Surfaces enhanced with HA are generally hydrophilic due to the highly polar nature of the molecule. HA is so hydrophilic that it becomes difficult to measure the water contact angle using traditional sessile water drop goniometry. In addition to those challenges the material will be in a hydrated state when in contact with blood, thus captive bubble technique was used to analyze

the hydrophilicity of the surface. By using the captive bubble technique, the films can be hydrated prior to measurement allowing the HA to swell with water as it would in human vasculature. Measurements were taken with a 260-F4 Ramé-Hart Goniometer. Samples were allowed to swell in DI water for at least 30 minutes before being taped to a slide, inverted, and submerged in a DI water tank for measurements. An air bubble was introduced to the inverted sample and the static contact angle was measured. The air bubble was expanded until a consistent receding contact angle was measured, and then in reverse the bubble was retracted until a consistent advancing contact angle was measured. Values are representative of the solid-liquid interface.

2.4.2 Results

Figure 2.7 shows the contact angles of the radiopacified samples before being treated with HA. Figure 2.8 shows the contact angles of the radiopacified samples after being treated with HA. All contact angles recorded on the HA treated samples were significantly different than their untreated controls except the advancing angle for 10% barium sulfate. In aggregate the respective static, advancing, and receding contact angles before treatment are 99.5 ± 1.9°, 106.8 ± 1.6°, and 96.9 ± 2.0°. After treatment the aggregate respective static, advancing, and receding contact angles are 44.0 ± 13.8°, 86.3 ± 5.9°, and 36.3 ± 11.6°. While almost all contact angles measurements of the treated samples are significantly different than their untreated controls it should be noted that the variation in contact angle is much greater on the treated samples. The decreased contact angle demonstrates impregnation of radiopaque materials does not prevent HA treatment of LLDPE.

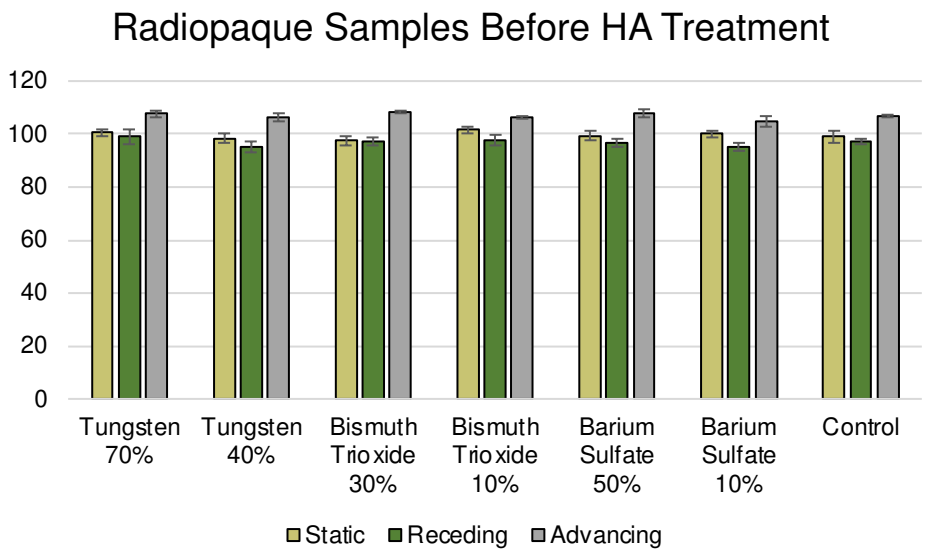

Figure 2.7: Goniometric data for the radiopacified samples prior to HA treatment.

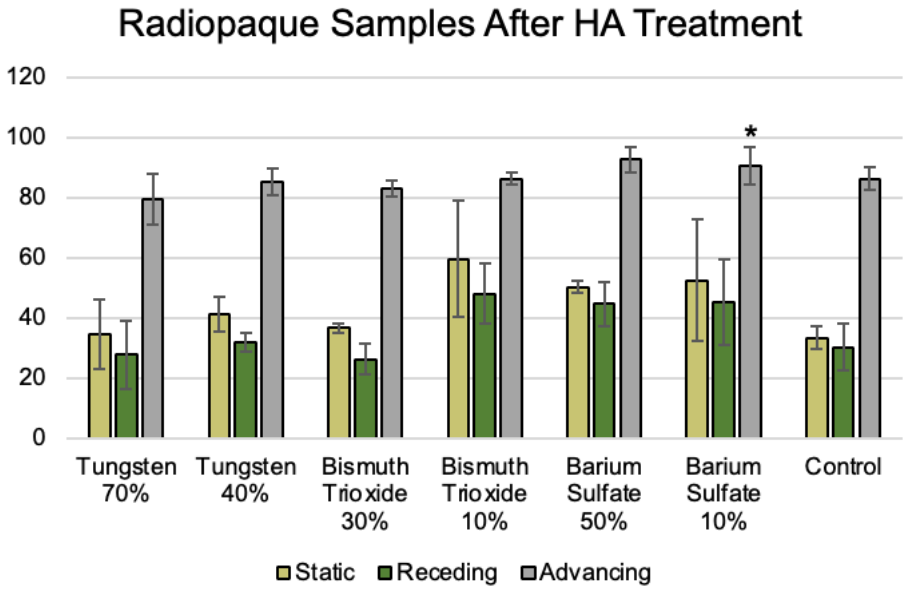

Figure 2.8: Goniometric data for the radiopacified samples after HA treatment. All samples were significantly different than their respective control before HA treatment, except for the advancing contact angle of 10% barium sulfate denoted with an asterisk (*).

2.4.3 Discussion

The results indicate that the HA treated samples are significantly more hydrophilic than the untreated controls with one exception. While the advancing contact angle of 10% barium sulfate was the only sample that was not significantly different (p value < 0.05) it should be noted that there was large variation in the contact angle of some of the radiopaque HA treated samples. Taking contact angles on these samples was difficult as the captive bubble often became trapped in between ridges of embedded radiopaque material. This was most present on the barium sulfate samples where the powder tended to pool or aggregate. As contact angle is a measure of the physical and chemical homogeneity of the surface it is likely that more homogenous distribution of the radiopaque material would produce lower variation in the data as seen in the control sample. The introduction of HA does introduce some chemical heterogeneity however the variation in contact angle is much lower than 10% barium sulfate and 10% bismuth trioxide. This leads to the conclusion that the HA treatment is effective at reducing the contact angle in radiopaque samples, and that more homogenous distribution of radiopaque materials may lead to more consistent captive bubble contact angle data.

While effective distribution may address some of the variation in contact angle data, it may be interesting to take surface roughness measurements and to try and correlate them to changes in contact angles. Advancing and receding angles would provide the most insight as the surface topology will affect the ability of the air bubble to advance and recede across the surface.

2.5 Uniaxial Tensile Testing

Uniaxial tensile testing was performed to determine if melt pressing radiopaque fillers into LLDPE had significant effects on the tensile properties of LLDPE films (Dowlex 2045G). Youngs modulus, yield stress, yield strain, elongation at break, ultimate tensile strength, and toughness were all evaluated. The heart valve leaflets should always be operating in the elastic region when

the heart valve is in use. Yielding would result in improper valve function and indicate the LLDPE leaflets are tending towards eventual failure. As such the most important properties are yield stress and yield strain considering the LLDPE film leaflets are expected to operate within the elastic domain of the material. As such failure mechanisms should be best predicted by yield stress and yield strain with these tests. The Young's modulus is also critical as a less stiff material may cause the leaflets to prolapse and a stiffer material may prevent the leaflets from properly opening and closing. As the test was completed to failure it seemed wise to evaluate other tensile properties such as ultimate tensile strength, toughness, and elongation at break for greater scientific understanding of any changes in uniaxial tensile failure mechanisms.

2.5.1 Methods

It should be noted that ASTM D882-18 was not followed, but rather another method using the ASTM D882-18 as a basis was evaluated against the ASTM standard and then used. See Appendix B.1, "Evaluation of non-ASTM Tensile Testing Protocol" for further details.

Two LLDPE films (6 cm x 6 cm) were weighed and one of three radiopaque powders (barium sulfate bismuth trioxide, or tungsten) were dispersed on top the first 6 cm x 6 cm LLDPE film. The second film was placed on top of the radiopaque powder sandwiching the radiopaque material between them. The LLDPE-radiopaque powder-LLDPE construct was placed between Kapton sheets and aluminum plates, and melt pressed at 150 °C for 3 minutes at approximately 100 PSI embedding the radiopaque materials. Control films were also pressed with no radiopaque powder.

The w/w percent of each material are as follows: Barium sulfate (50%± 5%), bismuth trioxide (40% ± 5%), and tungsten (70% ± 5%). Ex calculation barium sulfate: 50% ± 5% would be 0.1 grams LLDPE and 0.05 grams barium sulfate. While it should be noted that an accidental higher mass percentage was used for bismuth trioxide, this does represent a scenario in which the sample would be more likely to fail from aggregation of the radiopacifier in the melt. In fact,

this was seen on the barium sulfate samples but not in the bismuth trioxide samples. Regardless the higher mass would only make the films more radiopaque and was continued to be used in all further studies.

After melt pressing the films were weighed to determine the initial mass, swelled in xylenes overnight, rinsed with acetone, and dried under vacuum (-25 inHg) for at least 12 hours. The films were then weighed again to determine if the swelling process resulted in a loss of mass indicating the radiopaque powder was not completely embedded in the LLDPE. There was no detectable loss of mass seen in any film. The films were approximately 1 gram in mass and the balance used had a resolution of 0.001 grams, so any mass loss below 0.1% would not have been detected.

Tensile specimens (gauge length: 12 mm, width: 3.16 mm) were punched from the melt pressed films and pulled to failure at 500 mm/min using an Instron 4443 with a 50 N load cell. The thickness of each sample varied but was measured with calipers for each test. Yield stress, yield strain, elongation at break, ultimate tensile strength, and toughness were calculated.

Tensile specimens (gauge length: 12 mm, width: 3.16 mm) were punched from the melt pressed films and pulled to failure at 50 mm/min. The thickness of each sample varied but was measured for each test using digital calipers. Modulus was calculated from the lower strain rate data, as recommended by ASTM D882-18.

It should be noted that originally only barium sulfate samples were tested, as these samples were the most radiopaque as seen in figure 2.3. However, the barium sulfate films had a significant loss of mechanical properties when compared to melt press controls and plain 2045G films. To determine if other radiopaque fillers caused this same loss of mechanical properties, high weight percent tungsten and bismuth samples were evaluated. The plain 2045G film data was taken in the machine direction of the sample.

Data was evaluated for normality and equal variances. Data with equal variance was analyzed with an ANOVA and post hoc Tukey's test to determine significant differences ($n = 5$, p

value < 0.05). For data sets that did not have equal variance the Games-Howell test was performed (n = 5, p value < 0.05).

2.5.2 Results

Figure 2.9 shows the moduli for all samples. The melt press control and 50% barium sulfate samples had significantly lower moduli than the virgin 2045G samples.

Figure 2.10 shows the yield stress for all samples tested. Only the 50% barium sulfate samples had a significantly different yield stress when compared to the virgin 2045G LLDPE.

Figure 2.11 shows the yield strain for all samples tested. The 50% barium sulfate samples had a lower yield strain than virgin 2045G. The melt press control, 40% bismuth trioxide, and 70% tungsten samples all had significantly higher yield strains than the virgin 2045G samples.

Figure 2.12 shows the elongation at break for all samples tested. The melt press control, 40% bismuth trioxide, and 70% tungsten samples all had significantly higher elongation at break compared to the virgin 2045G sample.

Figure 2.13 shows the ultimate tensile strength for all samples tested. Only the 50% barium sulfate samples were significantly different than the 2045G samples.

Figure 2.14 shows the toughness for all samples tested. The melt press control and 40% bismuth trioxide samples had significantly greater toughness than the virgin 2045G samples.

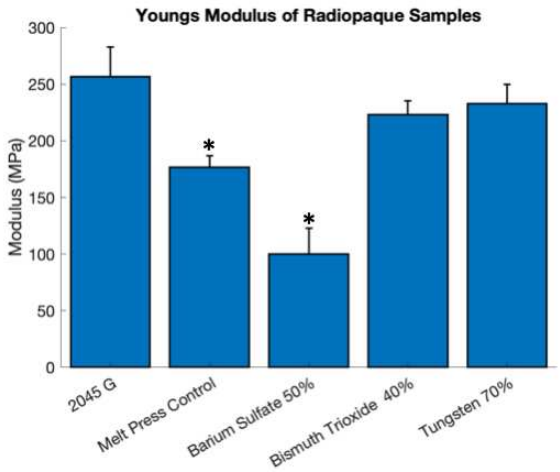

Figure 2.9: Young's modulus for radiopaque LLDPE samples. Error bars represent standard deviation and asterisks indicate that the samples had significantly lower moduli than the virgin 2045G samples. ($p < 0.05$)

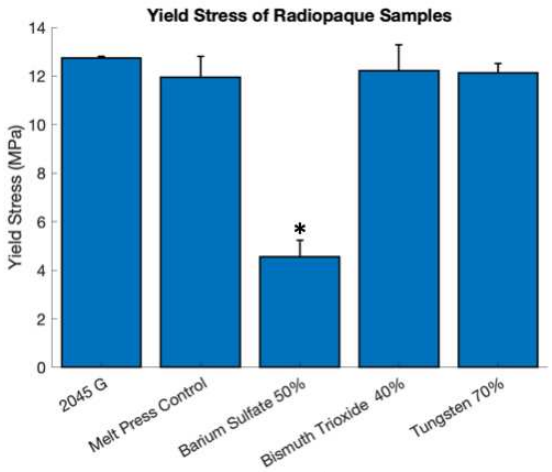

Figure 2.10: Yield stress for radiopaque LLDPE samples. Error bars represent standard deviation. Asterisks indicate that the samples had significantly different yield stress than the virgin 2045G samples. ($p < 0.05$)

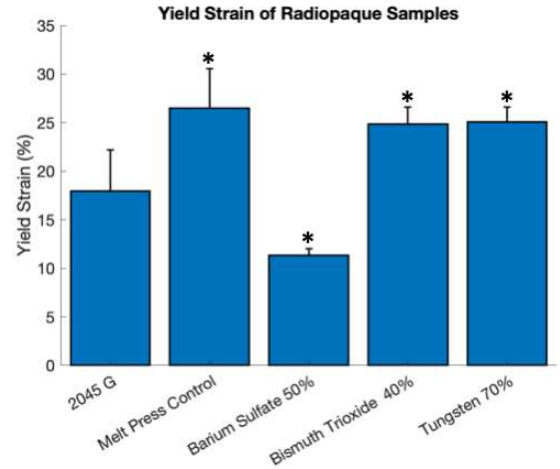

Figure 2.11: Yield strain for LLDPE samples. Error bars represent standard deviation. Asterisks indicate that the samples had significantly different moduli than the virgin 2045G sample ($p < 0.05$)

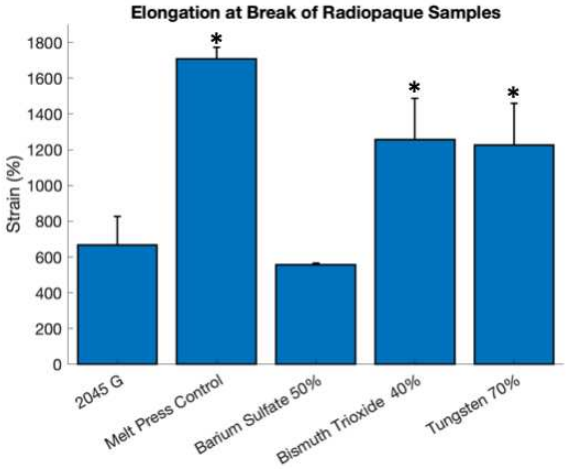

Figure 2.12: Elongation at break for LLDPE samples. Error bars represent standard deviation. Asterisks indicate that the samples had significantly different moduli than the virgin 2045G sample ($p < 0.05$)

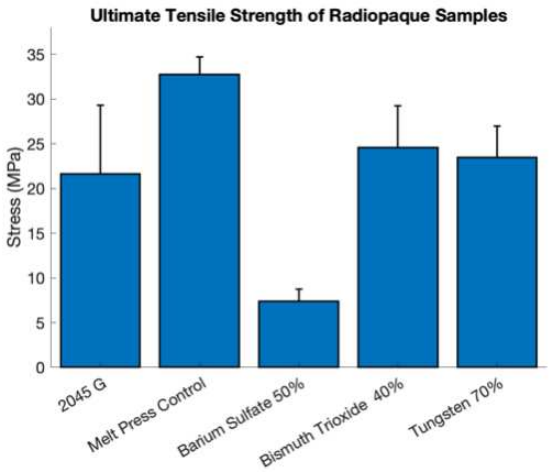

Figure 2.13: Ultimate tensile strength for LLDPE samples. Error bars represent standard deviation Asterisks indicate that the samples had significantly different moduli than the virgin 2045G sample ($p < 0.05$)

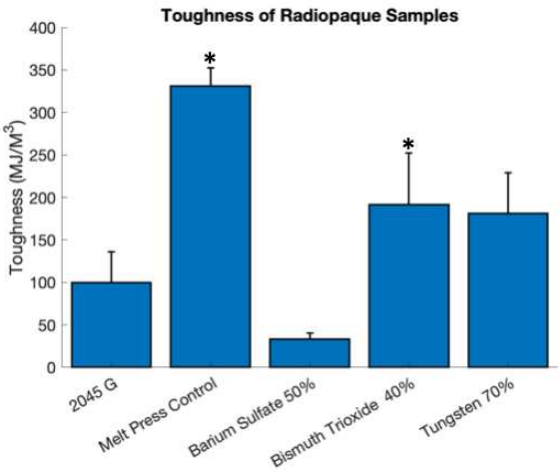

Figure 2.14: Toughness for LLDPE samples. Error bars represent standard deviation. Asterisks indicate that the samples had significantly different moduli than the virgin 2045G sample ($p < 0.05$)

2.5.3 Discussion

Moduli

Both the melt press control and barium sulfate had significantly lower moduli compared to the untreated 2045G material. This indicates melt pressing LLDPE reduces the stiffness of softens the material producing a lower modulus. Interestingly the LLDPE containing radiopaque fillers produced differing results. This is not completely unexpected as modulus is related to the molecular interactions of a material. Melt pressing the material the percent crystallinity and/or the orientation of the crystallinity may be altered, while adding fillers may act as a physical crosslinker.

The addition of barium sulfate reduced the modulus when compared to the melt press control while the bismuth trioxide and tungsten increased the modulus compared to the melt press control. This is not completely surprising as the less dense barium sulfate created large pools of powder within the melt pressed LLDPE which can be seen in figure 2.3. These pools create significant defects in the LLDPE that would rupture during tensile testing. The bismuth and tungsten are much denser and spread more evenly without pooling creating a more uniform

composite. The evenly dispersed radiopaque filler acted to stiffen the LLDPE which was not unexpected as Young's modulus is generally increased when adding filler to plastics[19,20]. The results demonstrate that the composite tungsten and bismuth films have a similar modulus to the 2045G films making them better candidates for use in a heart valve.

Yield Stress

Only the 50% barium sulfate samples had a significantly different yield stress than the 2045G films. In fact, the variation between all samples was remarkably low indicating all treatments except adding barium sulfate had little measurable effect on yield stress. This is likely due to the pooling of barium sulfate described in the discussion of moduli. Where the barium pooled rather than a distribution of powder in the LLDPE there was a pocket of barium surrounded by thin LLDPE. This thin layer of LLDPE then yielded at a much lower stress compared to all other samples.

Yield Strain

Again the 50% barium sulfate samples stood out as the only material to have a lower yield strain than virgin 2045G again likely due to powder pooling. The melt press control, bismuth trioxide, and tungsten samples had a higher yield strain to virgin 2045G. While this might be expected for the melt press control with a lower Young's modulus it is interesting to see in the bismuth trioxide and tungsten samples. Though the difference is statistically significant the total difference in mean yield strain is only 7-9%. The ultimate goal of this work is to create a thin radiopaque material that can be used in a heart valve, and these minor differences are unlikely to cause mechanical failure beyond what is seen in virgin 2045G LLDPE.

Elongation at Break

The melt press control, bismuth trioxide, and tungsten samples all had significantly greater elongation at break compared to the 2045G samples. This indicates the melt pressing process does have significant effects on the plastic properties of the LLDPE. This is not unexpected in the melt press control as the moduli of the melt press control was lower than that of virgin 2045G.

What is quite interesting is that the tungsten and bismuth samples which did not have significantly different moduli also had much greater elongation at break. This indicates that while some mechanical effects of melt pressing (modulus specifically) in the elastic region of the material is counteracted by adding tungsten and bismuth. some effects are seen in the plastic region of the material.

Ultimate Tensile Strength

The barium sulfate stands out as the only sample set to have a significant and reduced ultimate tensile strength compared to the untreated 2045G control indicating that the processes do not shift this particular tensile property away from native material.

Toughness

Finally, as would be expected from materials with greater elongation the melt press control, bismuth trioxide, and tungsten samples were all tougher than the 2045G. The tungsten sample was not significantly different, but this is by the barest of statistical margins as we see the tungsten films had very similar results to that of bismuth films.

Summary

Melt pressing 2045G films did have some significant effects on the tensile properties of the LLDPE as would be expected. Interestingly the addition of tungsten and bismuth trioxide at 70% and 40% respectively reversed the effects on the modulus, but not other tensile properties except for toughness on the 70% tungsten samples. This is likely because melt pressing the films affected the percent crystallinity and crystalline orientation imparted from the film blowing process. While these effects were not seen in the barium samples this is likely due to the difficulty in evenly distributing the radiopaque powder. This uneven distribution created pools of barium sulfate encapsulated in a thin layer of LLDPE resulting in decreased tensile properties. This decrease in mechanical properties in the elastic region of the material removed it from consideration as the polymer leaflets should mostly operate in the elastic region.

While the barium sulfate samples were removed from consideration, mechanical affects are still present in the melt press control, tungsten, and bismuth samples. To further understand what is causing these changes it would be prudent to run differential scanning calorimetry on LLDPE that has been melt pressed to determine if there are changes in the percent crystallinity that might be causing these changes in tensile mechanical properties.

Regardless, the most significant effects were seen in the plastic region of the material. These materials should not undergo major plastic deformation when used as heart valve leaflets. Plastic deformation would alter the shape of the leaflet which is vital to the efficacy of the valve. Of course, despite operating in the elastic region of the material, polyethylene will undergo some minor deformation over hundreds of millions of heartbeats. Rendering the material radiopaque can demonstrate how the leaflet movement and shape changes over hundreds of millions of cycles. These changes in shape and movement imaged in-vivo with computed tomography or fluoroscopy could allow for information driven redesign of the valve leaflets. In brief a material that can be evaluated over time and in-situ will allow each successive generation of valve leaflets to address issues that arrive with the previous generation of valve leaflets.

2.6 Hemodynamics

Vital to any potential TAVR leaflet material is an understanding of how the material functions under simulated heart conditions. To evaluate the hemodynamic performance the valves are mounted on a stent, placed in a left heart simulator (tuned to simulate flow from the left ventricle through the valve and into the aorta), and the flows and pressures across the valve are measured. The pressure gradient (ΔP) across the valve during forward flow is measured and averaged. This pressure gradient is used to calculate the effective orifice area (EOA) using the Gorlin Relation[21,22], seen below.

$$EOA = \frac{Q_{RMS}}{51.6\sqrt{\Delta P}}$$

Q_{RMS} (cm^3/s) is the root mean square of the flow rate through the aortic valve and ΔP (mmHg) is the pressure gradient across the valve curing that time. 51.6 is an empirical constant. Lower pressure drops indicate less energy from the heartbeat is expended opening and closing the valve leaflets and results in a greater effective orifice area.

The regurgitant fraction is another key parameter in understanding valve leaflet function and represents the amount of leakage through the valve during each heartbeat. It can be calculated as follows,

$$RF = \frac{CV + LV}{FV}$$

RF is the regurgitant fraction. CV is the closing volume. LV is the leakage volume. FV is the forward flow volume. A lower the regurgitant fraction indicates a higher performing valve as the lower this fraction is the better the valve is at preventing backflow through the orifice.

A study, *In vitro hemodynamic assessment of a novel polymeric transcatheter aortic valve*[22], published in 2019 compared the performance of an HA treated LLDPE valve to the Evolut and Sapien 3 commercially produced animal tissue valves. The study was carried out with a cardiac output of 5 L/min, a physiological pressure of 120/80 mmHg, and a heart rate of 60 beats/min. The results can be seen in table 2.2 below.

Table 2.2: Cardiac parameters for each heart valve leaflet

Sample	RF (%)	EOA (cm2)
HA-LLDPE	11.23 ± 0.55	2.08 ± 0.04
Evolut	15.74 ± 0.73	1.80 ± 0.04
Sapien 3	10.92 ± 0.11	2.10 ± 0.03

2.6.1 Methods

Leaflets were thermoformed from the melt press control, 70% tungsten, and 40% bismuth samples and mounted onto 26 mm diameter cobalt chromium stents. The valves were then mounted inside a rigid acrylic chamber and tested using a custom pulse duplicator left heart simulator in the Dasi laboratory at Georgia Tech under physiological flow conditions. The conditions are as follows systolic/diastolic pressure (120/80 mmHg), heart rate (70-72 bpm), and cardiac output (2.5 - 4 L/min). The cardiac output (total and forward flow only) and heart rate are reported for each test, but due to operator variation and other limitations these parameters were unable to be held consistent. Exact parameters for each valve can be seen in table 2.3 below A fluid of 60/40 water to glycerin was used to mimic the density (1.06 g/ml) and kinematic viscosity ($3.5 \cdot 10^{-6}$ m^2/s) of blood. Data of the flow rate, aortic pressure, and ventricular pressure were recorded at 100 Hz and used to calculate ΔP, EOA, and regurgitation fraction. Data was collected over 80 cycles. Only one valve of each type was measured.

Table 2.3: Cardiac parameters for each heart valve leaflet

Sample	Heart Rate (Beats/min)	Total Cardiac Output (L/min)	Forward Cardiac Output (L/min)
Melt Press Control	70.1	2.46	3.27
70% Tungsten	72.1	2.58	4.50
40% Bismuth	72.1	2.25	4.62

2.6.2 Results

The RF, ΔP, and EOA are reported in Table 2.4 below. The melt press control had the lowest RF, but also the highest ΔP, and lowest EOA. This indicates that the leaflets were able to close properly, but were relatively stiff. The tungsten and bismuth samples both had high regurgitant

fractions indicating the leaflets did not optimally close, but the low pressure gradient and higher effective orifice areas indicate the leaflets are more pliable.

Table 2.4: RF, ΔP, and EOA for each sample with standard deviations for 80 cycles

Sample	RF (%)	ΔP (mmHg)	EOA (cm^2)
Melt Press Control	20.1 ± 1.1	31.3 ± 2.1	0.73 ± 0.02
70% Tungsten	30.3 ± 2.9	20.9 ± 0.9	1.17 ± 0.05
40% Bismuth	34.4 ± 2.1	18.3 ± 1.3	1.32 ± 0.04

The flow rates, aortic pressures, and left ventricular pressures of the melt press control, 70% tungsten, and 40% bismuth are reported below in figures 2.15, 2.16, and 2.17, respectively.

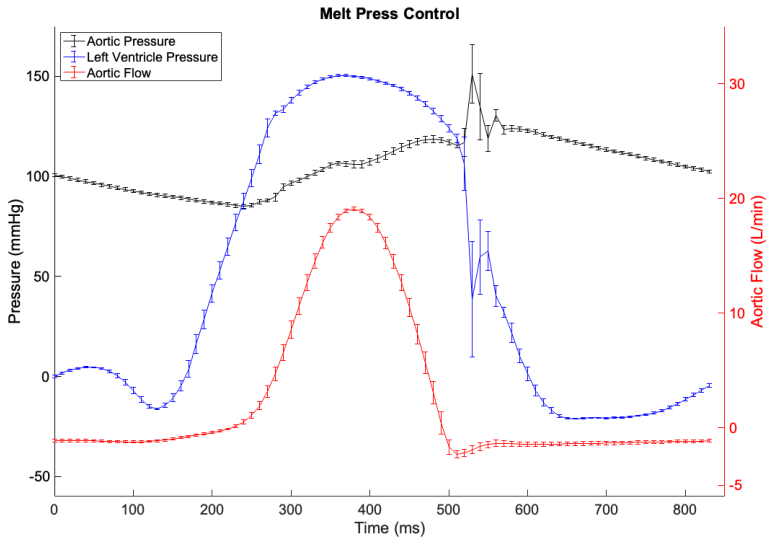

Figure 2.15: Aortic pressure (black), left ventricular pressure (blue), and flow rate (red) for the melt press control leaflets. The pressure axis in mmHg for aortic pressure and left ventricular pressure is on the left while the flow axis is on the right. Error bars represent standard deviation over the 80 cardiac cycles.

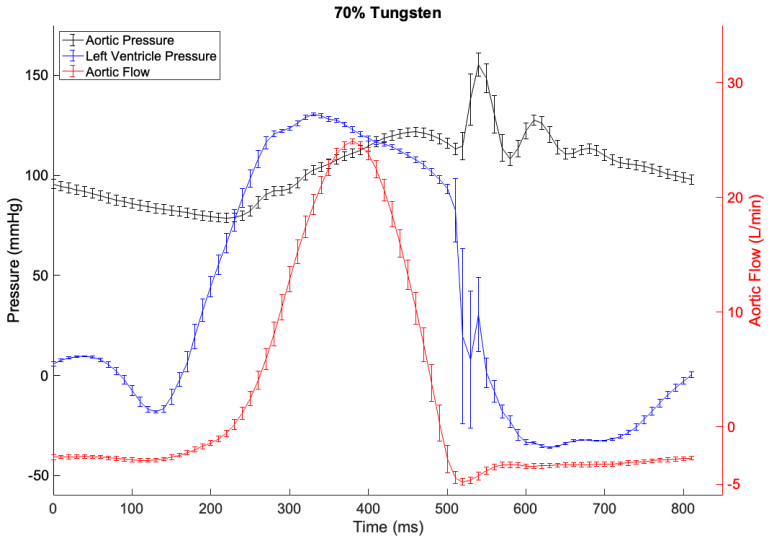

Figure 2.16: Aortic pressure (black), left ventricular pressure (blue), and flow rate (red) for the 70% tungsten leaflets. The pressure axis in mmHg for aortic pressure and left ventricular pressure is on the left while the flow axis is on the right. Error bars represent standard deviation over the 80 cardiac cycles.

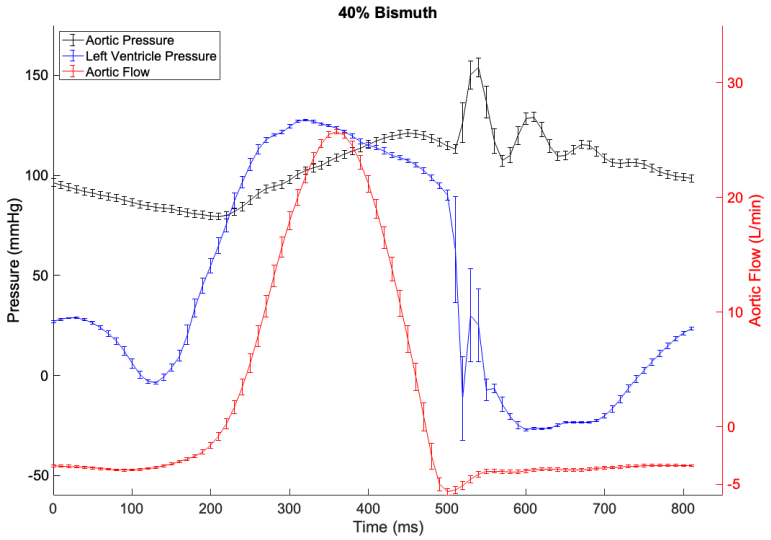

Figure 2.17: Aortic pressure (black), left ventricular pressure (blue), and flow rate (red) for the 40% bismuth leaflets. The pressure axis in mmHg for aortic pressure and left ventricular pressure is on the left while the flow axis is on the right. Error bars represent standard deviation over the 80 cardiac cycles.

2.6.3 Discussion

While the results indicate a sub optimal hemodynamic performance when compared to previous studies, specifically a lower EOA and a higher regurgitation fraction, when compared to commercial valves and the HA-LLDPE TAVR it does demonstrate that neither melt pressing, nor

melt pressing in tungsten or bismuth at 70% and 40% (w/w) respectively prevents the leaflets from functioning as a valve. Considering the very high weight percentages of tungsten and bismuth used, and the previously demonstrated range of loadings that provide x-ray visualization it demonstrates a very promising technique that can be used to introduce radiopacity into HA-LLDPE materials for use as a heart valve leaflet or blood contacting material. Further work is needed to optimize the loading percentages and the method of loading the radiopaque materials. For example, the radiopaque powders were melt pressed between sheets of blown LLDPE, however the previous study of an HA-LLDPE leaflet used blown LLDPE that had not been melt pressed. As noted in the tensile testing section, the thickness of the LLDPE varied after melt pressing, and to further note the films were thermoformed post melt pressing. Each of these post processing steps adds variation to the thickness and consistency of the material. If the radiopaque powders were introduced into the melt state LLDPE prior to blowing the LLDPE film the radiopaque material would be more evenly distributed and the thickness of the film would be more consistent. Introducing the powder in the melt state prior to blowing the film is not the only solution, the powder could be blended into the melt then injection molded or the material could be formed into sheets and press molded into the aortic leaflet shapes. Regardless of the method because polyethylene is a versatile and thermoplastic and the powder can be loaded into the material a variety of ways there is incredible potential to create a commercial radiopaque heart valve leaflet.

2.6 Fluoroscopic Insertion of Radiopaque LLDPE

To further demonstrate the radiopacity of the 70% tungsten and 40% bismuth LLDPE films, a C-Arm fluoroscope was used to image the radiopaque valve leaflets.

2.6.1 Methods

A GE OEC9800 C-arm was used to image LLDPE samples of 40% bismuth and 70% tungsten. Films were made as described in chapter 2.2, “Embedding Radiopaque Materials in LLDPE”, and then were subsequently thermoformed into valve leaflets using a Formech 450DT vacuum former and custom leaflet mold. Fluoroscopy of the 70% tungsten material had the following imaging parameters: 45 kVp, 0.39 mA, and 0.01 mGy. Fluoroscopy of the 40% bismuth material had the following imaging parameters: 48 - 49 kVp, 0.89 - 0.96 mA, and 0.12 - 0.15 mGy.

2.6.2 Results

Figure 2.18 shows the fluoroscopic images of the 70% tungsten leaflets.

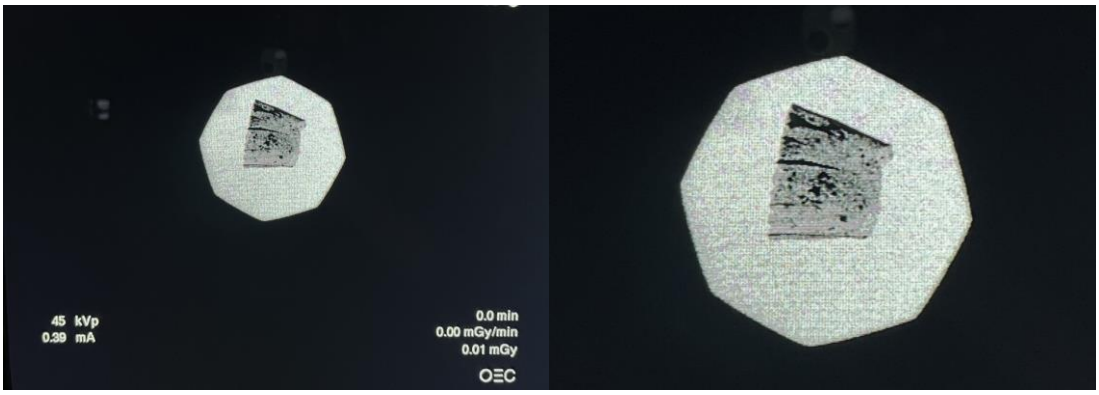

Figure 2.18: Fluoroscopy of 70% tungsten LLDPE heart valve leaflets

Figure 2.19 shows the fluoroscopic images of the 40% bismuth leaflets.

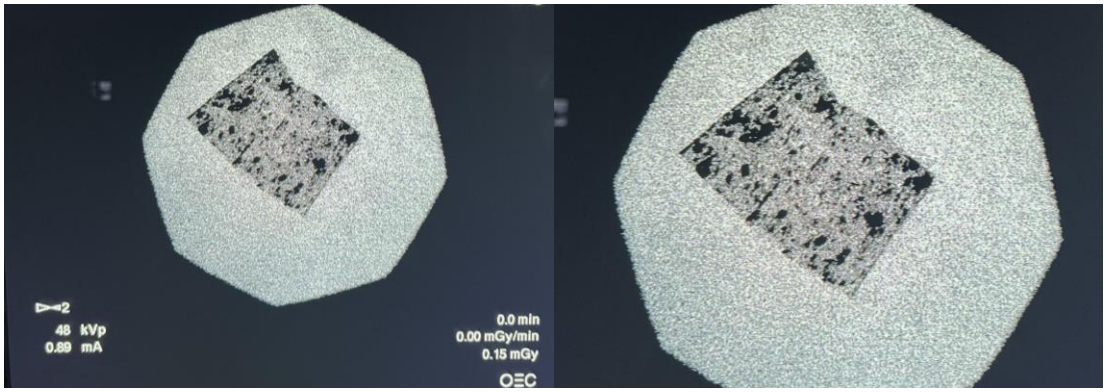

Figure 2.18: Fluoroscopy of 40% bismuth LLDPE heart valve leaflets

2.6.3 Discussion

Both the 40% bismuth and 70% tungsten demonstrate clear contrast when imaged using a c-arm fluoroscope. While further imaging, video of a radiopaque valve deployment, and video of the radiopaque valve in operation needs to be completed these initial images show that the radiopaque materials show up clearly when imaged with a fluoroscope. Video would demonstrate that valve movement of these radiopaque materials can be achieved. Once this has been shown the radiopaque leaflets should be deployed in an in-vivo model and imaged to demonstrate that the leaflet movement can be imaged through animal tissue.

2.7 Chapter Conclusions

The introduction of bismuth trioxide and tungsten both rendered HA enhanced LLDPE radiopaque using both traditional x-ray and c-arm fluoroscopy while only having minor effects on the material's hydrophilicity and tensile properties. While melt pressing alone and melt pressing in bismuth trioxide and tungsten did result in less-than-optimal hemodynamics they did not prevent the material from functioning as a valve leaflet. Barium sulphate did have such significant effects that it was removed from further studies performed in this dissertation. Specifically, the introduction of barium sulphate reduced all tensile properties to the point that there would be no reasonable expectation for the material to perform similarly to non-radiopacified LLDPE. As noted previously that these radiopacifiers have been introduced into the LLDPE simply by melt pressing the powder between sheets producing a radiopaque film with less consistency than other commercially available methods would produce. Commercially these radiopacifiers would be blended into the melt polyethylene and blown or cast into films producing an even distribution of the radiopaque powder throughout the thermoplastic. Unfortunately, this process is generally performed at scale and the cost of ordering such a material was beyond the scope of this academic pursuit. With that, melt pressing tungsten and bismuth trioxide at high weight

percentages between blown films generated a consistent and feasible material that retained the ability to form an IPN with HA and the tensile properties of blown LLDPE providing a promising method to generate the first ever synthetic and radiopacified heart valve leaflet.

2.8 References

1. Zhang, M. Surface Modification of Ultra High Molecular Weight Polyethylene with Hyaluronan for Total Joint Replacement Application. (Colorado State University, 2004).

2. Zhang, M. & James, S. P. Silylation of hyaluronan to improve hydrophobicity and reactivity for improved processing and derivatization. *Polymer* **46**, 3639–3648 (2005).

3. Bui, H. T. Development of hyaluronan enhanced expanded polytetrafluoroethylene and linear low density polyethylene for blood contacting applications, The. (Colorado State University, 2019).

4. Dean, H. *et al.* Development and Characterization of LLDPE-HA Materials for Cardiovascular Applications. *Submitt. Ann. Biomed. Eng.* **October**, (2012).

5. Bui, H. T., Harris, K. L., Li, E., Prawel, D. A. & James, S. P. Vapor Crosslinking of Hyaluronan-Polyethylene Interpenetrating Polymeric Network for Biomedical Applications. (2019).

6. Gill, H., Meier, D., Lai, A., Payne, G. W. & Sellers, S. L. Mechanisms of Transcatheter Valve Degeneration. *Card. Interv. Today* **17**, (2023).

7. Berger, M., Yang, Q. & Maier, A. X-ray Imaging. in *Medical Imaging Systems: An Introductory Guide* (eds. Maier, A., Steidl, S., Christlein, V. & Hornegger, J.) (Springer, 2018).

8. NIST: X-Ray Mass Attenuation Coefficients - Table 3. https://physics.nist.gov/PhysRefData/XrayMassCoef/tab3.html.

9. McKetty, M. H. The AAPM/RSNA physics tutorial for residents. X-ray attenuation. *RadioGraphics* **18**, 151–163 (1998).

10. Zaribaf, F. P., Gill, H. S. & Pegg, E. C. Characterisation of the physical, chemical and mechanical properties of a radiopaque polyethylene. *J. Biomater. Appl.* **35**, 215–223 (2020).

11. Abboud, M., Vol, S., Duguet, E. & Fontanille, M. PMMA-based composite materials with reactive ceramic fillers Part III: Radiopacifying particle-reinforced bone cements. *J. Mater. Sci. Mater. Med.* **11**, 295–300 (2000).

12. Húngaro Duarte, M. A. *et al.* Radiopacity of Portland Cement Associated With Different Radiopacifying Agents. *J. Endod.* **35**, 737–740 (2009).

13. Nisha, V. S. & Joseph, R. Preparation and properties of iodine-doped radiopaque natural rubber. *J. Appl. Polym. Sci.* **105**, 429–434 (2007).

14. Morabito, K. Radiopaque Medical Devices Improve Patient Safety. *J. Clin. Eng.* **38**, 175–177 (2013).

15. Radiopaque Polymer Formulations for Medical Devices. *mddionline.com* https://www.mddionline.com/materials/radiopaque-polymer-formulations-medical-devices (2000).

16. Mirji, S. P. Comparison of nano and micron sized radioapaque fillers in medical plastics. (University of Massachusetts Lowell).

17. Baleani, M., Cristofolini, L., Minari, C. & Toni, A. Fatigue strength of PMMA bone cement mixed with gentamicin and barium sulphate vs pure PMMA. *Proc. Inst. Mech. Eng. [H]* **217**, 9–12 (2003).

18. Ma, Z., Mao, Z. & Gao, C. Surface modification and property analysis of biomedical polymers used for tissue engineering. *Colloids Surf. B Biointerfaces* **60**, 137–157 (2007).

19. Jang, J. & Han, S. Mechanical properties of glass-fibre mat/PMMA functionally gradient composite. *Compos. Part Appl. Sci. Manuf.* **30**, 1045–1053 (1999).

20. Nurazreena, Hussain, L. B., Ismail, H. & Mariatti, M. Metal Filled High Density Polyethylene Composites – Electrical and Tensile Properties. *J. Thermoplast. Compos. Mater.* **19**, 413–425 (2006).

21. Bark, D. L. *et al.* Hemodynamic Performance and Thrombogenic Properties of a Superhydrophobic Bileaflet Mechanical Heart Valve. *Ann. Biomed. Eng.* **45**, 452–463 (2017).

22. Heitkemper, M., Hatoum, H. & Dasi, L. P. In vitro hemodynamic assessment of a novel polymeric transcatheter aortic valve. *J. Mech. Behav. Biomed. Mater.* **98**, 163–171 (2019).

CHAPTER 3: CYTOCOMPATIBILITY AND HEMOCOMPATIBILITY OF RADIOPACIFIED HA ENHANCED LLDPE

3.1 Chapter Introduction

The radiopaque materials introduced to the HA enhanced LLDPE were chosen because of their previous use in biomedical implants. However, as these materials have never been previously used for radiopacification of HA enhanced LLDPE, the final materials needed to be evaluated for cytocompatibility and blood compatibility. To evaluate cytocompatibility human dermal fibroblast cells were used to ensure the radiopaque material or that the process of impregnating LLDPE with radiopaque material was not cytotoxic to mammalian cells. Similarly, the material and process needed to be evaluated for causing thrombosis (i.e., blood clotting) and platelet activation.

These studies were undertaken to evaluate that the materials and the processes used to generate them did not create a cytotoxic effect or cause the material to lose previously evaluated hemocompatibility. This chapter reviews the results of these experiments into HA enhanced LLDPE radiopacified with bismuth trioxide and tungsten. Barium sulfate materials were not evaluated as it was demonstrated in chapter 2 that embedding barium sulphate significantly decreased the mechanical properties of HA enhanced LLDPE rendering a material that is unsuitable for heart valve leaflets.

3.2 Statistics

To ensure repeatability all studies were repeated twice on separate sets of samples, and both the static blood clotting assay and the platelet assays were repeated with two blood donors to ensure that any effects were not caused by a patient specific blood interaction. Data sets were evaluated for equal variance using Levene's test and evaluated for normality using the Anderson-Darling

test. Once these parameters were established significance was determined using ANOVA with post hoc Tukey's test (p value < 0.05). For data sets that did not have equal variance the Games-Howell test was performed (p value < 0.05). A post hoc power analysis was performed on all data sets to verify sample size with a minimum effect size of 0.8.

As the platelet assay results were not normally distributed a non-parametric test, Mood's median test (p value < 0.05), was used. Mood's median test determines the median of the compared samples and ranks the number of results above and below the median for each sample group. A chi square test is performed to determine the difference between samples.

All statistics were performed using Minitab 21 or MATLAB 2023a.

3.3 Cytocompatibility of Radiopacified HA/LLDPE

Cytocompatibility has many definitions, for the purpose of this work it will be defined as a material that is not cytotoxic to human dermal fibroblast cells. Cytocompatibility is the primary requirement of any biomaterial, as a cytotoxic material will harm any patient into whom it is implanted. LDH (Lactate dehydrogenase) assays are widely used as a method to determine if a material is cytotoxic[1–3]. LDH is a soluble enzyme found in the cytoplasm of all aerobic organisms, and is a critical part of energy production in the Kreb's cycle[4]. Due to is ubiquitous nature and presence in the cytoplasm, cells that are damaged or that undergo apoptosis release LDH into the media in which they reside, which can be used to measure the total amount of cell death[5]. There are a variety of ways to measure the presence of LDH and for this experiment a colorimetric assay was used. The assay functions as follows[6]:

1. Lactate, NAD+, diaphorase, and tetrazolium salt are added to the cell media.
2. In the presence of lactate and NAD+, the free LDH converts the lactate to pyruvate and the NAD+ to NADH.
3. Diaphorase then reacts with NADH and tetrazolium salt to form red formazan.

The red formazan concentration is representative of the amount of free LDH released by damaged and dead cells and can be measured using a plate reader. Higher concentrations of red formazan result in higher absorbance readings at 490 nm corresponding to higher cell death. As the red formazan has almost no absorbance past 650 nm[7], a reference wavelength of 680 nm is used to correct for absorbance not caused by the assay. To determine the minimum amount of cell death (positive control) cells are grown with no samples in the same type of well plate in which the cells are grown on the samples. To determine the maximum amount of cell death (negative control) a second set of cells are gown in the same type of well plate, but these are lysed prior to the assay to release all LDH present in the cells into the media. To determine the cytotoxicity percentage relative to 100% cytotoxic negative controls, the absorbance values are normalized to the negative and positive controls using the following equation.

$$\frac{Absorbance_{Sample} - Absorbance_{Postive\ Control}}{Absorbance_{Negative\ Control} - Absorbance_{Postive\ Control}} * 100 = Percent\ Cytotoxcicity$$

3.3.1 Methods

Radiopacified HA enhanced LLDPE samples were prepared as described in appendix A4, briefly either bismuth trioxide (40% w/w) or tungsten (70% w/w) was melt pressed between LLDPE sheets. The samples swollen in a 1% (w/v) solution of SHACTA in dry xylenes for two hours, elevated at a rate of 2 cm/hour out of the solution and crosslinked above a 10% (v/v) solution of TDI in xylenes. The samples were hydrolyzed to revert the SHATCA back to HA.

Eight mm diameter samples were punched from the radiopaque HA enhanced LLDPE films to demonstrate a scenario where a catastrophic failure has occurred and the embedded radiopaque powders are exposed directly to the cells cultured on the sample.

Samples were assessed for cytotoxicity using an LDH assay and the manufacturers protocol was followed (Themofisher Scientific, Cyquant™). Samples were sterilized with 70% alcohol for 24 hours prior to seeding, rinsed 2x with sterile deionized water, and allowed to hydrate

in phosphate buffered saline (PBS) for at least 1 hour prior to seeding. PBS was aspirated off immediately prior to cell seeding. 10,000 human dermal fibroblasts (PromoCell®, passage 5) were seeded and grown for 24 and 72 hours on the surface of each sample. 89% α-modified eagle media (α-MEM), 10% fetal bovine serum, and 1% penicillin/streptomycin growth media was used to culture the cells. After 24 and 72 hours of incubation with the cells an LDH cytotoxicity assay was performed per the manufacturer's instructions. 50µL LDH reagent was added to 50µL of incubated cell solution and allowed to react for 30 minutes protected from light. After 30 minutes, 50µL stop solution was added to each well and the absorbance was measured at 490 and 680 nm using a plate reader (BMG Labtech FLUOstarOmega). The absorbance of the 680 nm (background) was subtracted from the absorbance at 490 nm to evaluate cytotoxicity. A negative control was used to determine the maximum LDH release, in which the cells were lysed with 15µL Triton-X100 solution. A positive control was used to determine the minimum LDH released from apoptosis due to the culturing conditions on tissue culture polystyrene with no sample. The experiment was replicated twice, on two separate sets of samples.

3.3.2 Results

The results of the day 1 LDH are shown in figure 3.1. The untreated LLDPE, 70% tungsten, 40% bismuth trioxide, and melt press control samples all were significantly less cytotoxic compared to the negative and positive controls. Day 3 LDH assay results can be seen in figure 3.2 where all samples were not significantly different than the positive control but were significantly less cytotoxic compared to the negative control.

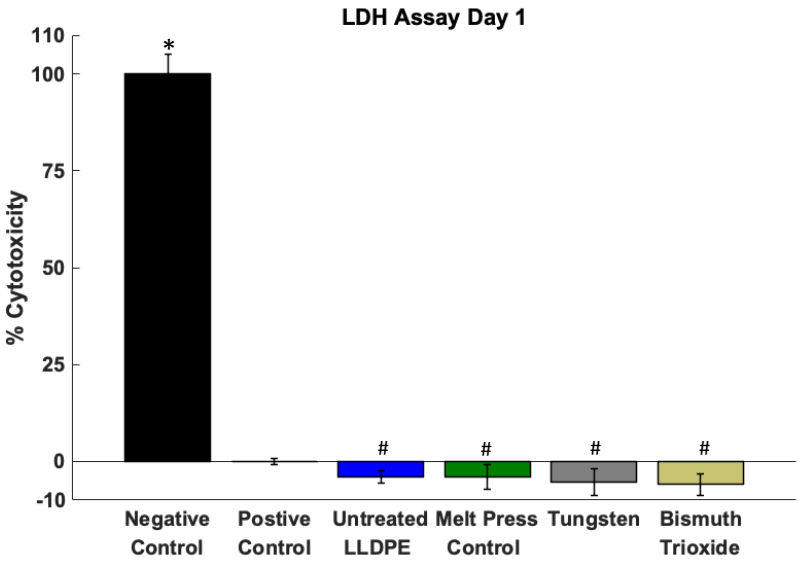

Figure 3.1: Day 1 LDH assay results. All samples were significantly different than the positive control with the negative control being significantly higher and all other samples being significantly lower. (p=0.05)

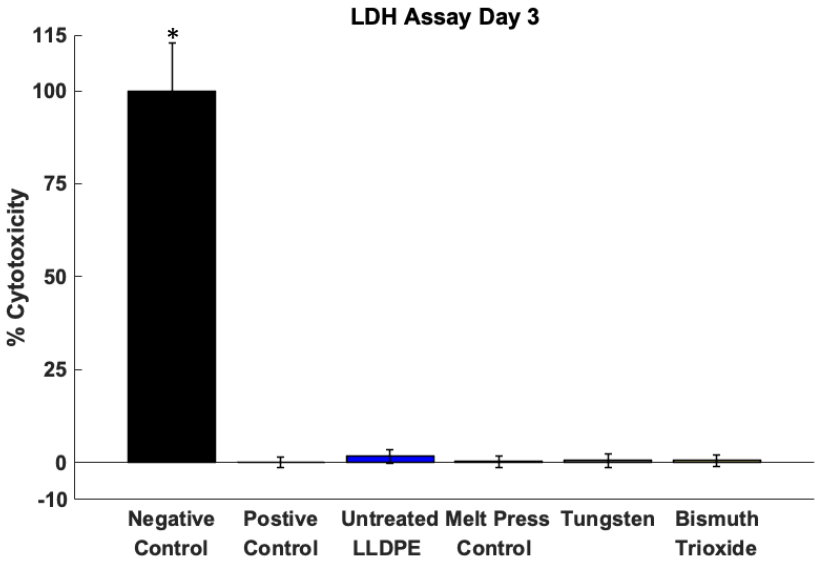

Figure 3.2: Day 3 LDH assay results. Only the negative control was significantly higher than the positive control. All other samples were not significantly different. (p=0.05)

3.3.3 Discussion

The results clearly demonstrate that human dermal fibroblasts grown on LLDPE samples release less LDH than lysed cells and do not release more LDH than human dermal fibroblasts grown in standard conditions on tissue culture polystyrene. This was true for all untreated LLDPE and HA treated LLDPE samples impregnated with bismuth, tungsten, and nothing (melt press control). As LDH release is indicative of cell death and cell membrane damage these results confirm that the process of melt pressing, and the addition of radiopaque powders does not have a cytotoxic effect. Furthermore, as the sample were punched from the melt pressed samples these samples represent a catastrophic failure scenario in which the embedded radiopaque powders are exposed, demonstrating that even if the LLDPE leaflets were to tear the material would not cause cell death.

Interestingly on day one the LLDPE whether treated with HA or not is less cytotoxic than standard tissue culture well plates, though the effect is not particularly strong. Regardless the radiopaque samples are not acutely cytotoxic after one or three days, and thus are prime candidates for use in generating a radiopaque polymeric heart valve leaflet.

3.4 Whole Blood Clotting on Radiopacified HA/LLDPE

Any ideal material used as a long-term blood contacting implantable device should not cause thrombosis, and as thrombosis can be triggered in a myriad of ways when coming into contact with a medical device whole blood interactions should be evaluated. To determine if radiopacified HA/LLDPE causes thrombosis an in-vitro hemolysis assay was performed. The assay is performed by collecting whole blood from a donor and plating the blood onto the surface of the assayed biomaterial, a negative control known to cause clotting (TCPS) [8,9], and into water to representing no clotting (positive control). After a set period of time the blood is eluted with DI water and the absorbance is measured at 540 nm. Greater absorbance indicates that there is

more free hemoglobin in solution. The more free hemoglobin in solution indicates less clotting caused by the material onto which the blood was plated. Less absorbance indicates greater clotting.

3.4.1 Methods

Prior to the study samples were sterilized and hydrated. Samples were placed in 70% ethanol for at least 12 hours, dried, and placed in sterile DI water for 24-36 hours before the experiment. This was to ensure there was not any blood reaction caused by contamination and to ensure the HA was completely hydrated before the experiment.

Immediately before blood collection sterile DI water was aspirated from the samples, and the samples were blotted dry to ensure excess water did not prevent blood clotting or dilute the final hemoglobin concentration. Blood was collected from a donor who had not taken any blood thinning agents or other medication for the past 10 days using uncoated vacuum tubes (BD vacutainer). The first tube containing the skin plug was not used.

5 μl of blood was immediately (within 5 minutes) placed on the surface of each sample and allowed to clot for 15 and 30 minutes. 5 μl of blood was also placed on TCPS (negative control) and 5 μl of blood was placed into 1000 μl of DI water to determine the maximum amount of hemoglobin released (positive control). After 15 and 30 minutes 1000 μl of DI water was added to each sample and the TCPS negative control. The samples were briefly shaken for 30 seconds at 100 RPM, then allowed to sit for 5 minutes so that unclotted hemoglobin is released into the DI water. After the absorbance is measured at 540 nm. Greater absorbance indicates that there is more free hemoglobin in solution. The more free hemoglobin in solution means that there was less clotting caused by the material onto which the blood was plated. The experiment was repeated with 2 separate donors, and 4 samples were used for each time point for each donor.

A detailed protocol can be found in appendix A.6, “Whole Blood Clotting”.

3.4.2 Results

Figure 3.3 shows the samples after 15 minutes of clotting. Figure 3.4 shows the results of blood clotting after 15 minutes on all samples. All samples and the negative control had less absorbance indicating greater clotting compared to the positive control. There were no differences between the negative control and the samples.

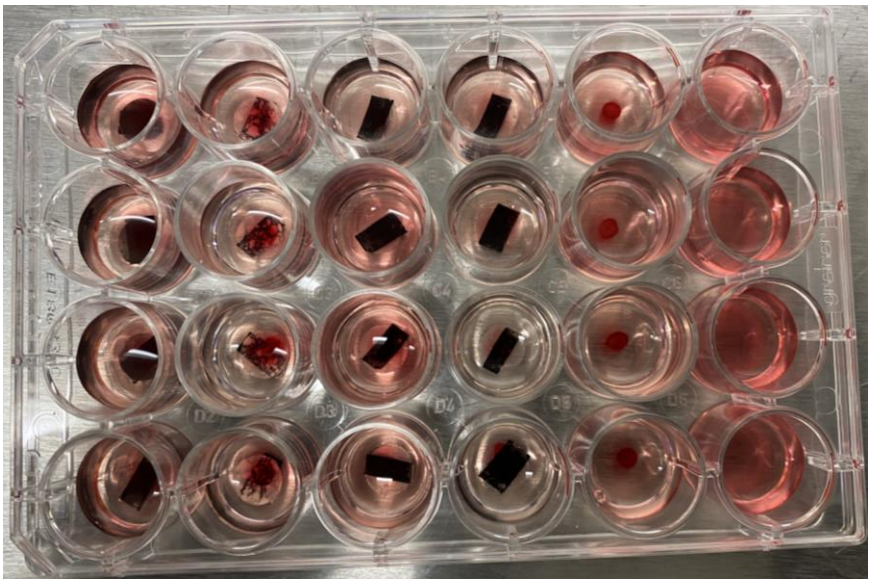

Figure 3.3: Blood clotting on samples after 15 minutes. All samples in a column are the same. From left to right the columns are 70% tungsten (HA) , 40% bismuth (HA), melt press control (HA), untreated LLDPE, TCPS, and the positive control.

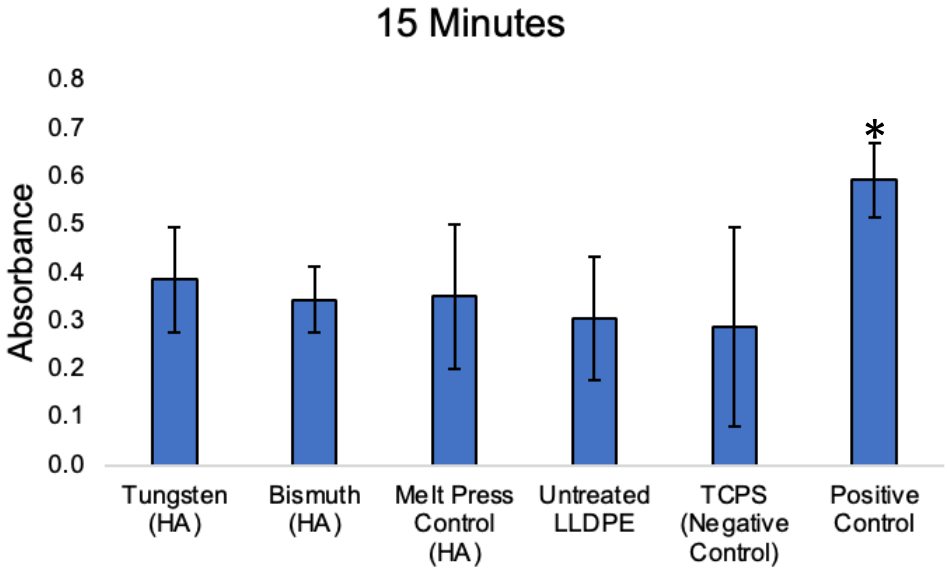

Figure 3.4: Absorbance of blood clotting on radiopacified HA/LLDPE samples after 15 minutes. Asterisk indicates significant difference between TCPS (negative control) (p=0.05)

Figure 3.5 shows the samples after 30 minutes of clotting. Figure 3.6 shows the results of blood clotting after 30 minutes. Again, all samples had less absorbance than the positive control, however at 30 minutes all LLDPE samples had more absorbance indicating less clotting compared to the negative control TCPS.

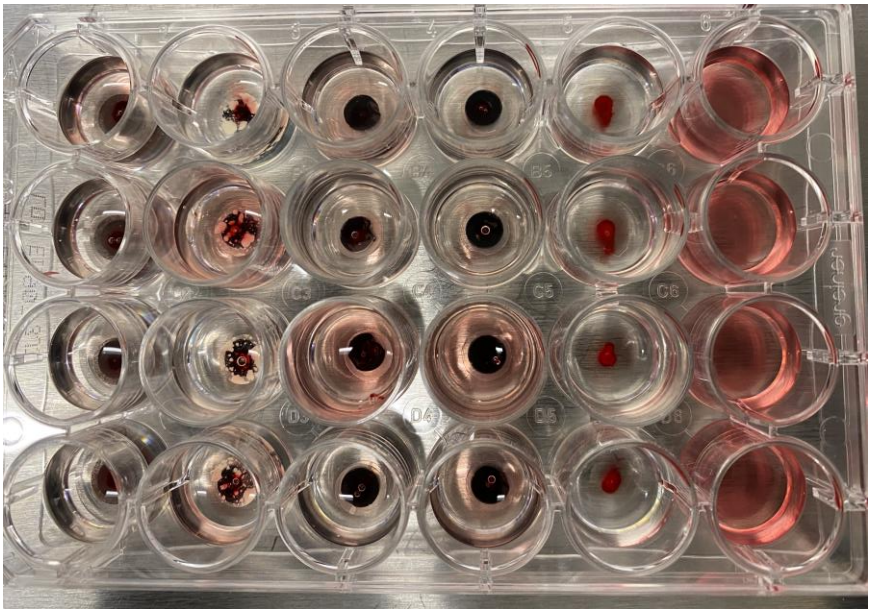

Figure 3.5: Blood clotting on samples after 30 minutes. All samples in a column are the same. From left to right the columns are 70% tungsten (HA) , 40% bismuth (HA), melt press control (HA), untreated LLDPE, TCPS, and the positive control.

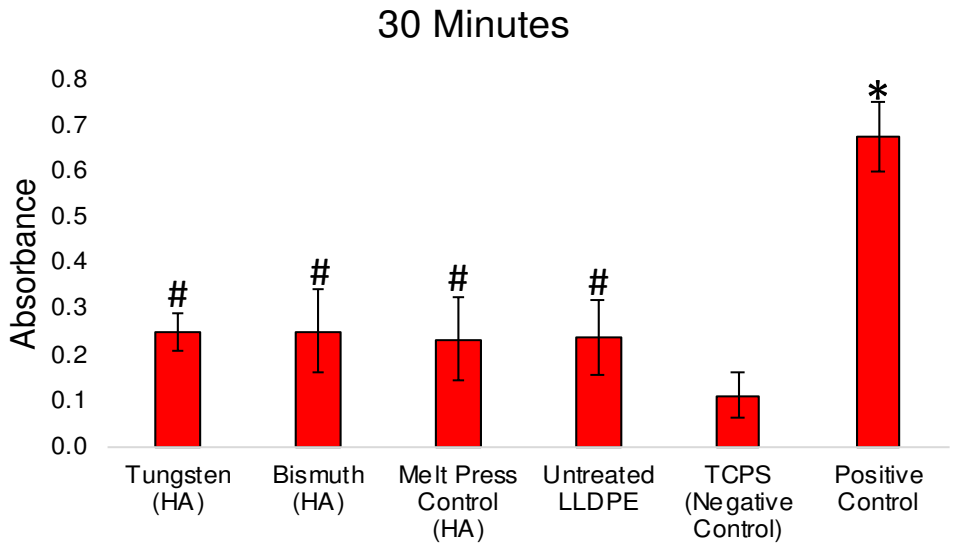

Figure 3.6: Absorbance of blood clotting on radiopacified HA/LLDPE samples after 30 minutes. Hashtag indicates significant difference between TCPS (negative control) (p=0.05), asterisk indicates significant difference between TCPS and all samples (p=0.05).

3.4.3 Discussion

There were not significant differences in the samples compared to the known clotter and negative control, TCPS, in the absorbance readings after 15 minutes. The variation in short term blood clotting can also be seen in the well plate photo, where most samples and the TCPS control appear red from the unclotted hemoglobin released into the DI water. This indicates that over a short period of time the neither the HA treated samples nor the LLDPE control prevented blood clotting when compared to TCPS. However, it should be noted that there were significant amounts of variation in the results as indicated by the error bars, and that at 15 minutes there has been less opportunity for the blood to clot. As there is less time for clotting against the surface, it may be more difficult to identify whether the material has the ability to reduce clotting compared to the negative control TCPS. This can also be seen in the results as there is greater absorbance in the 15 minute samples compared to the 30 minute samples and the 15 minute averages are much closer to the positive control in which there is no clotting. In summary all samples and the negative control were significantly lower than the positive control, but had no difference between each other. This difference between the positive control and all samples is expected as the positive control represents the complete absence of clotting. Even if a sample were able to prevent clotting at the surface, the blood exposed to air will dry and clot to some degree. This clotting will certainly be greater than the positive control where the blood is placed immediately in water and cannot clot. Nevertheless, it appears that over 15 minutes neither the presence of HA, nor the difference in material between LLDPE and TCPS is significantly different from each other.

There were significant differences between the samples and the TCPS negative control after 30 minutes. This can be seen in the absorbance results and the sample image in figure 3.5 and 3.6. Most notably we see in the blood clotting image that there is very little redness in the water solution for the TCPS samples indicating very little hemoglobin release. On all other

samples the solution is slightly red though there is well to well variation. The absorbance results are clear that the LLDPE samples had more absorbance and therefor less clotting than the negative TCPS control. The variation seen visually between samples can also be seen in the data in the error bars. Interestingly, there was no difference between the HA treated samples and the untreated LLDPE. This was not expected as one might think the presence of HA, a molecule present in the glycocalyx with known anticoagulant properties[10,11], might prevent whole blood clotting to a greater degree than LLDPE alone. Regardless, LLDPE does prevent clotting over 30 minutes when compared to TCPS and melt pressing LLDPE with or without the introduction of radiopacifiers does not reduce this effect.

These results indicate that the introduction of radiopacifiers does not create a significant negative effect on blood clotting, however static blood testing is only one way to evaluate a material for an ability to reduce thrombosis. Furthermore, while static blood testing does indicate a materials ability to prevent blood clotting the assay is limited. First in that the blood is exposed to air for this test while the application for the material would not be. Second in that it is a static test while the blood interaction will be dynamic when the material is used a leaflet. While the assay is imperfect it does have value as an in-vitro evaluation that can be paired with other assays to provide indications of how the material will perform in-vivo. One such assay explored in the following section is platelet adhesion and activation on the materials.

3.5 Platelet Activation on Radiopacified HA/LLDPE

Platelets play a key role in thrombogenesis. There primary role upon injury to a blood vessel is to aggregate at the injury forming a physical blockage to prevent further blood loss[12,13]. However, platelet aggregation is the final stage of platelet activation, and the stages of activation are as follows: 1. Round, platelets are not activated and have a round shape without extending pseudopodia, 2. Dendritic, platelets are partially activated having limited and short pseudopodia extending from the cell, 3. Spreading dendritic, platelets are activated having multiple

pseudopodia extending from the cell and flattening against the material surface, 4. Spreading, platelets are fully activated, hyaloplasmic spreading has occurred, and limited pseudopodia may still be present, 5. Fully spreading, platelet granulation begins to occur and hyaloplasmic spreading is complete, 6. Aggregation, platelets have aggregated on the surface of the material promoting thrombus formation[6,14–16]. Each platelet stage can be seen in figure 3.7

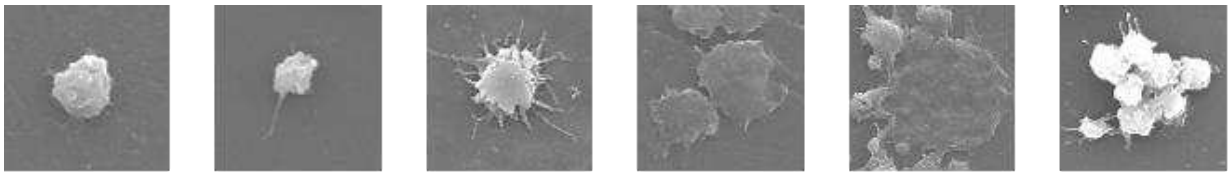

Figure 3.7: Stages of platelet activation. From left to right each image represents a platelet moving further along the activation stages. From left to right the stages are as follows: Round, dendritic, spreading dendritic, spreading, fully spreading, and aggregating.

An ideal long-term implant that is a blood contacting should prevent platelet adhesion and activation to the surface, but in practice the material should greatly reduce adhesion and activation rather than completely prevent it. To examine whether the introduction of radiopacifiers and subsequent formation of an HA IPN with the LLDPE was able to reduce platelet adhesion and activation an assay was performed in which platelet rich plasma was incubated on the surface of the samples. Platelets adhered to the sample were chemically fixed, imaged using a scanning electron microscope, and blindly evaluated for percent coverage on surface as well as for the percent of each stage of activation.

3.5.1 Methods

Prior to the experiment, eight mm samples were punched from all sample groups and sterilized in 70% ethanol for at least 24 hours. TCPS and aluminum punches were sanded and washed prior to sterilization to remove rough edges that can cause platelet activation. Samples then rinsed 2x in sterile deionized water and were adhered to 8 mm aluminum punches using double sided carbon tape in a sterile bio safety cabinet. The double-sided tape had little to no exposure

as it was between the aluminum and sample. Aluminum punches were used to ensure samples did not float in the plasma which would prevent platelet adhesion from occurring on the surface. Aluminum was chosen as recent publications have shown that only small aluminum nanoparticles affect platelet activation while large nanoparticles do not[17]. As such it was expected that the aluminum pucks would not cause platelet activation. The samples were placed in a 24 well plate with one ml of sterile DI water to hydrate overnight prior to platelet exposure.

Blood was collected in EDTA coated tubes (BD vacutainer) and gently rocked to ensure the EDTA was well mixed with the blood. The tubes were spun at 150 g for 15 minutes and allowed to rest for another 15 minutes. The plasma was carefully collected and pooled. Immediately prior to plating the plasma the sterile DI was aspirated from all samples. One ml of plasma was placed on each sample and the samples were shaken at 100 RPM for two hours in an incubator at 37 °C and 5% CO_2.

After two hours the plasma was aspirated from the samples and the samples were gently rinsed 2x with phosphate buffered saline to remove unadhered platelets. The samples were placed in a 0.1 M sodium cacodylate, 0.1 M sucrose, and 3% (v/v) glutaraldehyde and DI water fixative solution for 45 minutes followed by 10 minutes in a 0.1 M sodium cacodylate, 0.1 M sucrose in DI water buffer solution. The platelets were then dehydrated by placing them in 35%, 50%, 70%, 100% ethanol and DI water solutions for 10 minutes each. Samples were allowed to air dry after the final 100% ethanol solution and placed in a desiccator for storage.

Samples were coated with 10 nm of gold and imaged with a scanning electron microscope (JEOL 6500F) with a 10 kV accelerating voltage. Four images were taken of representative areas of each sample, two at 250x magnification and two at 1000x magnification. Images were then deidentified and given to two independent (blinded) evaluators. Evaluators were asked to use the 250x image to determine the approximate percent coverage of platelets to the nearest quartile (0%, 25%, 50%, 75%, and 100%). Evaluators were asked to determine what percent of the

platelets were at each stage of activation (round, dendritic, spreading dendritic, spreading, fully spreading, and aggregation) as described above.

The experiment was performed twice on two separate sets of samples (n = 4 for each set of samples, n = 8 total) with two separate blood donors. Results shown are for all samples with all donors and evaluators.

Detailed protocols of the platelet activation and SEM fixing can be found in appendices A.7, “Platelet Activation” and A.8, “SEM Fixing”.

3.5.2 Results

Figure 3.8 shows representative images of each sample. It should be noted that there was variation in the platelet adherence on each sample that can be seen in the data shown in subsequent figures. However, it can be clearly seen that there are more platelets on the known platelet activator TCPS and untreated LLDPE. There appears to be less activation on the HA treated radiopaque samples and the melt press control. Further images of each sample can be found in appendix B.2 “SEM images of Platelets on Radiopacified Samples”.

Percent coverage can be seen in figure 3.9. There is a large amount of variation in the results, however all HA treated samples had significantly less coverage that the LLDPE and TCPS samples. The high variation is to be expected as the evaluators were limited to using quartile rankings. The LLDPE samples also had significantly less coverage than the TCPS samples. Considering TCPS is known to activate platelets this is result is expected but demonstrates that LLDPE itself is less prone to platelet adherence, and that the treatment with HA significantly reduces adherence. Vitally the radiopaque and melt press control samples show that neither melt pressing nor the introduction of radiopacifiers causes increased adherence on the surface of the HA/LLDPE material.

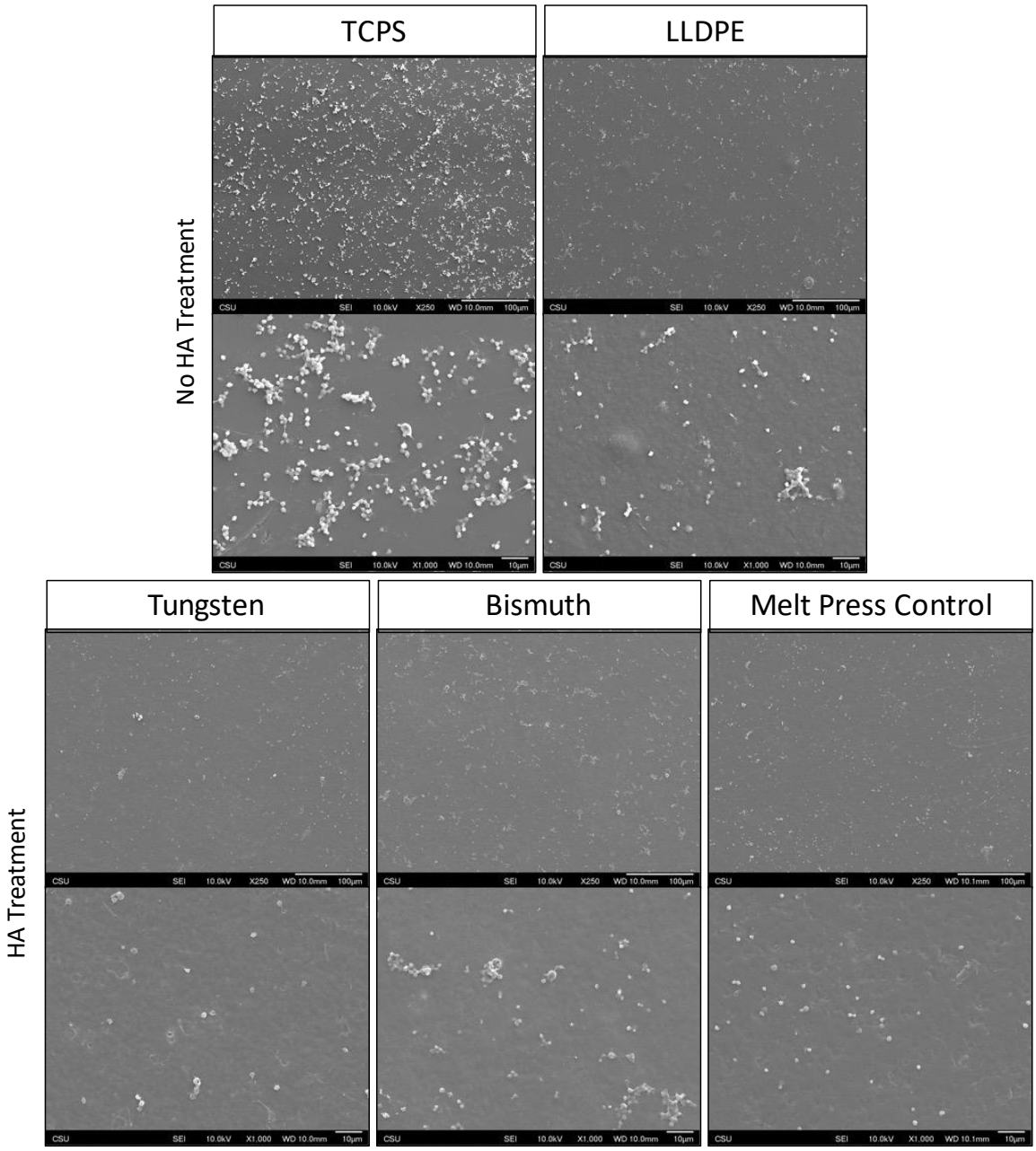

Figure 3.8: Representative SEM images of fixed platelets on each sample. High concentrations of aggregated platelets can be seen on the TCPS images. A variation of stages of activation can be seen on the untreated LLDPE images. HA treated samples with embedded tungsten, bismuth, and the melt press control have the least amount of platelets and appear to have platelets in the round and dendritic stages. Some aggregated platelets can be seen on the bismuth sample shown.

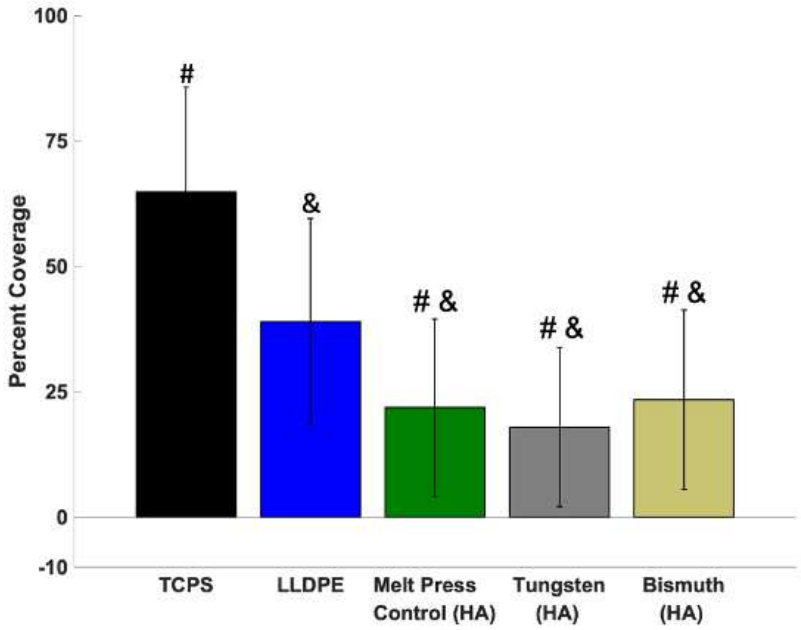

Figure 3.9: Percent coverage of platelets on radiopacified HA/LLDPE samples. # indicates a significant difference compared to LLDPE. & Indicates a significant difference compared to TCPS. All samples had less coverage than TCPS and all HA treated samples had significantly less coverage than TCPS and the untreated LLDPE. ($n = 8$, $p < 0.05$).

Figure 3.10 shows the results of each stage of platelet activation on each sample. Samples treated with HA are labeled as such on each graph, for the purpose of discussion the melt press control, tungsten, and bismuth samples are all HA treated while the LLDPE (also referred to as untreated LLDPE) and TCPS samples are not. All samples had a significantly higher percentage of round platelets, the first and least activated platelet stage, compared to TCPS. Only the melt press control had a significantly higher percentage of round platelets compared to untreated LLDPE. The untreated LLDPE and melt press control samples both had more dendritic platelets than the TCPS while the bismuth and tungsten samples were not different than the LLDPE or TCPS. There were no differences between samples for the spreading dendritic

platelets, however this was the most common platelet classification for most samples. Only the melt press control and TCPS had higher averages for other classifications, which were round and aggregation respectively. Both the bismuth and tungsten had more spreading platelets than the TCPS. There were no differences between samples for the fully spread classification. For aggregation TCPS was significantly higher than all samples including the untreated LLDPE. Of the HA treated samples, only the tungsten samples had significantly less aggregation than the LLDPE samples.

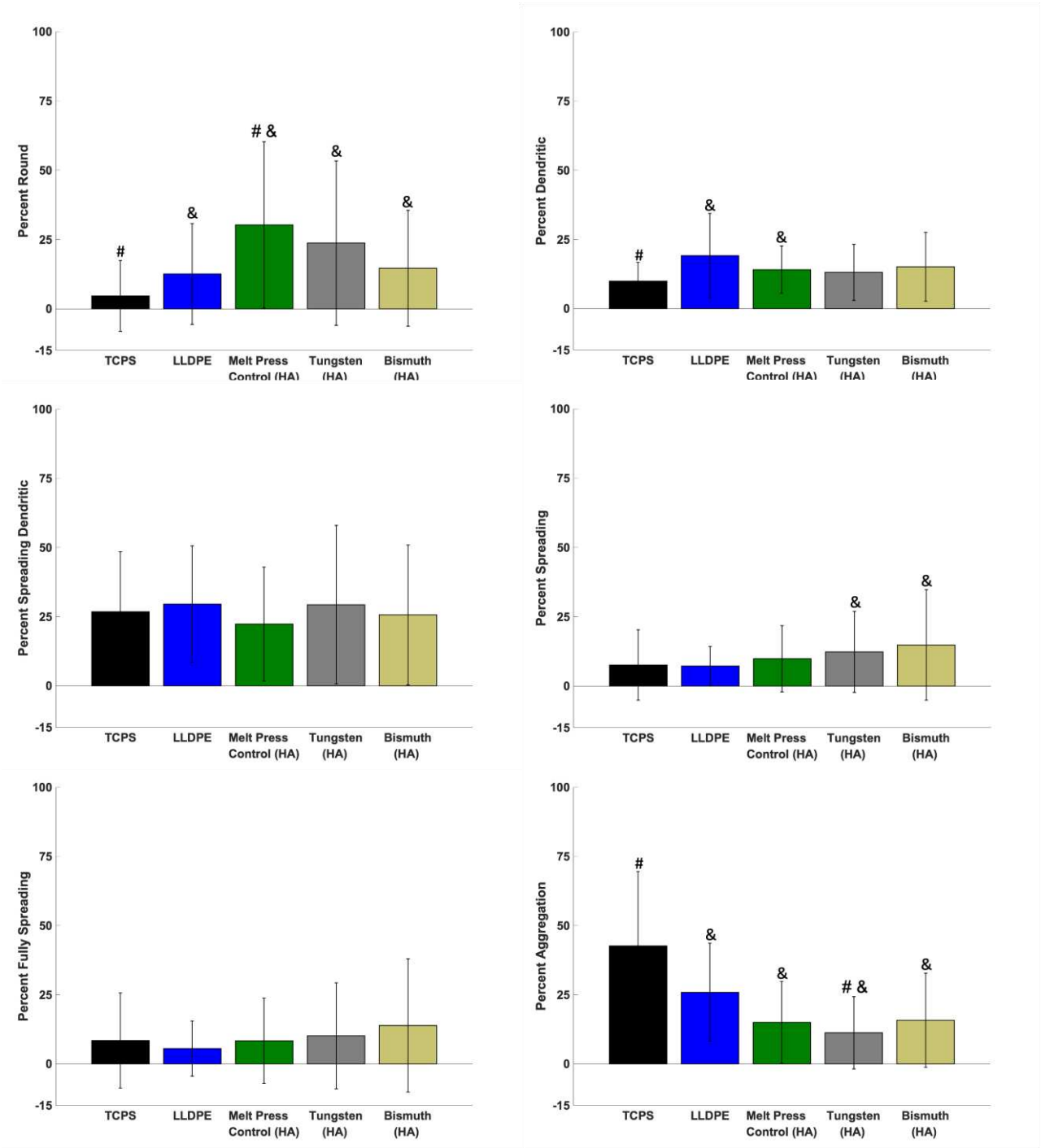

Figure 3.10: Percent of each stage of activation on radiopacified HA/LLDPE samples. "#" indicates a significant difference compared to LLDPE. "&" Indicates a significant difference compared to TCPS.

3.5.3 Discussion

It is clear that LLDPE prevents platelet adherence when compared to the known platelet activator TCPS, and it is clear that HA treatment of melt press samples further reduces adherence as seen in the percent coverage evaluation. With that it should be noted that using observers to estimate percent coverage is a subjective method of evaluation. For transparency the SEM images can be found in appendix C.1 “SEM images of Platelets on Radiopacified Samples”. To ensure the observers did not have greatly different characterizations of platelet data, the data was plotted separately and compared. The data by observer can be found in appendix C.2 “Platelet Data by Observer”. Ideally an objective quantitative method such as cell staining with calcien combined with image analysis would be used to determine the coverage on the surface. This type of evaluation was beyond the scope of this dissertation but should be considered in future work. In the platelet images there are clear indications that all LLDPE samples that were melt pressed had some surface damage. A short exploration into this is presented in appendix C.3 “Notes on Surface Morphology of Melt Pressed LLDPE from SEM images”.

The percent coverage clearly demonstrate that HA treatment reduces platelet adherence. However, it is not clear that HA treatment prevents the activation of platelets once they become adhered. While there was some statistical significance in the intermediate stages between samples there was not a clear trend. The results for the primary and least activated stage and the final and most activated stage does present a clearer picture. Looking at the results for round platelets (least activated or un-activated) only the melt press control sample had significantly more platelets than both the TCPS and untreated LLDPE. However, all LLDPE samples whether untreated with HA (LLDPE) or treated with HA (melt press control, tungsten, and bismuth samples) had significantly more round platelets than the TCPS indicating that all of these materials are less prone to furthering platelet activation. This also indicates that neither melt pressing nor the introduction of tungsten or bismuth causes increased platelet activation. Looking

at the results for aggregated platelets (most activated) again all LLDPE samples whether untreated with HA (LLDPE) or treated with HA (melt press control, tungsten, and bismuth samples) had significantly less aggregated platelets than the TCPS samples. These results indicate again that LLDPE whether HA treated, melt pressed, or melt pressed with radiopacifiers is less prone to activating platelets when compared to TCPS.

There are several further points to be made when reviewing this data. First is the lack of normality resulted in the need to use the non-parametric Mood's median test to evaluate the data which has less power than other statistical methods. As such the significance should viewed as less concrete than other data presented. Second and more importantly is that the percentage of each stage of platelet activation is not weighted. As such though the TCPS samples clearly had a greater number of platelets the percent of each stage of activation may not have differed despite there being a large difference in the number of activated platelets. For example, if a sample had 100 platelets and 40 of them were aggregated, it would have the same amount of aggregation of a sample with 10 platelets and 4 of them aggregated. Thus, the percent coverage indicating greater platelet interaction with the material should be taken into consideration when evaluating the stages of activation. Another way to examine the data that might allow more straightforward evaluation would be to evaluate the platelets as un-activated (round) and activated (all other platelet stages). This may provide a simpler result demonstrating how the samples affect the activation of platelets.

With respect to the significance of the data, several clear conclusions can be drawn. First and foremost is that HA treatment on LLDPE samples that have been melt pressed with or without tungsten and bismuth reduces the number of platelets adhered to a sample compared to untreated LLDPE and TCPS. Second is that untreated LLDPE itself prevents platelet adhesion compared to TCPS. Third is that all LLDPE samples whether treated with HA, melt pressed, or radiopacified have a greater percentage of the least activated round platelets and a lower percentage of the most activated aggregated platelets, indicating that LLDPE prevents platelet

activation. Taking both sets of data into account this indicates that the HA treatment reduces overall platelet adhesion and LLDPE prevents activation regardless of whether the LLDPE has been melt pressed or radiopacified. As such LLDPE leaflets with embedded tungsten or bismuth are viable candidates for use in an artificial heart valve.

3.6 Chapter Conclusions

Neither melt pressing nor the introduction of tungsten or bismuth trioxide into LLDPE that was subsequently treated with HA cause a cytotoxic effect with human dermal fibroblasts, nor did it induce increased blood clotting on the surface of these materials. Interestingly LLDPE itself caused less clotting than TCPS, however the clear increase in platelet adhesion on untreated LLDPE relative to HA treated LLDPE does indicate that the HA treatment creates a more ideal blood contacting material. It should also be noted that while the HA treatment does reduce overall platelet adhesion it did not create a significant effect as to the percent of each stage of platelet activation across all HA treated samples. Regardless, the radiopaque samples did not induce greater cytotoxicity, increase blood clotting, increase platelet adherence, nor did they cause greater platelet activation. These results indicate the bismuth and tungsten HA/LLDPE materials have potential to be used as the first ever radiopaque heart valve leaflets. While the results are promising several further investigations should be considered.

The materials were not demonstrated to be acutely cytotoxic, however a leaching study should be carried out to determine that over a long period of time no cytotoxic molecules or particles can diffuse out of the materials that would be harmful to mammalian cells[18,19]. Short term animal studies in which a dynamic blood interaction occurs with the material should also be considered to determine if the materials are able to reduce thrombosis under flow[20,21]. With that, acute and chronic juvenile sheep studies remain the gold standard for evaluating aortic heart valves[22,23], and should be the primary studies used to evaluate a radiopaque valve that has been

optimized to produce in-vitro hemodynamics comparable to currently available commercial aortic valve replacements.

3.7 References

1. E. Vasey, C. *et al.* Amphiphilic tri- and tetra-block co-polymers combining versatile functionality with facile assembly into cytocompatible nanoparticles. *Biomater. Sci.* **7**, 3832–3845 (2019).

2. Kosowska, K. *et al.* Gradient Chitosan Hydrogels Modified with Graphene Derivatives and Hydroxyapatite: Physiochemical Properties and Initial Cytocompatibility Evaluation. *Int. J. Mol. Sci.* **21**, 4888 (2020).

3. Ding, K. *et al.* A PEGylation method of fabricating bioprosthetic heart valves based on glutaraldehyde and 2-amino-4-pentenoic acid co-crosslinking with improved antithrombogenicity and cytocompatibility. *Acta Biomater.* **144**, 279–291 (2022).

4. Gasmi, A. *et al.* Krebs cycle: activators, inhibitors and their roles in the modulation of carcinogenesis. *Arch. Toxicol.* **95**, 1161–1178 (2021).

5. Parhamifar, L., Andersen, H. & Moghimi, S. M. Lactate Dehydrogenase Assay for Assessment of Polycation Cytotoxicity. in *Nanotechnology for Nucleic Acid Delivery: Methods and Protocols* (eds. Ogris, M. & Oupicky, D.) 13–22 (Humana Press, 2013). doi:10.1007/978-1-62703-140-0_2.

6. Bui, H. T. Development of hyaluronan enhanced expanded polytetrafluoroethylene and linear low density polyethylene for blood contacting applications, The. (Colorado State University, 2019).

7. Denizot, F. & Lang, R. Rapid colorimetric assay for cell growth and survival: Modifications to the tetrazolium dye procedure giving improved sensitivity and reliability. *J. Immunol. Methods* **89**, 271–277 (1986).

8. Grunkemeier, J. M., Tsai, W. B. & Horbett, T. A. Hemocompatibility of treated polystyrene substrates: Contact activation, platelet adhesion, and procoagulant activity of adherent platelets. *J. Biomed. Mater. Res.* **41**, 657–670 (1998).

9. Bui, H. T., Friederich, A. R., Li, E., Prawel, D. A. & James, S. P. Hyaluronan enhancement of expanded polytetrafluoroethylene cardiovascular grafts. *J. Biomater. Appl.* **33**, 52–63 (2018).

10. Mestechkina, N. M. & Shcherbukhin, V. D. Sulfated polysaccharides and their anticoagulant activity: A review. *Appl. Biochem. Microbiol.* **46**, 267–273 (2010).

11. Jiang, Y., Guo, Y., Wang, H., Wang, X. & Li, Q. Hydrogel coating based on dopamine-modified hyaluronic acid and gelatin with spatiotemporal drug release capacity for quick endothelialization and long-term anticoagulation. *Int. J. Biol. Macromol.* **230**, 123113 (2023).

12. Kamath, S., Blann, A. D. & Lip, G. Y. Platelet activation: assessment and quantification. *Eur. Heart J.* **22**, 1561–1571 (2001).

13. Gachet, C. & Cazenave, J. P. ADP induced blood platelet activation: a review. *Nouv. Rev. Fr. Hematol.* **33**, 347–358 (1991).

14. Goodman, S. L. Sheep, pig, and human platelet–material interactions with model cardiovascular biomaterials. *J. Biomed. Mater. Res.* **45**, 240–250 (1999).

15. Goodman, S. L., Cooper, S. L. & Albrecht, R. M. Integrin receptors and platelet adhesion to synthetic surfaces. *J. Biomed. Mater. Res.* **27**, 683–695 (1993).

16. Zang, Y., Popat, K. C. & Reynolds, M. M. Nitric oxide-mediated fibrinogen deposition prevents platelet adhesion and activation. *Biointerphases* **13**, 06E403 (2018).

17. Taterra, D. *et al.* Aluminum Nanoparticles Affect Human Platelet Function In Vitro. *Int. J. Mol. Sci.* **24**, 2547 (2023).

18. Guo, B., Sun, Y., Finne-Wistrand, A., Mustafa, K. & Albertsson, A.-C. Electroactive porous tubular scaffolds with degradability and non-cytotoxicity for neural tissue regeneration. *Acta Biomater.* **8**, 144–153 (2012).

19. BURAL, C., AKTAŞ, E., DENIZ, G., ÜNLÜÇERÇI, Y. & BAYRAKTAR, G. Effect of leaching residual methyl methacrylate concentrations on in vitro cytotoxicity of heat polymerized denture base acrylic resin processed with different polymerization cycles. *J. Appl. Oral Sci.* **19**, 306–312 (2011).

20. Glynn, J. J., Polsin, E. G. & Hinds, M. T. Crosslinking decreases the hemocompatibility of decellularized, porcine small intestinal submucosa. *Acta Biomater.* **14**, 96–103 (2015).

21. Yao, Y., Zaw, A. M., Anderson, D. E. J., Hinds, M. T. & Yim, E. K. F. Fucoidan functionalization on poly(vinyl alcohol) hydrogels for improved endothelialization and hemocompatibility. *Biomaterials* **249**, 120011 (2020).

22. Prawel, D. A. *et al.* Hemocompatibility and Hemodynamics of Novel Hyaluronan–Polyethylene Materials for Flexible Heart Valve Leaflets. *Cardiovasc. Eng. Technol.* **5**, 70–81 (2014).

23. Flameng, W. *et al.* Factors influencing calcification of cardiac bioprostheses in adolescent sheep. *J. Thorac. Cardiovasc. Surg.* **132**, 89–98 (2006).

CHAPTER 4: EVALUATION AND OPTIMIZATION OF HA LLDPE FILM TREATMENT

4.1 Chapter Introduction

The initial goal of creating a biomaterial with HA was to create a lubricious surface on ultra-high molecular weight polyethylene for use in knee replacements[1–4]. The technique used porous preform of ultra-high molecular weight polyethylene that allowed silylated HA to be crosslinked as a microcomposite then returned to its native state. This process generated a self-lubricating surface that was later commercialized into a partial resurfacing knee replacement under the trade name Biopoly®. This HA surface on the polyethylene demonstrated lasting biological compatibility, inspiring further investigations into other uses for HA-polyethylene materials, namely as an artificial heart valve leaflet[5,6].

While using a porous preform was necessary to generating a microcomposite with ultra-high molecular weight polyethylene, this technique was not ideal for LLDPE films. LLDPE films have much lower crystallinity and lower molecular weight[7] and thus would be difficult to mold into a porous preform. Rather than using a porous surface the silylated HA was allowed to diffuse directly into LLDPE swollen in xylenes and then crosslinked in a xylene/ poly(hexamethylene diisocyanate) solution. The resulting interpenetrating polymer network (IPN) between HA and LLDPE was robust. However, the crosslinking step required the reswelling of the silyl HA-LLDPE in xylenes allowing the un-crosslinked silyl-HA to diffuse out of the material and away from the surface. This reswelling process created materials which had inconsistent HA deposition across the LLDPE surface.

To create a more consistent and confluent layer of HA a vapor crosslinking method was evaluated. HA-LLDPE films were placed above a solution of toluene diisocyanate dissolved in xylenes. The xylene vapor caused the HA-LLDPE films to swell without the loss of unbound HA

while the toluene diisocyanate crosslinked the HA in place[8,9]. The resulting materials had greater confluency of HA at the surface, and consistently lower contact angles.

Interestingly a second wrinkle was added to the treatment process in which the silyl HA/xylenes solution was drained away slowly from the films prior to crosslinking rather than simply pulling the films from solution. Only two draining rates (1.8 cm/hr and 45 cm/hr) were tested due to the limitations of the process. It was noted however that the lower draining rate generated a greater surface density of HA as measured with quantitative TBO indicating that draining the solution slowly generated a more confluent and denser silyl HA surface prior to crosslinking. This realization demonstrated that the surface density and confluency of HA was potentially controllable.

This discovery gave rise to significant questions. Though it was understood that the HA was diffusing into the LLDPE to create an IPN, is it diffusing through the bulk of the material or is it concentrated near the surface? Why does the draining rate change the amount of HA at the surface? To what degree can the amount of HA at the surface be controlled and does this have an effect on rendering the LLDPE compatible with blood cells so that it can function as a heart valve leaflet? This chapter attempts to explore and answer some of these questions in an attempt to create processes to generate a more consistent HA surface on LLDPE.

While the HA-LLDPE demonstrated great promise for use as an artificial heart valve leaflet[10,11], the techniques used to generate the HA-LLDPE heart valve leaflets had onerous requirements such as solvent distillation, treatment under a dry nitrogen blanket, and draining the silyl-HA/xylene solution under vacuum. Furthermore, while it was understood that the process generated an IPN between the silyl-HA and the LLDPE it was not understood if this IPN was present throughout the bulk of the LLDPE material or whether the diffusion of silyl HA into the LLDPE was limited. This chapter reviews the investigation into optimizing the treatment of LLDPE by reducing the complexity of the treatment process, and the investigation into using different

molecular weight HA as a method to determine the depth of penetration of HA into the bulk of LLDPE films.

4.2 Preliminary Work on the simplification of HA-LLDPE treatment

The first of two simplifications of the treatment process arrived from necessity. Previously the treatment of the films was performed under a dry nitrogen blanket in a glove bag, however the facility in which the treatments were performed lost its dry nitrogen supply. The second simplification, the removal of xylene distillation, arose to decrease safety risks. Solvent distillation is a dangerous process that involves the volatilization of flammable xylenes past their flash point[12] to further dry and store a chemical. This is unnecessary as solvents such as xylenes can easily dried and stored over molecular sieves[13]. Due to the lack of a dry nitrogen supply and the desire to create a safer process a preliminary experiment was performed in which blown LLDPE films (Dowlex 2045G) were treated with HA as described in chapter 2, with one exception. Rather than withdrawing the films from solution at a 2 cm/hr under vacuum (-15 inHg) the solution was drained away. This was because the film elevator described later in this chapter had not yet been designed and built at the time the preliminary experiment was carried out. The films were then evaluated by TBO staining and captive bubble contact angle.

4.2.1 Methods

More detailed methods can be found in chapter 2, section 2.1.1 Hyaluronan Enhancement of LLDPE. Briefly blown LLDPE films were cleaned, swollen in a 1% silyl-HA/xylene (w/v) solution for 2 hours at 50 °C, then the solution was drained away under vacuum. The films were dried for at least 3 hours then crosslinked above a 10% TDI/xylene (v/v) solution for 1 hour at 60°C. The films were then hydrolyzed and dried.

Films were evaluated for static, advancing, and receding contact angles using the captive bubble contact angle goniometry in DI water and were also stained with TBO to visually evaluate

the distribution of HA across the surface. More detailed methods on TBO staining can be found in chapter 2 section 2.3.1, and more detailed methods on captive bubble goniometry can be found in chapter 2, section 2.4.1.

Historical data[8] from the James group of films treated under a nitrogen blanket and with distilled xylenes is used to compare to films treated in atmosphere with non-distilled xylenes referred to as "Simplified".

4.2.2 Results

The historic contact angle data and the simplified contact angle data with images of the TBO stained samples inlaid can be seen in figure 4.1. The static, receding, and advancing contact angles for the historically treated samples are 32 ± 12°, 25 ± 9.1°, and 57 ± 19° respectively (n=3, $p<0.05$). The static, receding, and advancing contact angles for the simplified treatment samples are 27.9 ± 6.4°, 23 ± 3.7°, and 72 ± 15° respectively (n =3, $p < 0.05$). There were no significant differences between the simplified and historic data.

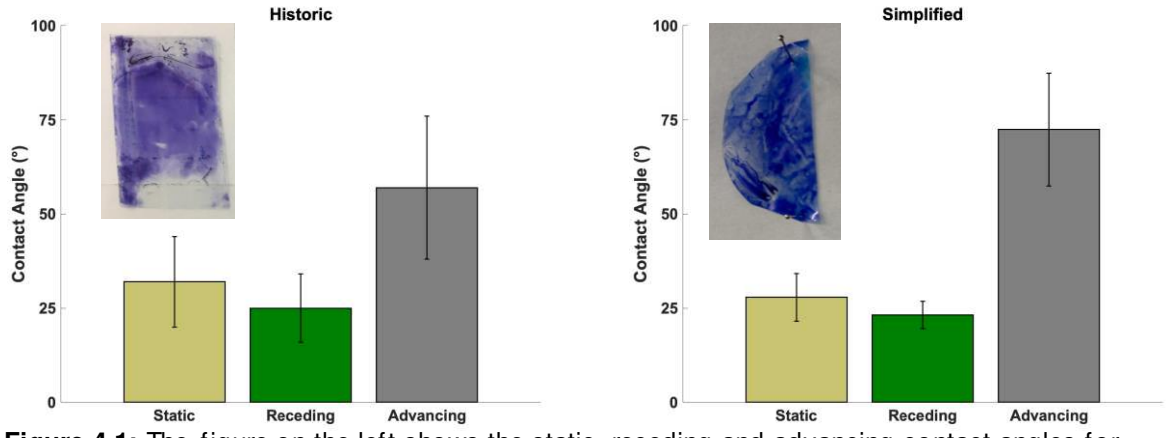

Figure 4.1: The figure on the left shows the static, receding and advancing contact angles for samples historically treated samples with a TBO stained sample inlaid. The figure on the right shows the static, receding and advancing contact angles for samples treated in the simplified method with a TBO stained sample inlaid. There were no differences between the historic and simplified static, receding, and advancing contact angles respectively (n = 3, $p < 0.05$).

4.2.3 Discussion

Previous research had been taken with extreme care to ensure that each film sample was produced in the most optimal environment possible, but due to unforeseen circumstances and safety evaluations these environmental considerations were relaxed. The results clearly demonstrate there was not a significant reduction in the hydrophilicity of the HA treated samples indicating that treatment under nitrogen and with distilled xylenes is unnecessary to the process. While the TBO results appear different in color this may be due to the lighting conditions and cameras used. Regardless both samples clearly have a consistent TBO stain across the surface indicating a relatively confluent presence of HA. Ideally a quantitative TBO assay would have been performed to compare the concentration of HA at the surface. Unfortunately, this experiment was not performed on the simplified sample at the time. However subsequent quantitative TBO studies were performed on films using the simplified treatment method demonstrating that the rate of HA on the surface can be controlled. Beyond this the relaxation of both treatment under nitrogen and solvent distillation are ideal for the commercialization of this process. Creating a gas tight chamber would introduce significant complexity and cost to a scaled treatment process, and solvent distillation at large scales is energy intensive and costly as well. These preliminary results indicated that the treatment process is more robust than previously thought. They also provide a basis to greatly reduce the price and complexity of creating a scaled an automated HA treatment process to generate HA-LLDPE heart valve leaflets.

4.3 Evaluation of film withdrawal rates and vacuum pressure on the consistency of HA confluence on LLDPE films

After preliminary results indicated that certain aspects of the treatment process could be relaxed without altering the hydrophilicity of the samples, a second investigation was undertaken to determine the optimal rate of withdrawal and whether the “accessible” HA polymer repeat units

on the surface of the samples was affected by the vacuum pressure and temperature during withdrawal. When the HA-LLDPE IPN is formed some of the HA polymer is trapped within the LLDPE. This HA is not "accessible" at the surface. Only HA repeat units accessible at the surface will interact with the surrounding environment which will be referred to as "active" HA. To determine whether or not the velocity of withdrawal affects active HA a custom device known as the "film elevator" was built. The film elevator slowly withdraws the LLDPE films from the silyl HA/xylene solution at controlled rates.

4.3.1 Methods

Blown LLDPE films were treated as described in chapter 2, section 2.1.1, with several variations. First after two hours of swelling in a 1% silyl HA/xylene solution, the films were slowly withdrawn under a 15 inHg vacuum at 50 °C at the following rates: 10 cm/hr, 5 cm/hr, and 2 cm/hr. Due to an error one set of films were withdrawn two times once at about 5 cm/hr then repeated at 2 cm/hr at the initial -15 inHg vacuum and 50 °C temperature. The film had the highest concentration of TBO, but as the withdrawal was repeated it was determined that the experiment should be completed at 2 cm/hr with a single withdrawal. This ensured that any changes were due to the rate of withdrawal and not the repeated withdrawal.

After it was determined that 2 cm/hr was the optimal rate of withdrawal, films were withdrawn under atmospheric pressure at 2 cm/hr and at 50 °C, and 65 °C. While these experiments were carried out under atmospheric pressure, the vacuum oven was used to maintain the temperature during film withdrawal. Lastly lower molecular weight (MW) HA (100 kDa) was silylated and used to treat a film with the following withdrawal conditions 2 cm/hr, 50 °C, 15 inHg vacuum. It should be noted that all previous samples had been treated with silyl HA derived from higher MW 700 kDa HA. It should be noted that there is a large range of MW's of HA, both in the human body and produced commercially[14,15]. 100 kDa and 700 kDa MW HA

would be considered by many to be high MW, for the purposes of this dissertation they will be referred to as low and high MW HA respectively.

Contact angle was measured as described in chapter 2, section 2.4.1, and TBO staining was performed as described in chapter 2 section 2.3.1.

To determine the concentration of TBO on the surface of the samples an elution assay was carried out. First a serial dilution of TBO in 50% acetic acid and 50% deionized water was carried out from a concentration of 1 μM to 20 μM in triplicate. The absorbance of 100 μl of each concentration was measured at 630 nm using a plate reader (BMG Labtech FLUOstarOmega) and averaged. The results were plotted and the trendline was used to determine the concentration of TBO vs absorbance. The absorbance curve can be seen in figure 4.2.

After TBO staining three punches of 8 mm were taken from each sample and placed in 3 ml of 50% acetic acid and 50% deionized water for one hour to elute the TBO from the surface. Samples were gently rocked at least 3 times throughout the hour to encourage elution. After 100 μl of the eluent was plated in triplicate for each sample and measured at 630 nm to determine the concentration of TBO in the eluent. The concentration and nominal sample surface area was used to calculate the concentration of TBO on the surface which directly correlates to the number of carboxyl groups present on the surface and should correlate to the amount of accessible HA repeat units at the surface. This assumes that HA repeat units provide the only available source of stainable carboxyl groups. It should be noted that only HA repeat units able to be solvated by water and acetic acid at the surface are measured. These will be referred to as "available HA repeat units" or "active HA" HA repeat units embedded and crosslinked in the LLDPE are unable to be reached by the TBO stain and the eluting solution.

$$Concentration\,TBO\left(\frac{\mu\,\mathrm{mol}}{L}\right) * 0.003\,(L) * \frac{1}{\pi * \left(4\,(mm)\right)^2} = TBO_{surface\,concentration}\left(\frac{\mu\,\mathrm{mol}}{mm^2}\right)$$

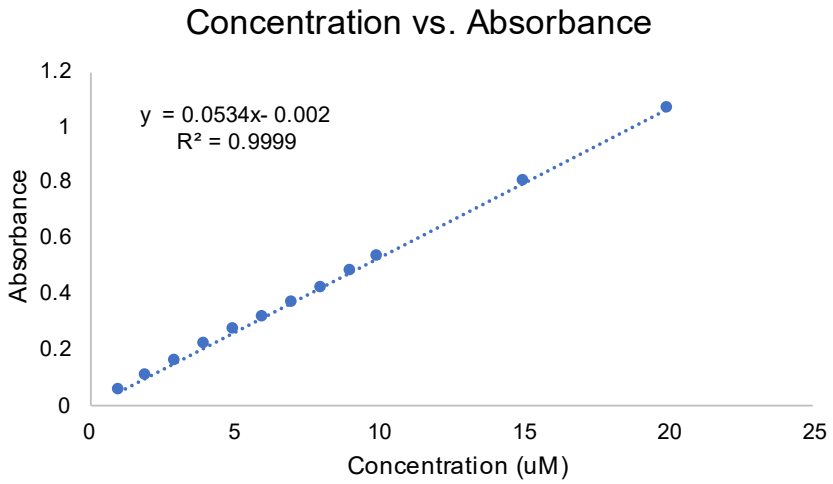

Figure 4.2: Relationship between concentration of TBO and absorbance at 630 nm.

4.3.2 Results

Figure 4.3 shows the contact angle results for each sample treatment. The description of the treatment is below each set of static, advancing, and receding contact angles. From top to bottom each row describes the withdrawal rate of the film from the silyl-HA/xylene solution, the relative vacuum pressure, the temperature, and if present a fourth factor in the treatment (specifically the accidental 2x withdrawal sample and the use of lower MW HA (100kDa vs 700 kDa)). Columns with an asterisk indicate a significantly higher contact angle than the corresponding column with a hashtag. Columns with no marking were not different than any other column according the post-hoc Tukey's test.

Only the 5 cm/hr, -15 inHg, and 50 °C sample had a significantly higher static contact angle than other samples, specifically the following: 10 cm/hr, -15 inHg, and 50 °C samples , 2 cm/hr, -15 inHg, and 50 °C (2x withdraw) samples, and 2 cm/hr, -15 inHg, and 50 °C (low MW) samples. Both the 5 cm/hr, -15 inHg, and 50 °C samples and the 2 cm/hr, -15 inHg, and 50 °C had a higher receding contact angle compared to the 2 cm/hr, -15 inHg, and 50 °C (low MW) samples. No samples had significantly different advancing contact angles.

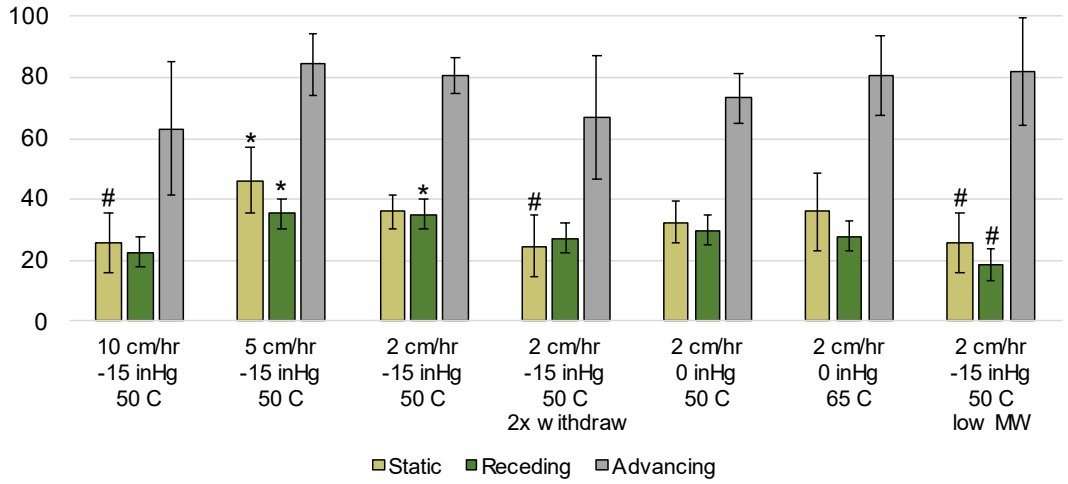

Figure 4.3: Static, receding, and advancing contact angle for LLDPE samples with altered withdrawal parameters. The top row describes the withdrawal rate. The second row describes the relative vacuum pressure, the third row describes the temperature, and if present the fourth row describes an extra parameter change. Asterisks indicate significant difference when compared to hashtags ($n = 9$, $p < 0.05$)

Figure 4.4 shows the surface density of available HA repeat units as measured through quantitative TBO analysis along with an image of a TBO stained sample prior to punching and elution. The two sample sets withdrawn at 2 cm/hr, -15 inHg, and 50 C both had significantly higher concentrations of HA repeat units compared to all other samples. Though the sample withdrawn twice it did not have significantly more available HA at the surface. The samples withdrawn at higher temperature (65 °C) and at atmospheric pressure and the samples treated with low MW HA had significantly more available HA at the surface compared to the samples withdrawn at higher rates and the sample set treated at 2 cm/hr but at 50 °C.

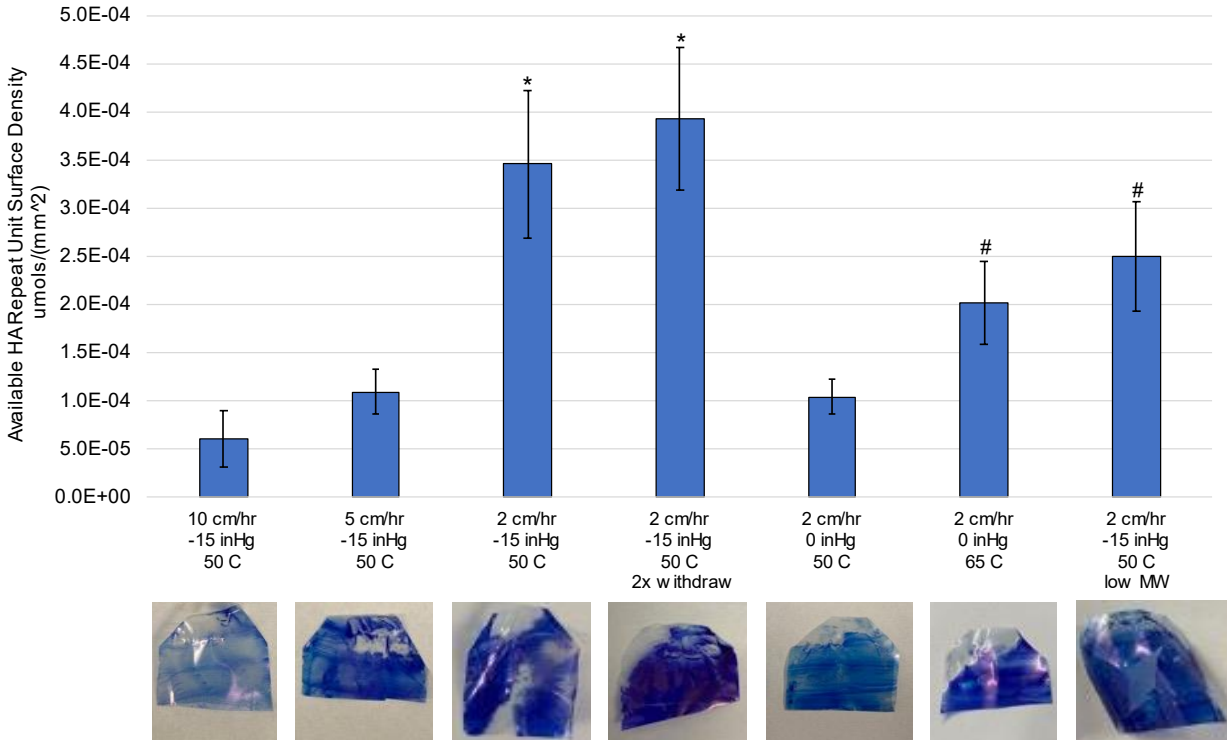

Figure 4.4: Available HA repeat units and images of TBO stained films of films with varied withdrawal rates, temperatures, and vacuum pressures. Asterisks indicate significantly more available HA repeat units compared to all samples, and hashtags indicate significantly more available HA repeat units compared to unmarked samples (n=9, $p < 0.05$)

4.3.3 Discussion

The contact angle results indicate that regardless of treatment withdrawal conditions or the MW of the HA the treatment process is fairly robust at generating an IPN between LLDPE and HA that produces a hydrophilic surface. There was a statistically significant reduction in static and receding contact angles for the samples treated with low MW HA compared to some but not all samples. Specifically, the samples treated at 5 cm/hr and 2 cm/hr at 50 °C and -15 inHg. However, there is not a consistent trend, nor do the contact angles correlate with the available HA units measured by quantitative TBO. In fact, it appears the samples treated at 5 cm/hr may have simply been outliers as the contact angle was higher than both the 2 cm/hr samples and 10 cm/hr samples performed with the same temperature and atmospheric vacuum. Without the 5

cm/hr samples the only difference between any samples is between the samples treated with low and high MW HA and only for the receding contact angle. Though there are no clear trends in contact angle vs treatment method, this data does demonstrate that within the varied parameters (rate of withdrawal, temperature, atmospheric pressure, and MW of HA) the treatment process is able to generate a hydrophilic surface on LLDPE films. As hydrophilic surfaces have been shown to decrease fibrinogen adsorption[16], platelet adhesion[17], and blood clotting[9,16] which are necessary to producing a blood compatible implantable material, each treatment shown should produce a heart valve leaflet material that prevents thrombosis.

Beyond the lack of trends captive bubble contact angle is performed manually. This can create some variation in contact angle measurements between users. Because of the time and large number of samples, and the need to take multiple measurements on each sample multiple lab members recorded contact angle data. Despite these challenges it is clear is that regardless of the treatment conditions the contact angles are much lower than untreated LLDPE. Untreated LLDPE contact angle can be found in chapter 2.4.2.

The TBO assay results indicate that reductions in the rate of withdrawal clearly generate an HA-LLDPE IPN with more available HA at the surface of the samples. This can be seen in the general trend across the first three samples in which the rate of withdrawal was reduced from 10 cm/hr to 2 cm/hr. It is also clear that the vacuum pressure helps to produce more active HA at the surface as the samples treated at atmospheric pressure both had lower amounts of available HA compared to the sample treated at a vacuum pressure of -15 inHg. Finally, we see that the lower molecular weight HA produces less available HA at the surface than a sample treated with higher MW HA under the same conditions. This should be kept in mind during the following section as TBO stained low MW HA was more easily detected by EDS. With this discussion it should be noted first that HA availability at the surface is important for improving the blood compatibility of LLDPE for use in heart valve leaflets as shown in chapter 3, however

concentration of the available HA still needs to be evaluated against the clotting and platelet adherence and activation before further conclusions can be drawn.

Regardless of blood compatibility characteristics, this work demonstrates that the HA treatment process is robust and can be tailored. The tailoring can occur through the velocity at which a film is withdrawn from the silyl-HA/xylene solution, the vacuum pressure at which the withdrawal occurs, the temperature at which the withdrawal occurs, and the MW of the HA used. Importantly it was determined that the treatment can occur in atmospheric pressure without losing the induced hydrophilicity of the LLDPE from the HA, indicating that this onerous aspect of the treatment process can be removed for commercial scale up.

Lastly of most importance it should be noted that all aspects that can increase the rate of drying increased the amount of available HA. Specifically slower withdrawal rates, higher temperature, and higher vacuum were all correlated with increased available HA at the surface. While continually increasing available HA may be worthwhile, it is likely that at a certain point HA surface density provides negligible gains in blood compatibility. The amount of HA at the surface should be evaluated against blood compatibility characteristics and the rate of degradation of HA in the presence of hyaluronidase to determine the optimal commercial HA treatment parameters for LLDPE when used as a heart valve leaflet.

4.4 Evaluation of HA penetration through LLDPE films with 700 kDa HA (High MW HA) and 100 kDa HA (Low MW HA)

While it has been verified that the HA treatment process creates an IPN with blown LLDPE films[5,9], no one had successfully determined how far the silyl HA was able to diffuse into the bulk of the LLDPE films. A method was developed to freeze fracture the HA films such that the resulting fractured cross section that could be evaluated for the presence of HA. Once this method was established, it became theoretically possible to determine how deep the HA was diffusing into the

bulk of the polymer material through energy dispersive X-ray spectroscopy (EDS, X-Max Silicon Drift Detector (SDD) 80 mm^2, Oxford Instruments). It was hypothesized that the lower MW HA used the further it might be able to diffuse into the swollen LLDPE. To test this an experiment was put together to treat LLDPE samples with different MW HA and measure the depth of penetration through the fractured cross section using EDS.

While this work will not delve into the results initially the films were stained with ruthenium red and coated in gold prior to SEM imaging. This was due to the Lα peak of ruthenium occurring at 2.56 keV which did not overlap the Lα peak of gold at 2.12 keV. The ruthenium did not generate a uniform stain nor was it easily detectable by EDS so further options were explored.

While it was initially considered TBO staining was ruled out for EDS mapping as the characteristic element sulfur present in TBO has a Kα peak of 2.30 which had significant overlap with the Lα peak of gold at 2.12 keV. The molecular structure of TBO can be seen below in figure 4.5. As gold coating was necessary and the only available method to generate the conductive surface needed for SEM and EDS mapping at the time, the work was put aside. Fortunately, the Analytical Resources Core at Colorado State University was able to revive a carbon coater which was used to generate a conductive surface that did not have overlapping EDS peaks with the characteristic atom of the TBO stain.

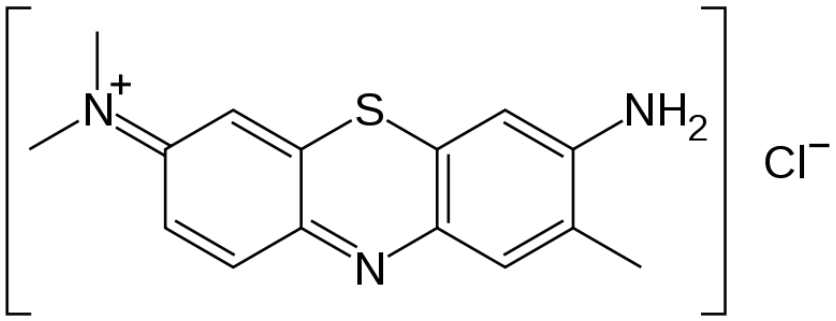

Figure 4.5: Chemical structure of toluidine blue O.

4.4.1 Methods

Blown LLDPE films were treated as described in chapter 2, section 2.1.1 with one set of films being treated with high MW HA (700 kDa) and a second set of films being treated with low MW HA (100 kDa). The HA surfaces were stained with TBO according to chapter 2 section 2.3.1. These initial samples were carbon coated and subsequently evaluated with EDS mapping to ensure that the sulfur peak provided by the TBO stain was identifiable. An accelerating voltage of 15 keV was used to ensure there would be enough counts to produce clear spectra peaks.

After the initial evaluation a second set of treated films were placed in liquid nitrogen for 30-45 seconds, removed from the freezing solution, and hit with a hammer to induce brittle fracture across the sample. After the fracture surface was cut from the sample and marked to denote where the fracture occurred. The freeze fracturing protocol can be found in appendix A.9. "Freeze Fracturing" After the fracture samples were re-hydrolyzed. This ensured that HA previously buried in the bulk of the sample that was now exposed at the fracture surface was hydrolyzed. After the samples were stained with TBO, coated in carbon, and analyzed with point EDS.

Originally EDS mapping was attempted but due to the significant amount of time it takes for the EDS scans to take place and the fact that the scans did not provide enough resolution and data to determine the distribution of sulfur across the sample point scans were performed at the edge of the sample and then deeper into the cross section. The depth and volume from which characteristic x-rays are generated in EDS analysis depends on the accelerating voltage of the electron beam and the density of the material being examined. It can vary from several hundred nanometers to 4 microns. With an accelerating voltage of 15 keV and a carbon sample the depth can volume was estimated to be 1-2 microns[18].

4.4.2 Results

The Kα peaks of key elements are as follows: Carbon – 0.277, Nitrogen – 0.392, Oxygen – 0.525, Sodium – 1.041, Aluminum – 1.486, Silicone – 1.739, Sulfur – 2.307, and Chlorine at 2.621. Copper has an Lα peak at 0.930 and Gold has an M peak at 2.12 keV[19].

Figure 4.6 shows the results of EDS mapping the surface of control, high MW, and low MW samples. Two maps in two locations were taken from each sample to confirm results. Clear oxygen and silicone peaks can be seen on all samples at approximately 0.5 and 1.75 keV. Nitrogen peaks can be seen on both the high MW and low MW samples at about 0.4 keV, however the peaks are much less defined on the high MW samples. The same trend follows for the sulfur peaks at 2.3 keV, however on one high MW sample the sulfur peak is barely distinguishable from the background.

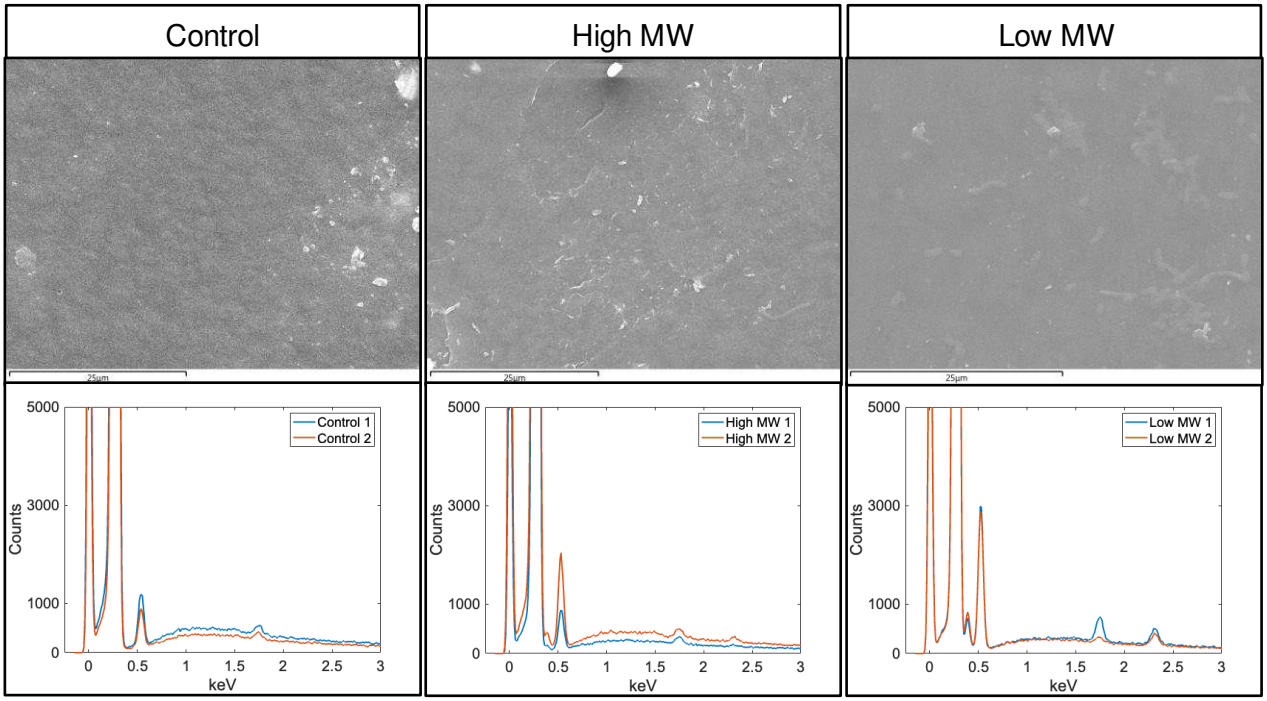

Figure 4.6: SEM images and EDS spectra of control, high MW, and low MW samples stained with TBO. Scale bars shown are 25 μm.

Figure 4.7 – Figure 4.10 show the result of point EDS along both the edge of the freeze fractured samples and moving towards the interior. On the top left is the image of the cross

section of the sample. On the top right is a magnified image on the edge of the sample with the point EDS locations shown. Below are the EDS spectra taken at each point. EDS produces characteristic x-rays from an approximately spherically shaped volume with a diameter of several microns within the bulk of the sample. As such each point shown should be understood to be representing 1-2 microns across and into the sample. Points were taken at least 3 microns apart to prevent large areas of overlap.

Figure 4.7 shows the cross section, EDS spectra locations, and EDS spectra of point EDS taken on the control sample. Clear carbon and oxygen peaks can be seen on all spectra except on spectra 21. This is interesting because the point location was selected just off the edge of the sample indicating that if the spectra are taken from a location past the edge of the fracture the resulting spectra will show a flat baseline and a very low relative carbon peak. This is important to note as some of the SEM images have significant charging at the edge where point EDS was taken. Charging was caused as higher acerating voltages were necessary to get a better EDS signal.

There is a second interesting note to be made which is that spectra 22 taken from a more interior point has clear peaks at 1.5, 0.9, and 2.1 keV which are the Kα, Lα, and M peaks of aluminum, copper, and gold respectively. The sample holder is regularly coated in gold. The samples were propped with aluminum foil and grounded with copper tape indicating that occasionally the background environment is picked up by EDS. The final note to make on the control sample is a clear lack of a peak at 2.3 keV where the characteristic x-ray Kα peak of sulfur is found

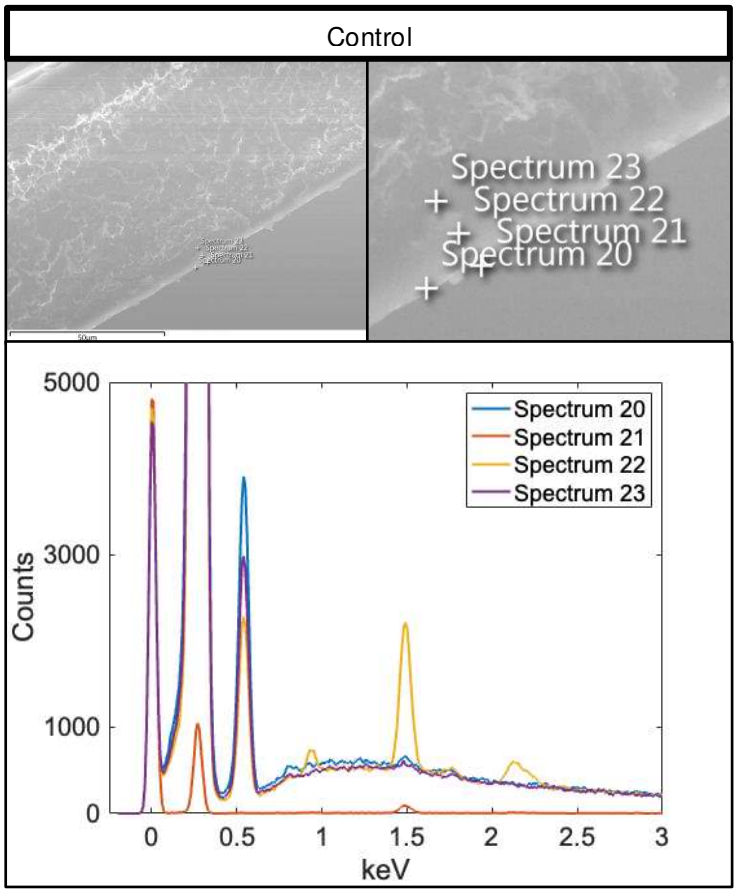

Figure 4.7: SEM images and point EDS spectra of the cross section of a freeze fractured control sample. Scale bar shown is 50 μm.

Figure 4.8 shows two cross sections of LLDPE samples treated with high MW (700 kDa) HA. On the High MW 1 sample shown on the left we can see the clear charging effects that make it difficult to identify the edge of the sample. Despite the difficulty of locating the exact edge only spectrum 6 has a small peak at 2.3 keV where the characteristic x-ray Kα peak of sulfur is found. Even that peak is so small it is hard to draw a conclusion that there is TBO bound to HA and no other spectra on the sample has even a semblance of a peak. This aligns with the EDS map across the surface a sample treated with high MW HA in figure 4.6 where the sulfur peaks were also difficult to distinguish from the background.

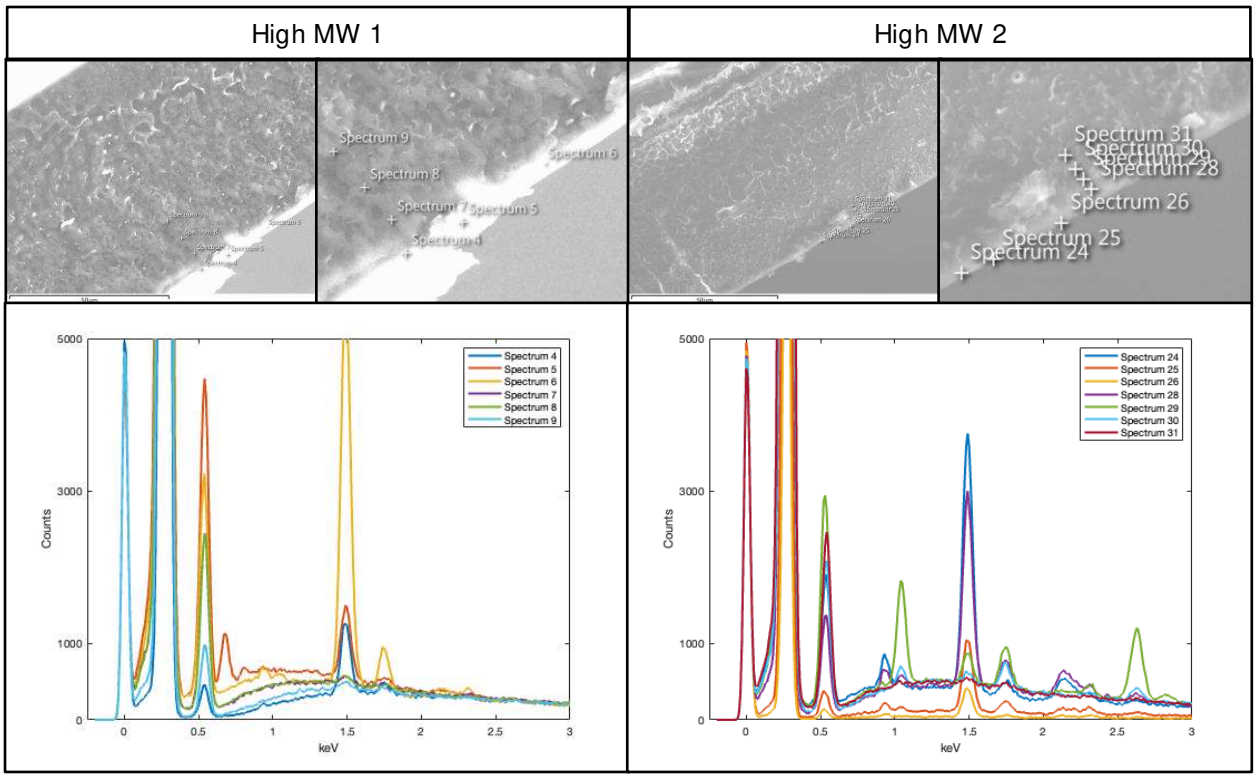

Figure 4.8: SEM images and point EDS spectra of the cross sections of a freeze fractured high MW HA treated samples. Scale bar shown is 50 μm.

On the high MW 2 sample shown on the right spectra 25 and 26 clearly missed the cross section as the curves have a flat baseline. Spectra 28 and 29 both have clear peaks at 2.3 keV indicating the presence of sulfur from TBO bound to HA that are difficult to see on figure 4.8, however figure 4.9 shows the same spectra but focused between 2.0 and 2.5 keV. Here it can be seen that the sulfur peaks are present on spectra 28 and 29 but not on any other spectra. This

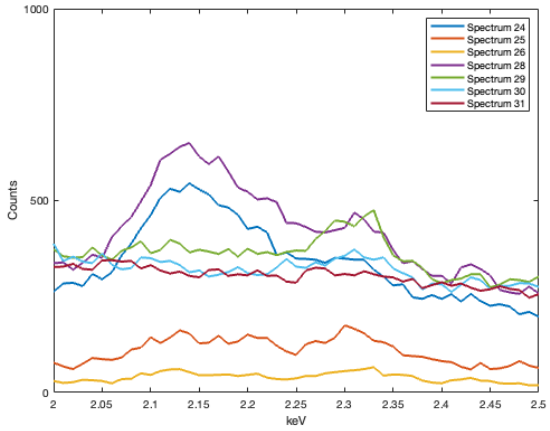

Figure 4.9: High MW 2 EDS spectra between 2 and 2.5 keV

is interesting as both are taken from interior points (still less than 5 μm from the edge), but the spectra 24 taken right at the edge does not have a sulfur peak.

While less relevant to the identification of the location of HA, spectra 29 and 30 both have peaks at the following locations indicating presence of the corresponding element: Sodium – 1.041, Aluminum – 1.486, Silicone – 1.739, and Chlorine at 2.621. The sodium and chlorine are most likely present from the hydrolysis process in which the samples are submerged in multiple NaCl solutions. Silicone is found in both the vacuum pumps and oil baths used in the lab and often contaminate samples. The aluminum is present from the sample props made from aluminum foil.

Figure 4.10 shows the cross sections of two LLDPE samples treated with low MW (100 kDa) HA. For the low MW 1 sample seen on the left clear sulfur peaks (2.3 keV) are found in spectra 10 and 11 taken at the very edge of the sample as are peaks associated with copper, aluminum, and silicone (0.9, 1.5, 1.7 keV respectively). Spectra 12, 13, and 14 taken towards the interior of the cross section do not have sulfur copper, aluminum, or silicone peaks.

For the low MW 2 sample spectra 15 and 16 taken at the edge both have clear sulfur peaks (2.3 keV) while spectrum 17 taken slightly towards the interior of the cross section has a smaller but still clear sulfur peak. All three of these spectra have the copper, aluminum, and silicone peaks seen previously while spectra 18 and 19 do not.

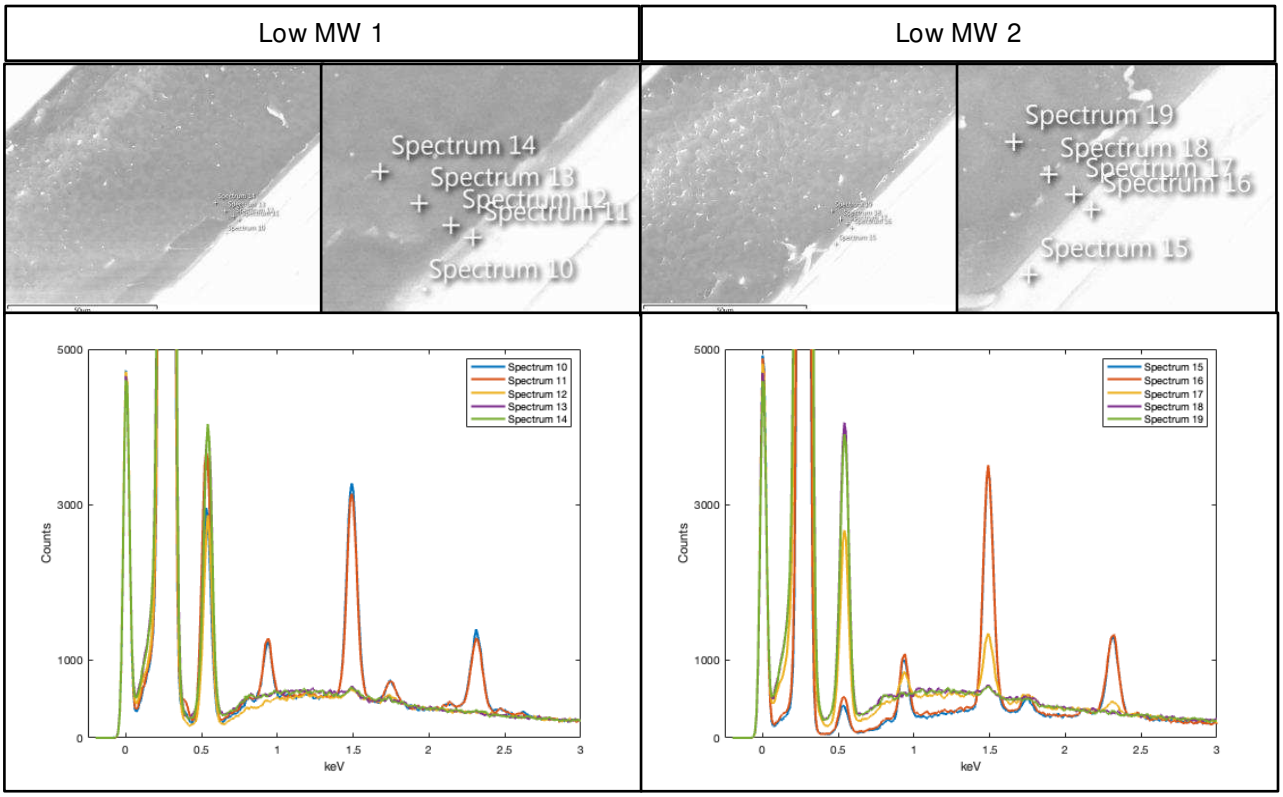

Figure 4.10: SEM images and point EDS spectra of the cross sections of a freeze fractured low MW HA treated samples. Scale bar shown is 50 μm.

4.4.3 Discussion

The initial hypothesis when this research was undertaken was that the low MW (100 kDa) HA would be able to diffuse deeper into the LLDPE samples during treatment. The results however, do not demonstrate such a clean picture of the process.

The initial maps demonstrate that despite low contact angles and the clear presence of TBO, that sulfur is hard to detect with EDS on the high MW samples, but is clearly detected on low MW samples. As sulfur is the key element being detected from the TBO stain it is then difficult to draw direct comparisons between the high and low MW samples. What is interesting is that previous TBO elution assay results showed much more TBO on the high MW samples. This may indicate that when the films are stained in the TBO water solution the high MW HA is able to

solvate and stain while the low MW HA is bound more tightly to the surface. Once the films are removed from solution and dried the bound TBO is buried within the high MW HA but is more available with the low MW HA.

When examining the freeze fractured high MW samples only the high MW 2 sample had a sulfur peak. This peak on spectra 28 and 29 was detected a few microns into the fracture but the same results were not seen on the high MW 1 sample.

With the freeze fractured low MW samples sulfur is clearly present on the edge of both samples and can be detected somewhat interiorly on the low MW 2 sample as seen in spectra 17. The results are not repeated on the low MW 1 sample however where sulfur is only seen at the very edge.

What is clear is that there is no sulfur present on the control sample and there was sulfur detected on the edges of the treated samples. Also, sulfur was detected several microns deep into the fracture of one high and low MW HA treated sample. Sulfur was also not detected on any EDS spectra taken more than several microns deep into the fracture of any sample. Though only limited conclusions can be drawn from this limited evidence, it does indicate that HA diffuses a few microns deep into the LLDPE, but not further. This HA is crosslinked in place and forms an IPN at more than a superficial level but is not present through the bulk of the material.

These results indicate further studies should be investigated to determine the depth of penetration of HA into the LLDPE samples. Ion beam milling could give greater insight into the depth of penetration of the HA IPN, whether it be used in conjunction with SEM/EDS or more directly using TOF-SIMS. By slowly milling the sample and determining the characteristic atomic profile as the sample is milled it might be possible to determine the presence and relative amounts of HA through the bulk of the LLDPE. Another experiment that could be carried out would be to allow the LLDPE to swell for different periods of time. It may be that the silyl HA molecules can diffuse easily into the first several microns but that path becomes more tortuous deeper into the material and that diffusion becomes exponentially slower. Lastly even lower MW HA could be

used to create an IPN, however this experiment is not without risk as if the HA MW is low enough it may not be able to be crosslinked enough to generate a stable IPN.

4.5 Chapter Conclusions

The formation of an IPN between HA and LLDPE is a robust process that can be carried out effectively in a variety of conditions and with HA of different molecular weights. The process changes do not have major significant effects on the hydrophilicity of the HA-LLDPE material as seen in the contact angle results, but they do affect the amount of HA available to be stained by TBO. Considering HA is a dynamic molecule whose MW does have an effect on its biological properties[20], further investigation into whether low MW affects the cytotoxicity and blood compatibility as explored in chapter 3 is warranted. While these investigations are critical to ensuring the HA-LLDPE leaflets do not elicit negative biological responses this chapter assumes the presence of HA will elicit these effects and is focused on whether the process can be optimized for manufacturing.

To that question it can clearly be stated that the distillation of xylenes and the treatment of LLDPE under nitrogen is not necessary to produce an IPN between HA and LLDPE that is confluent across the surface. Furthermore, the data shows that the treatment conditions and withdrawal rate does have an effect on the amount active HA, but does not have major effects on the material's hydrophilicity.

Though more commercial in nature, further investigations should be made into ways that enhanced drying affects the confluence of HA on the surface of the LLDPE materials. It takes several hours to complete withdrawal and this will be a significant bottleneck in the treatment of LLDPE with HA. Acceleration of the withdrawal process without the loss of active HA could create significant savings. The use of a co-solvent that is more volatile than xylenes such as chloroform may accelerate drying.

Beyond accelerating drying there may be gains to be had by treating LLDPE samples with a mixture of different MW HA. The quantitative TBO results indicate that more active HA is present on high MW samples compared to low MW samples treated under the same conditions however the EDS mapping was able to detect TBO stained low MW HA better than TBO stained high MW HA. This indicates that in solution there is more active HA present with high MW HA, possibly because the HA is able to be semi solvated and extend away from the surface. However on a molecular level at the surface low MW HA may be more evenly distributed.

In conclusion some onerous processes can be relaxed in the treatment of LLDPE with HA and the treatment process can be further optimized for the commercial production of heart valve leaflets made from HA-LLDPE.

4.6 References

1. Zhang, M., King, R., Hanes, M. & James, S. P. A novel ultra high molecular weight polyethylene–hyaluronan microcomposite for use in total joint replacements. I. Synthesis and physical/chemical characterization. *J. Biomed. Mater. Res. A* **78A**, 86–96 (2006).

2. Zhang, M., Pare, P., King, R. & James, S. P. A novel ultra high molecular weight polyethylene–hyaluronan microcomposite for use in total joint replacements. II. Mechanical and tribological property evaluation. *J. Biomed. Mater. Res. A* **82A**, 18–26 (2007).

3. Zhang, M. Surface Modification of Ultra High Molecular Weight Polyethylene with Hyaluronan for Total Joint Replacement Application. (Colorado State University, 2004).

4. Beauregard, G. P. & James, S. P. Synthesis and characterization of a novel UHMWPE interpenetrating polymer network. *Biomed. Sci. Instrum.* **35**, 415–419 (1999).

5. Prawel, D. A. *et al.* Hemocompatibility and Hemodynamics of Novel Hyaluronan–Polyethylene Materials for Flexible Heart Valve Leaflets. *Cardiovasc. Eng. Technol.* **5**, 70–81 (2014).

6. Dean, H. *et al.* Development and Characterization of LLDPE-HA Materials for Cardiovascular Applications. *Submitt. Ann. Biomed. Eng.* **October**, (2012).

7. Chen, Y., Zou, H., Cao, Y. & Liang, M. Melt miscibility of HDPE/UHMWPE, LDPE/UHMWPE, and LLDPE/UHMWPE blends detected by dynamic rheometer. *Polym. Sci. Ser. A* **56**, 630–639 (2014).

8. Bui, H. T. Development of hyaluronan enhanced expanded polytetrafluoroethylene and linear low density polyethylene for blood contacting applications, The. (Colorado State University, 2019).

9. Bui, H. T., Prawel, D. A., Harris, K. L., Li, E. & James, S. P. Development and Fabrication of Vapor Cross-Linked Hyaluronan–Polyethylene Interpenetrating Polymer Network as a Biomaterial. *ACS Appl. Mater. Interfaces* **11**, 18930–18941 (2019).

10. Bui, H. T. *et al.* Transcatheter Heart Valves: A Biomaterials Perspective. *Adv. Healthc. Mater.* **10**, e2100115 (2021).

11. Heitkemper, M., Hatoum, H. & Dasi, L. P. In Vitro Hemodynamic Assessment of a Novel Polymeric Transcatheter Aortic Valve. *J. Mech. Behav. Biomed. Mater.* **98**, 163–171 (2019).

12. Hristova, M. Measurement and prediction of binary mixture flash point. *Cent. Eur. J. Chem.* **11**, 57–62 (2013).

13. Williams, D. B. G. & Lawton, M. Drying of Organic Solvents: Quantitative Evaluation of the Efficiency of Several Desiccants. *J. Org. Chem.* **75**, 8351–8354 (2010).

14. Hornof, M., de la Fuente, M., Hallikainen, M., Tammi, R. H. & Urtti, A. Low molecular weight hyaluronan shielding of DNA/PEI polyplexes facilitates CD44 receptor mediated uptake in human corneal epithelial cells. *J. Gene Med.* **10**, 70–80 (2008).

15. Schanté, C. E., Zuber, G., Herlin, C. & Vandamme, T. F. Chemical modifications of hyaluronic acid for the synthesis of derivatives for a broad range of biomedical applications. *Carbohydr. Polym.* **85**, 469–489 (2011).

16. Simon-Walker, R. HEMOCOMPATIBILITY OF HYALURONAN ENHANCED LINEAR LOW-DENSITY POLYETHYLENE FOR HEART VALVE LEAFLET APPLICATIONS. (Colorado State University, 2018).

17. Lee, J. H. & Lee, H. B. Platelet adhesion onto wettability gradient surfaces in the absence and presence of plasma proteins. *J. Biomed. Mater. Res.* **41**, 304–311 (1998).

18. Crist, B. V. SEM-EDS Information Depth. *The XPS Library of Monochromatic XPS Spectra* https://xpslibrary.com/sem-eds-information-depth/.

19. BEARDEN, J. A. X-Ray Wavelengths. *Rev. Mod. Phys.* **39**, 78–124 (1967).

20. Snetkov, P., Zakharova, K., Morozkina, S., Olekhnovich, R. & Uspenskaya, M. Hyaluronic Acid: The Influence of Molecular Weight on Structural, Physical, Physico-Chemical, and Degradable Properties of Biopolymer. *Polymers* **12**, 1800 (2020).

CHAPTER 5: SARS-COV-2 SPIKE PROTEIN ADHESION ON NONWOVEN POLYPROPYLENE USED IN PERSONAL PROTECTIVE EQUIPMENT (PPE)

5.1 Chapter Introduction

The largest zoonotic pandemic since the Spanish influenza, COVID-19, resulted in millions of lives lost and billions in economic damage[1–3]. Any efforts that can be made to rapidly address novel pandemics should be investigated, especially as the increasing global population and interconnectedness increases the risks for additional pandemics[4,5]. This chapter addresses an effort into developing treatments for nonwoven polypropylene used in most face masks to decrease the spread of COVID-19 by increasing adsorption of the SARS-CoV-2 virion to the material. Furthermore, the processes entailed can be carried out rapidly and relatively inexpensively in the evaluation of any material for use in PPE to address any novel viral or bacterial threat.

5.1.1 Background on SARS-CoV-2 and PPE

As of July, 2021, the CDC has reported over one million deaths attributed to COVID-19 in the US[6]. The CDC (Centers for Disease Control and Prevention) recommends healthcare personnel who work with COVID-19 patients wear personal protective equipment (PPE) including gloves, isolation gowns, N95 respirators, and goggles/face shield to protect themselves from infection[7]. While PPE protects healthcare personnel from infection, it can also encourage the spread of disease between patients through contact transmission[8,9]. Polypropylene (PP), polyethylene (PE), and polyethylene terephthalate (PET) are materials commonly used to make isolation gowns and N95 masks[10–13]. These plastics are easily manufactured into PPE, but recent evidence has shown that plastic, PP in particular, provides SARS-CoV-2 viability up to 72 hours, while on

cardboard the virus only had viability up to 24 hours[14]. Use of plastics-based PPE by healthcare personnel could be facilitating the transfer of SARS-CoV-2 between patients, and further research into known material alterations to decrease SARS-CoV-2 viability on PPE surfaces could provide a significant reduction in the spread of COVID-19 both in hospitals and across the globe as mask use becomes widespread. While entirely new materials for PPE could be investigated to decrease the viability of SARS-CoV-2, it will take years to fully investigate, design, manufacture, and build a robust supply chain for these. Alterations to current PPE, specifically N95 masks would be much faster, and our research group has already developed a method for incorporating a non-toxic and potentially viricidal biological polymer, hyaluronic acid, into plastics[15–18]. Furthermore, we have developed a more cost-effective method to introduce PEG into the nonwoven PP used in N95 masks. Our data demonstrates PEG treated masks retain the spike protein of SARS-CoV-2 at a significantly greater rate than untreated masks potentially providing a route to reduce transmission.

Under the "Guide to the Selection and Use of Particulate Respirators" NIOSH (The National Institute for Occupational Safety) describes N95 masks as masks that filter 95% of particulates and aerosols down to 0.3 micrometers in size[19]. While no materials are specified for use by NIOSH both 3M and Honeywell describe the filtration layer of their masks as nonwoven polypropylene[12,13]. Polypropylene, discovered in 1954, is a widely used polymer in the medical industry due to its high temperature resistance and ease of molding[20]. Polypropylene can be altered with O_2 plasma to induce carbonyl, carboxyl, ester, and hydroxyl groups at the surface inducing hydrophilicity and creating the potential to graft other polymers to the surface[21–24]. Acrylic acid, polyethylene glycol, hyaluronic acid, and chitosan have all been grafted to various surfaces through oxygen and other plasma treatments[24–27]. While N95 masks are currently the standard PPE for use by medical professionals to prevent the contracting and spread of SARS-CoV-2, the size of single virus particles are 0.06 - 0.120 micrometers in size, far below the required 0.3 micrometer aerosol particle size required by NIOSH[28]. Furthermore, polypropylene surfaces were

demonstrated to allow viable SARS-CoV-2 virions to survive for up to 72 hours, while cardboard only allowed the virus to survive 24 hours[14]. The authors only note the cardboard is "locally sourced", however most cardboard is made from cellulose. Cellulose is comprised of repeating glucose units linked with ether bonds, Hyaluronic acid is comprised of repeating β-1,4-d-glucuronic acid-β-1,3-*N*-acetyl-d-glucosamine linked with ether bonds, and polyethylene glycol (PEG) has repeated ether bonds forming the entire molecular structure[29–31]. With SARS-CoV-2 being capable of surviving on polypropylene for three days any surface modification to N95 masks is warranted, and with the ability to create further adhesion and multiple routes for surface modification of polypropylene, PEG and hyaluronic acid are promising candidates for the enhancement of N95 masks against SARS-CoV-2.

The COVID-19 pandemic has demonstrated the global need for rapid prototyping of antiviral and antibacterial materials that can be used by frontline medical workers and the general population. As the SARS-CoV-2 virion is primarily transmitted through respiration the most important piece of PPE in preventing transmission is the face mask[32]. PP used in facemasks has been shown to harbor live SARS-CoV-2 for up to 72 hours, indicating that while the mask may prevent aerosolized droplets from being respired it creates a surface hazard that can carry the disease[14]. The spike protein of SARS-CoV-2 is hydrophobic and is extensively decorated in mannose glycans providing a plethora of hydrogen bond donors[33,34]. A hydrophilic surface decorated in hydrogen bond acceptors has the potential to trap and inactivate the disease by creating electrostatic hydrogen bonds with the protein and causing it to denature through conformational changes induced by interactions with the hydrophilic surface. As the virion is seen to survive for long periods of time on hydrophobic PP (the most commonly used material in disposable face masks) developing a novel cost-effective method to induce a viricidal effect on the material has potential to reduce transmission.

HA is known to have viricidal effects against HIV, is a hydrophilic polymer with seven hydrogen bond acceptors per 401.3 Daltons (each repeat unit of the polymer) and has been used

to generate a microcomposite on synthetic hydrophobic polymers[15,17,18]. PEG is another hydrophilic polymer which has one hydrogen bond accepter per 44.05 Daltons and has been grafted to polypropylene using oxygen plasma[24]. Furthermore, the methods used to alter the nonwoven PP are well studied and documented to be non-toxic. Oxygen plasma treatment of polypropylene is a well-documented method for use in blood filtration and wound dressing. PEG is widely used in drug delivery and has been evaluated for cytotoxicity[35–38]. Finally hyaluronic acid is a naturally occurring polymer that our group has extensively evaluated for cytotoxicity and have been successfully implanted in multiple large animal models[15,18,39,40]. This chapter reviews a study into the treatment of nonwoven PP with HA and PEG and the resultant effects on spike protein adhesion. A briefer version can be found in the journal *Materials Advances* under the title "Treatment of Nonwoven Polypropylene to Increase Adsorption of SARS-CoV-2 Spike Protein"[41].

5.2 Treatment of Polypropylene Textiles

5.2.1 Plasma Grafting of Polyethylene Glycol onto Nonwoven Polypropylene

Non-woven polypropylene (PP) fabric of disposable face masks (Makena) was activated with oxygen plasma (PlasmaEtch) for 60 seconds. Following plasma activation PP samples were placed in a 25g/L solution of PEG (MW 3,350 kDa Sigma Aldrich) in 200 proof ethanol for 15 minutes allowing the PEG to adsorb to the activated PP sample surfaces. Samples were dried under vacuum (-635 mmHg) for 10 minutes to remove ethanol. The adsorbed PEG was grafted to the surface with a second oxygen plasma treatment for 300 seconds. Excess PEG was removed by rinsing in methanol for 15 minutes, followed by a rinsing in ethanol for 15 minutes. Finally, the PP samples were dried under vacuum (-635 mmHg) for 10 minutes to remove methanol and ethanol. Sham controls underwent the same process except the shams were submerged only in ethanol rather than a PEG/ethanol solution after the plasma activation step.

5.2.2 Hyaluronic Acid complexed with Cetyltrimethylammonium (HACTA) Spray Treatment of Nonwoven Polypropylene

Sodium hyaluronate (Lifecore biomedical) and cetyltrimethylammonium bromide (CTAB) were dissolved in DI at 0.3% (w/v) and 1.0% (w/v) respectively. The solutions were mixed, and the precipitate (HA-CTA) collected, washed with DI water (5x), dried under vacuum (-635 mmHg, 12 hours), and cryoground at -196 °C into a powder. The HA-CTA was then dissolved in 200 proof ethanol at 0.4% (w/v) and 50 °C for 3 hours or until no HA-CTA powder was observed. The HA-CTA/ethanol solution was sprayed onto the nonwoven PP layer at 25-30 PSI using an airbrush (Powermate). The airbrush was held approximately 4 cm from the sample and the solution sprayed at 0.1 ml/cm^2 which correlates to a deposition of HA-CTA at 0.4 mg/cm^2. The material was flipped, and the process repeated for the second side of the PP material. The sample was dried for 1 hour under vacuum at -635 mmHg.

A 2% (v/v) solution of toluene diisocyanate (TDI) in xylenes was prepared by mixing the two liquids for 15 minutes at room temperature. The dry HA-CTA sprayed PP material was cut into circles approximately 6.35 cm in diameter and allowed to crosslink in the vapor above 10 ml of the TDI/xylene solution at 60 °C for 1 hour. The crosslinked samples were dried under vacuum overnight at -635 mmHg. After drying the samples were hydrolyzed by placing each sample in 20 ml of 0.2 M NaCl in DI/ethanol (1:1, v/v) solution and sonicating for 1 hour. The solution was changed and the sonication repeated 3x. Samples were placed in 20 ml of DI/ethanol (3:2, v/v) for 2 hours, followed by sonication in DI for 30 minutes. Finally, samples were dried under vacuum -635 mmHg overnight.

5.3 Attenuated Total Reflectance-Fourier Transform Infrared Spectroscopy (ATR-FTIR)

ATR-FTIR measures the infrared absorption spectra of a materials surface. The wavelengths absorbed correspond to the chemical bonds found in the material.

5.3.1 Methods

ATR-FTIR (Nicolet 6700) spectra were taken on days 1,7, 14, 21, and 28 after treatment to assess the chemical composition of the PP fabrics and the stability of the samples over 28 days while stored. Samples were placed on the ATR crystal and run for 32 scans on the spectrometer. ATR-FTIR is known to penetrate a sample 0.5-2 microns depending on the material being tested[42], due to this depth of penetration the FTIR curves shown present material properties in the bulk more so than atomic surface properties. MATLAB R2020b was used to plot the FTIR data.

5.3.2 Results

The following peaks seen in all spectra can be attributed to chemical groups found in PP: alkane C-H stretching at 2915 cm^{-1}, methylene group C-H bending at 1455 cm^{-1}, and methyl group C-H bending at 1375 cm^{-1}. Aliphatic ether stretching was expected between 1150-1085 cm^{-1} on the PEG treated samples. However, the small peak seen at 1165 cm cm^{-1} is unchanged between the control and PEG treated samples. Hydroxyl O-H group stretching is seen at 3550-3200 cm^{-1} and secondary amide N-C=O stretching 1640 cm^{-1} are seen on the HA treated samples

Figure 5.1 shows the control, PEG treated samples for day 1 and day 28, and the PEG sham samples for day 1 and 28. Days 7, 14, and 21 had no difference and were omitted for clarity. Figure 5.2 shows the control and HA treated samples for day 1 and day 28. Days 7, 14, and 21 had no difference and were omitted for clarity.

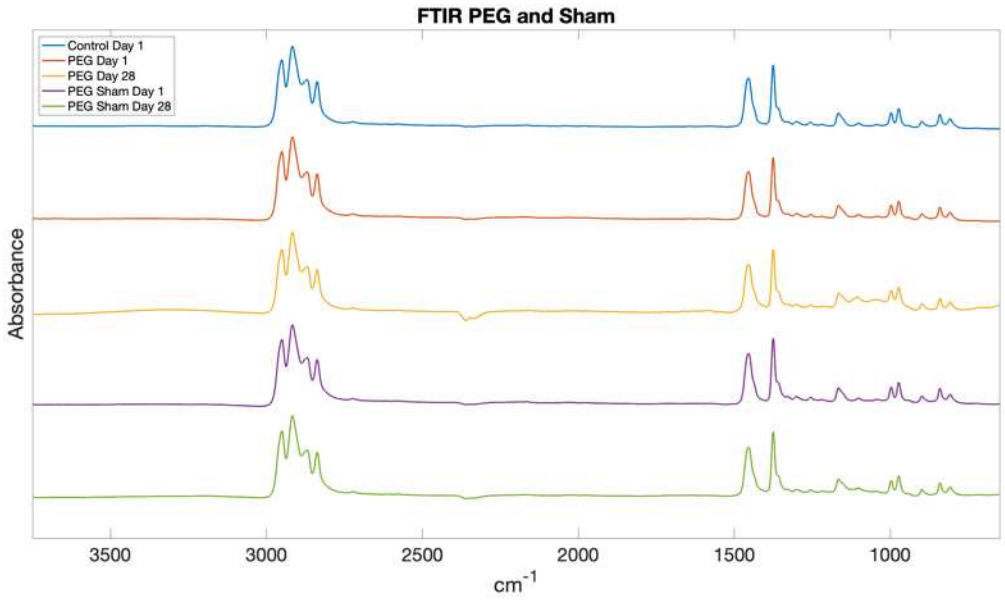

Figure 5.1: FTIR curves for PEG and sham samples.

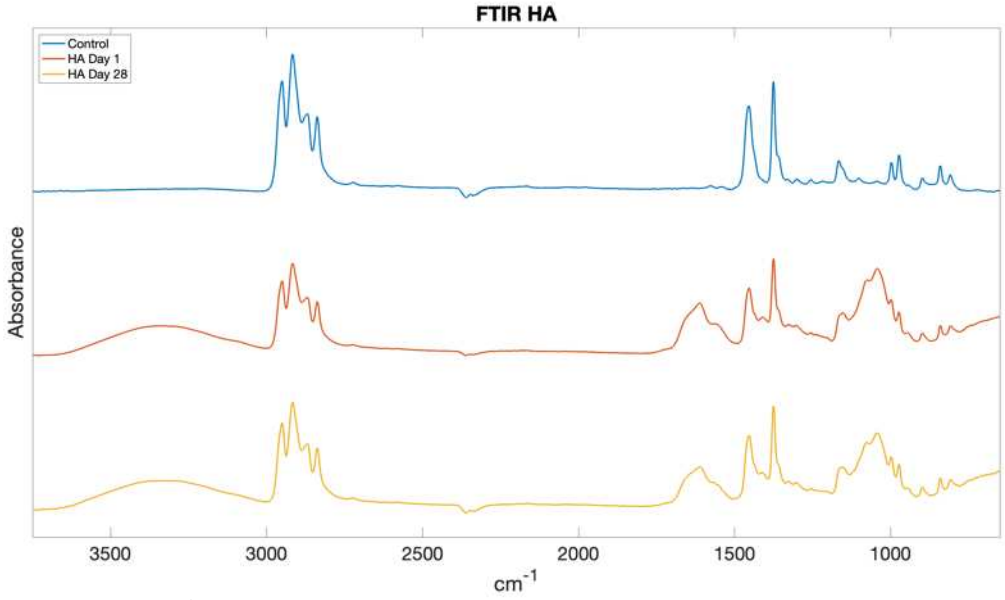

Figure 5.2: FTIR curves for HA treated samples.

5.3.3 Discussion

The PEG and sham samples have no differences from the control indicating that the top 1-2 microns of material are predominately PP. While this indicates that the bulk of the material does not contain PEG, further XPS and contact angle results demonstrate the surface of the material has been altered by the PEG treatment. Due to the known depth of penetration of FTIR it is possible that a thin layer of PEG is grafted to the surface, yet it does not constitute enough of the material to absorb significant IR waves compared to the PP textile.

The HA treated samples have hydroxyl O-H group stretching at 3550-3200 cm^{-1} and secondary amide N-C=O stretching at 1640 cm^{-1}. This clearly indicates the PP materials have been coated in the crosslinked HA creating a microcomposite on the surface. No change is seen over the 28-day study.

5.4 Contact Angle Goniometry

Contact angle goniometry is most often used to determine the two-dimensional surface characteristics pertaining to the interaction between liquids and solids. However, the method can be used to evaluate the surface and bulk interactions between textiles and other three-dimensional materials and liquid droplets. When evaluating nonwoven PP textiles for use as a COVID-19 enhanced PPE face mask it is important to understand how water may absorb and adhere to the material as COVID-19 is primarily transmitted through aerosolized water droplets respired by infected persons[43–45]. Due to the three-dimensional characteristics of the PP fabric contact angles was assessed by depositing a droplet of water on the surface taking the static contact angle over 5 minutes to determine if the material absorbed the water and the rate at which the contact angle changed as the material structure interacted with the droplet of water.

5.4.1 Methods

Water contact angle (260-F4 Ramé-Hart Instrument) goniometry measurements were taken on days 1, 7, 14, 21, and 28 after treatment. A droplet of water was placed on the surface of the sample and the contact angle between the surface of the sample and the droplet was recorded over 5 minutes. MATLAB R2020b was used to calculate the mean and standard deviation of the contact angle.

5.4.2 Results

Figure 5.3 shows the control samples and PEG treated samples for day 1, and day 28. Figure 5.4 shows the control samples and PEG sham samples for day 1 and 28. Figure 5.5 shows the control samples and HA samples for day 1 and 28. Days 7, 14, and 21 were omitted for clarity, and they did not have any significant differences between day 1 and 28. PEG and HA treated samples had a significantly lower contact angle than the PP control at all time points. The PEG sham sample did not have a significantly lower contact angle at any time point.

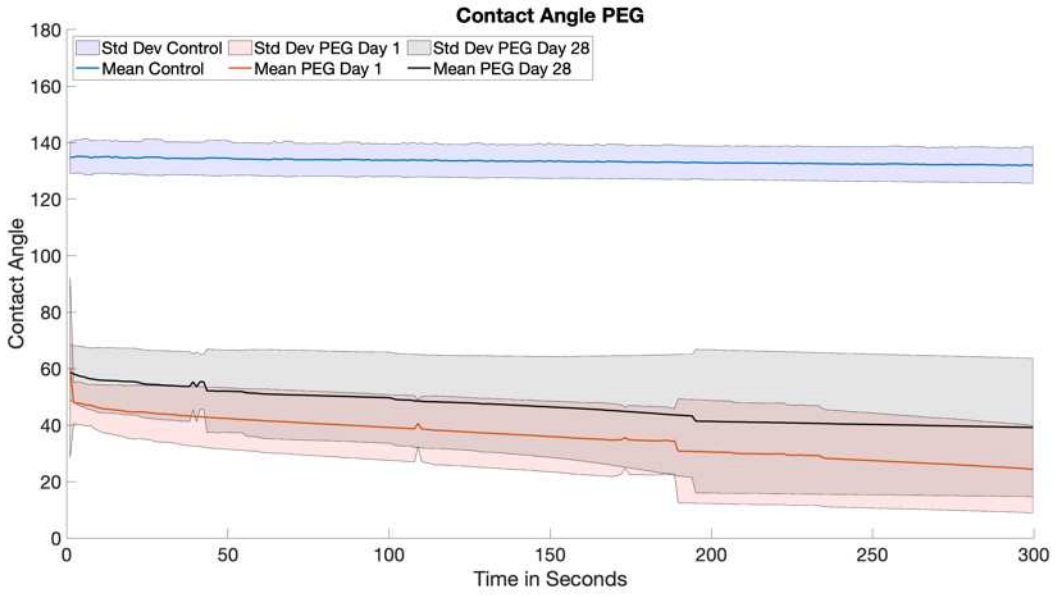

Figure 5.3: Contact angle of water on the surface of PP samples treated with PEG.

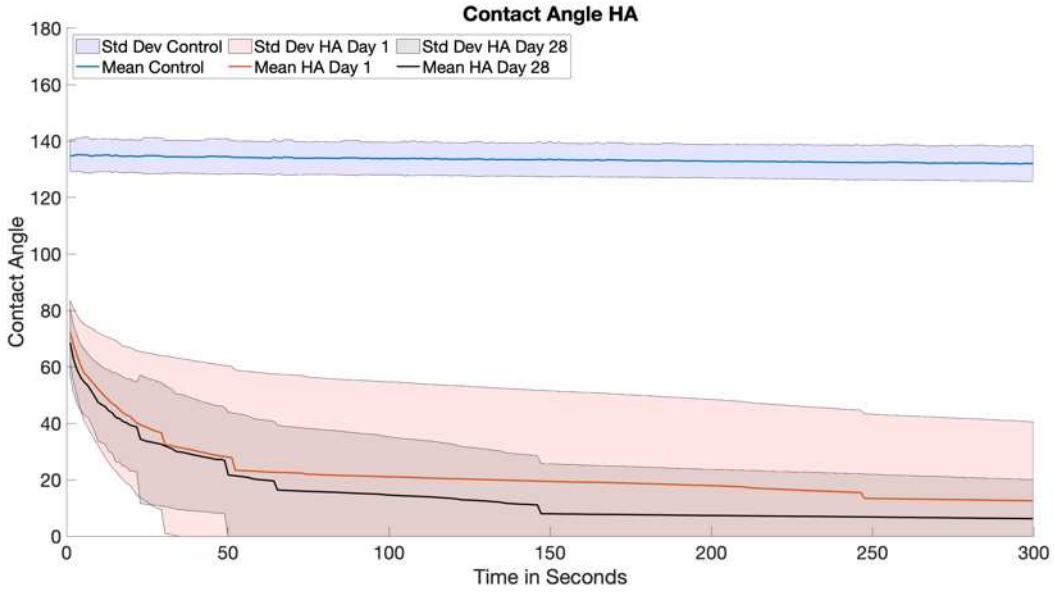

Figure 5.5: Contact angle of water on the surface of PP samples treated with PEG.

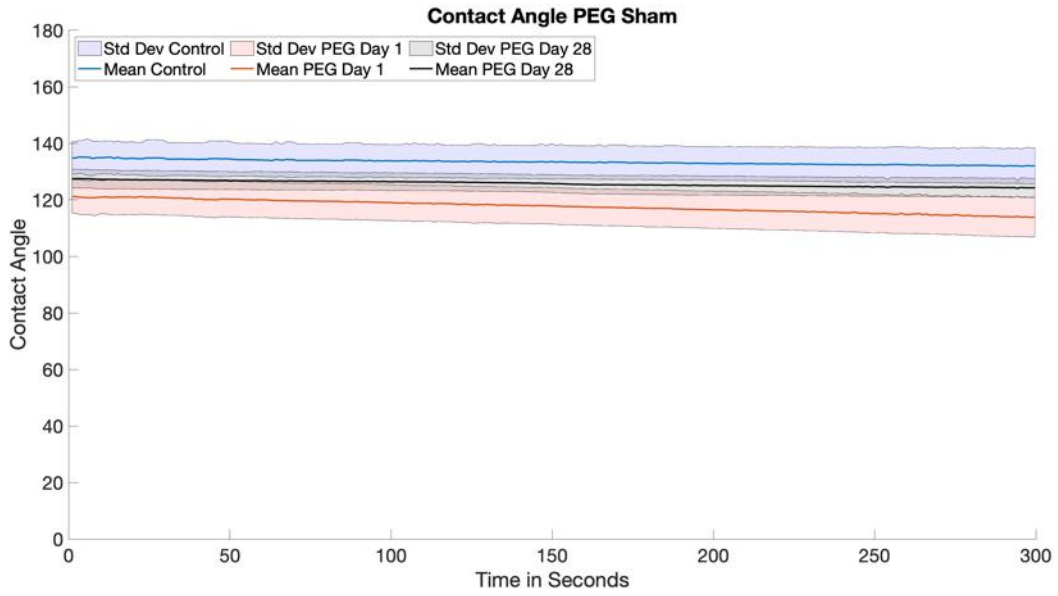

Figure 5.4: Contact angle of water on the surface of PP samples treated with PEG.

5.4.3 Discussion

The PEG treated PP samples had consistently lower contact angles than the control PP from day 1 to day 28, however there was a slight increase over that time. The sham samples were never significantly different than the controls at any time point. PEG is a hydrophilic polymer and grafting PEG to the PP surface introduced significant hydrophilicity that was retained over the course of 28 days when stored with no protection on a shelf. The sham PEG controls did not have or retain significantly lower contact angles indicating that the PEG treatment does in fact change the surface chemistry and that the PEG will stay grafted to the sample over 28 days.

The HA treated PP samples had consistently lower contact angles compared to the control from day 1 to day 28, with most samples completely absorbing the water droplet over the 5 minutes of testing. These results indicate that the HA microcomposite creates a hydrophilic structure on the nonwoven PP that is stable for at least 28 days.

5.5 X-ray photoelectron spectroscopy (XPS)

X-ray photoelectron spectroscopy (XPS) is used to identify the atomic composition in the top 10-20 nm of a solid surface. Briefly X-rays of a known energy are focused onto a surface, and a detector senses photo emitted electrons from the surface. Based on the energy of the electron detected and the energy of the x-ray photons sent to the surface the binding energy of the electron can be determined and correlated to the atomic species that emitted an electron of that energy.

5.5.1 Methods

A PHI-5800 spectrometer X-ray photo-electron spectroscopy was used to analyze the surface chemistry. A monochromatic Al-K X-ray source operated at 15 kV was used for the study and the emitted photoelectrons were collected at a takeoff angle of ~45° relative to the PP sample surface. Survey spectra were collected from 0 to 1100 eV with a pass energy of 187.85 eV. High-

resolution spectra were collected for oxygen (O 1s) and Carbon (C 1s) from 280 to 294 eV and 526 to 538 eV, respectively. The atomic composition of the PP samples was calculated using peak fit analysis with Multipack software. Before taking spectra, samples were dried under vacuum (-635 mmHg) overnight. Spectra were collected every 7 days from day 1 to day 28 to determine if the elemental composition of the surfaces changed over 1 month of shelf storage.

5.5.2 Results

Day 1 results are shown in figure 5.6 and table 5.1. The PEG and sham samples have an increased oxygen to carbon ratio compared to the control. Some silicone is seen on the sham, control, and HA samples most likely due to contamination from silicone oils used in the vacuum systems in the lab. As would be expected nitrogen and sodium are seen on the HA sample due to the presence of nitrogen in HA and the use of sodium chloride in the hydrolysis process. Sodium ions also should replace the cetyltrimethylammonium (CTA) counter ion seen in HACTA.

Table 5.1: Elemental composition of day 1 PP samples as analyzed by XPS.

Sample	Carbon	Oxygen	Nitrogen	Silicon	Others
PEG	86.3	13.7	0	0	0
Sham	70.42	21.29	1.15	7.14	0
Control	90.15	5.35	0	4.5	0
HA	72.83	19.42	4.89	1.77	1.08(Na)

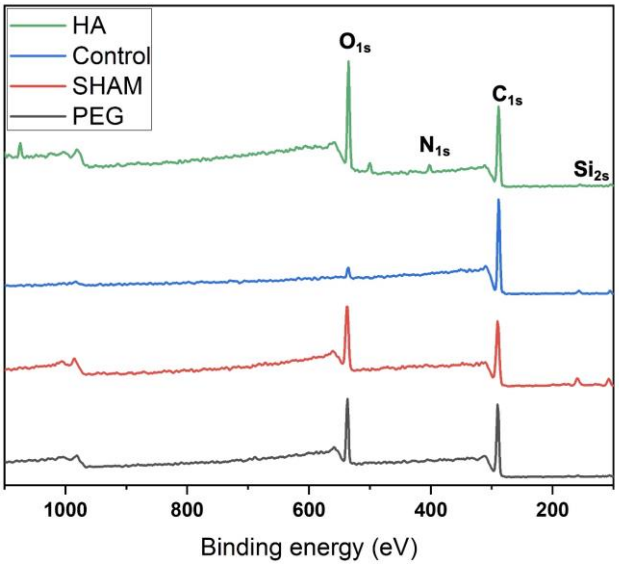

Figure 5.6: XPS spectra of Day 1 PP samples.

Day 28 results are seen in figure 5.7 and table 5.2. The PEG sample and sham samples continued to maintain significantly higher carbon to oxygen ratios compared to the control over the 28-day study. Interestingly the PEG sample had almost double the oxygen to carbon ratio at day 28 compared to day 1. All samples had silicon on the surface at the end of the study. As they were stored in the lab it's likely the silicone oils used for pump oils and heating baths or vacuum grease used on ground glass joints contaminated the surface over the course of the study. HA samples continued to have a higher oxygen to carbon ratios compared to the control and had continued presence of nitrogen and sodium.

Table 5.2: Elemental composition of day 28 PP samples as analyzed by XPS.

Sample	Carbon	Oxygen	Nitrogen	Silicon	Others
PEG	73.81	24.56	0	0.99	0
Sham	68.69	24.33	0	6.98	0
Control	93.09	4.21	0	2.69	0
HA	60.45	32.23	3.36	0.96	2.83 (Na)

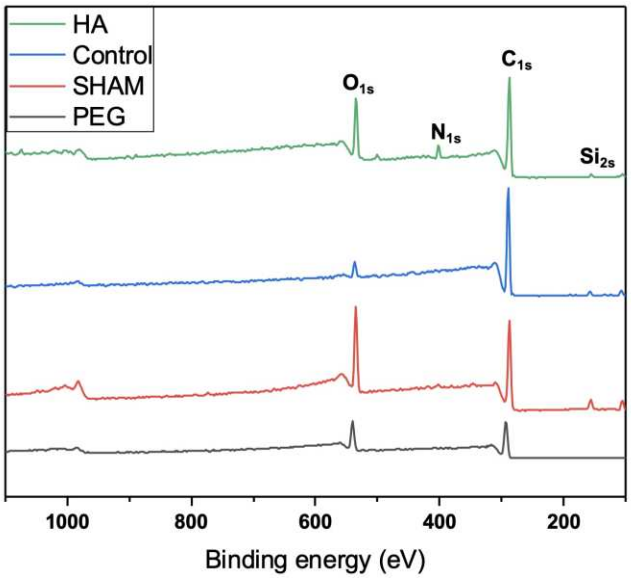

Figure 5.7: XPS spectra of Day 28 PP samples.

5.5.3 Discussion

The PEG sham results from day 1 showing an increase in oxygen on the surface of the samples indicate that exposure to oxygen plasma alters the surface chemistry of the PP. With this it is reasonable to assume that the lower oxygen to carbon ratio of the PEG samples compared to the sham indicated that the PEG is covering some of the oxygen groups from the plasma by binding to the surface. XPS alone would not confirm this however the contact angle data demonstrating that the PEG samples are significantly more hydrophilic than the sham samples indicate a lasting change.

The increased oxygen to carbon ratios, the new presence of nitrogen and sodium strongly indicate the presence of HA on the HA treated samples. This claim is further bolstered by the FTIR and contact angle results on day 1.

After 28 days, the PEG sham maintained a higher oxygen to carbon ratio over the course of the study indicating the oxygen plasma treatment is durable over time, but does not induce significant hydrophilicity as seen in the contact angle data. The PEG samples had an increase in

the oxygen to carbon ratio on day 28 which may be due to variation in the PEG grafting across the surface. The shifting oxygen ratios did not have a significant effect on the hydrophilicity of the samples as seen in the contact angle data. It should be noted that XPS analyzes a much smaller area compared to contact angle. This increased resolution indicates the PEG grafting is not ubiquitous across the surface. HA samples also saw an increase in oxygen to carbon ratios over the study indicating variation across the surface however the presence of nitrogen without great variation indicates the HA treatment is more confluent over the sample. Neither control sample nor the PEG sham sample had a change in the oxygen to carbon ratio indicating there was not some type of contamination that introduced oxygen to the surface.

5.6 Uniaxial Tensile Testing

Uniaxial tensile testing was performed on all PP samples to determine if the treatments would change the mechanical properties of the material creating an inferior fabric that may not be suitable for use.

5.6.1 Methods

Tensile testing was performed according to ASTM D3822. Dog bone samples were punched from the material with a gauge length of 15 mm and a width of 3.16 mm. The samples were pulled at a constant rate of extension of 10%/min or 1.5mm/min until failure. The Youngs' modulus was calculated from 1%-3% strain where all samples exhibited linear behavior. Testing was performed on an Instron 4442 with the 50 N load cell. Plots were generated with MATLAB R2020b, moduli were calculated using a linear polynomial fit from the curve fitting toolbox in MATLAB R2020b, and statistics were performed using Minitab. Samples stored in ambient conditions before testing.

5.6.2 Results

The tensile strain at break (tensile failure) occurred in the non-woven polypropylene and the Youngs' modulus can be seen in table 5.3.

Table 5.3: Tensile failure and Youngs' modulus of non-woven polypropylene samples. *The PEG Sham samples had an outlier fail at 27% strain.

Sample	Control	PEG Sham	PEG	HA
Tensile Failure (Strain %)	29-39	63-75*	31-47	18-25
Youngs Modulus (MPa)	0.345 ± 0.043	0.271 ± 0.047	0.362 ± 0.058	0.574 ± 0.020

The PEG sham samples failed at much higher strain compared to all other samples apart from one outlying PEG sham sample. The HA treated samples failed at a lower strain than all samples. Only the HA treated samples had a significantly different modulus compared to the control and all other samples when compared using a one-way ANOVA and post hoc Tukey's test. The modulus of the HA sample was much higher 0.574 ± .020 MPa compared to the next highest PEG at 0.362 ± 0.058. The stress stain curves for each sample set can be seen in figures 5.8 – 5.11.

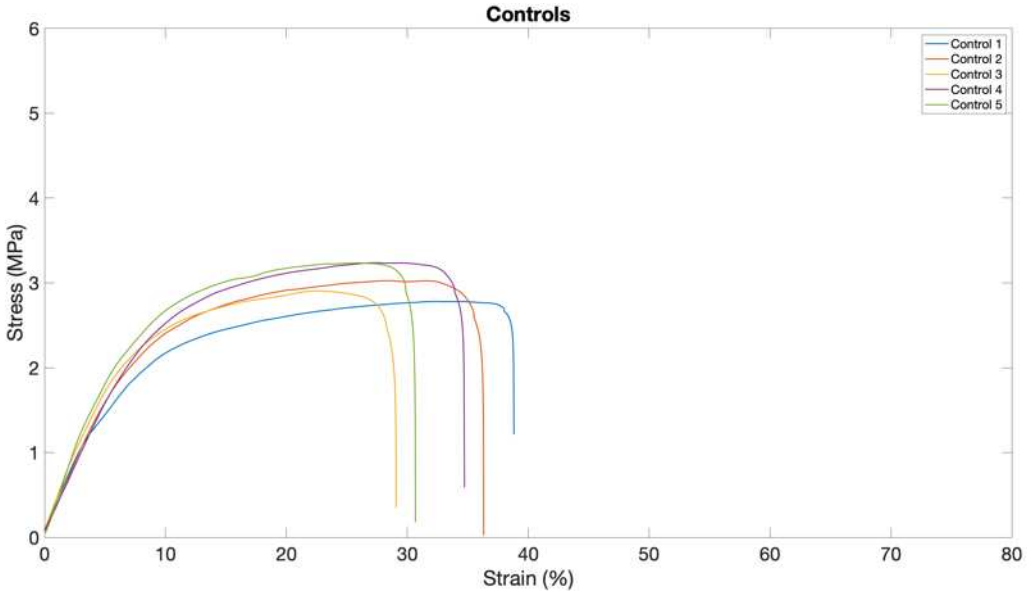

Figure 5.8: Stress vs strain data for control PP samples

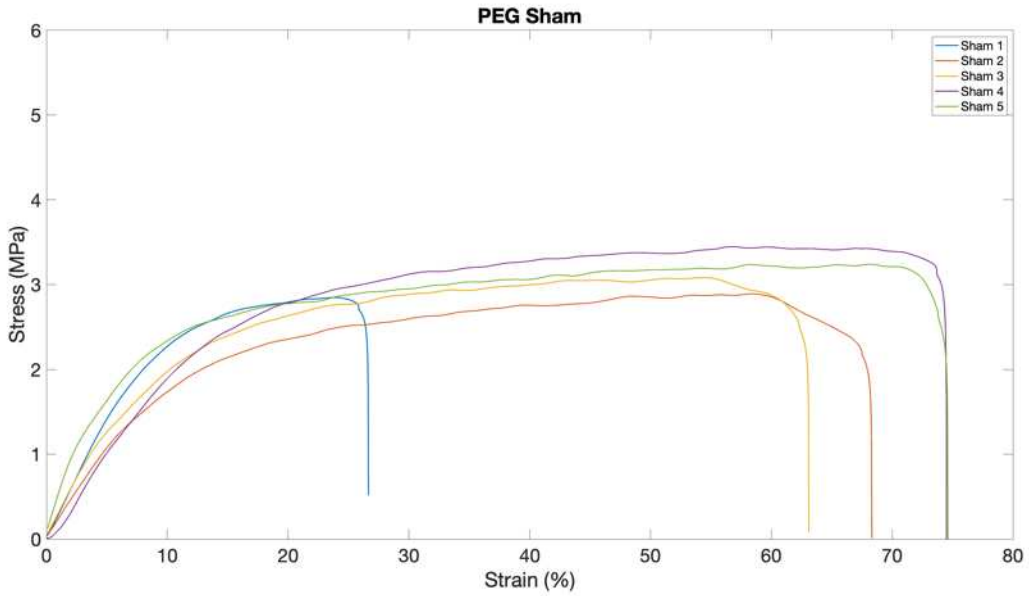

Figure 5.9: Stress vs strain data for PEG sham samples

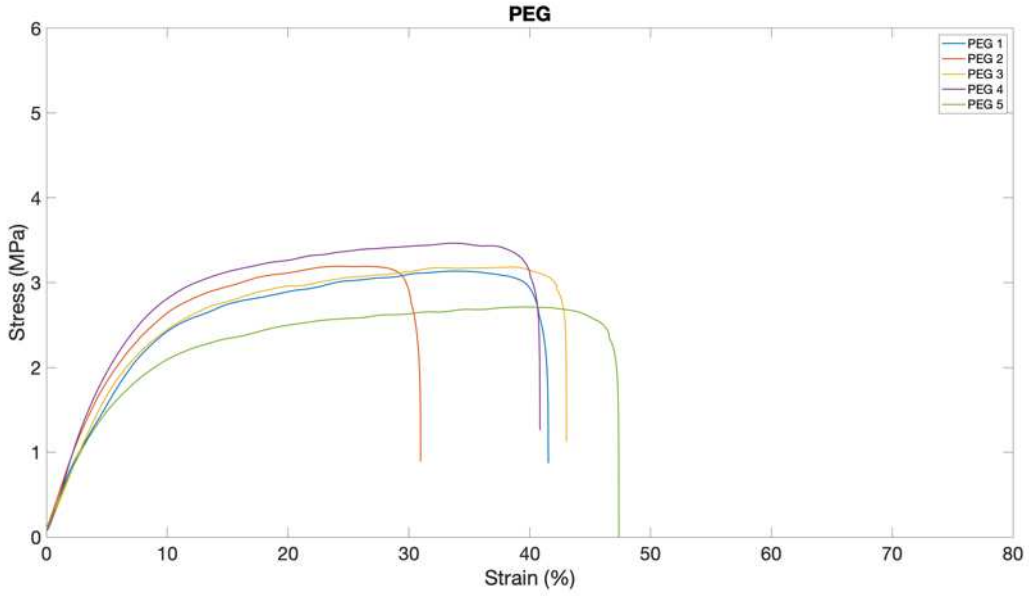

Figure 5.10: Stress vs strain data for PEG sham samples

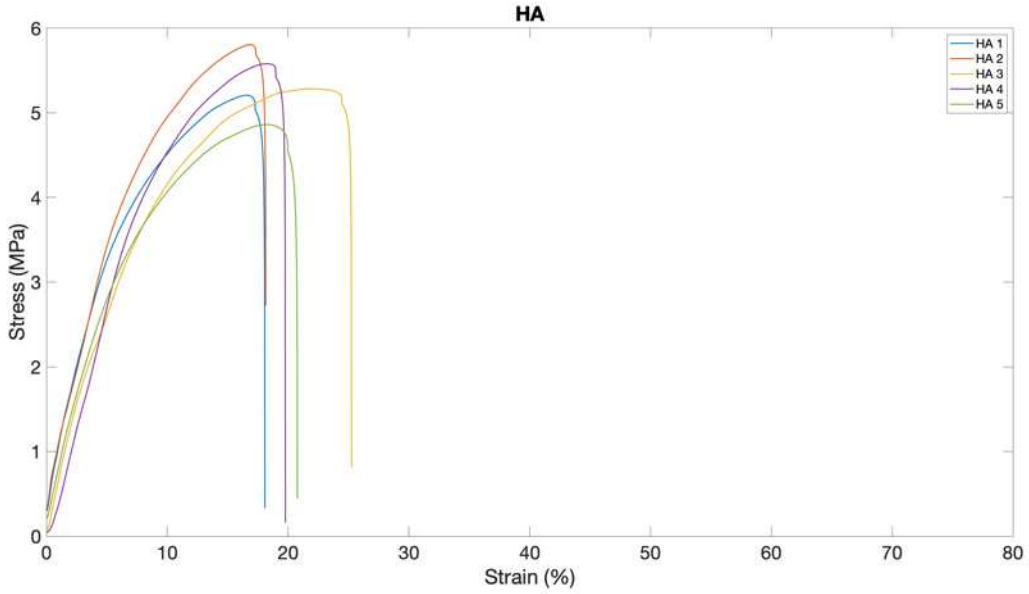

Figure 5.11: Stress vs strain data for HA samples.

5.6.3 Discussion

The PEG, PEG sham, and control samples did not have statistically different Youngs' moduli. With the exception the of outlying sample the PEG sham samples did have much greater strain to break (63% - 75%) compared to the PEG (31% - 47%) and control (29% - 39%) samples. The greater strain to break seen in the PEG sham samples may be due to soaking the non-woven PP in ethanol and methanol allowing the fabric to swell and disentangle. The PEG samples also underwent the soaking process indicating they too should have greater strain to break, however the introduction of the PEG molecules and grafting through plasma treatment most likely resulted in light crosslinking of the disentangled PP. The longevity over 28 days of the PEG as indicated by XPS and contact angle demonstrates the PEG is bound to the PP resulting in the potential for crosslinking the PP fibers.

The increased modulus and reduced strain to break seen in the HA samples is due to the creation of a secondary network of material being deposited over the surface and that network

being crosslinked in place. The crosslinked HA acts to reinforce the material at low strain, but restricts the movement of non-woven PP fibers resulting in lower strain at break.

All samples were stored in ambient conditions prior to testing, due to the demonstrated hydrophilicity of the PEG and HA samples it is likely the samples may have different tensile properties at high humidity.

5.7 Water Vapor Transmission Rate (WVTR)

WVTR was measured to understand the breathability of the treated and untreated polypropylene mask samples. W3/062 Water Vapor Transmission Rate Test System (Labthink, Boston, USA) was used which provided the WVTR in units of g/m^2-day. ASTM D6701-16 method was followed to conduct the experiment.

5.7.1 Methods

Six samples from each of the treated (HA, PEG and PEG sham) and untreated (control) masks were cut to instrument specification using the die cutter provided by the manufacturer. The samples were loaded on the machine and the experiments were initially conducted at 36°C and 82% relative humidity (RH). However, due to the hydrophilic and heavily porous nature of the samples (transmitters), transmission was beyond the measurement capability of the instrument. To continue the RH of the instrument was reduced to between 55~60%. All results presented were performed between 55~60% RH. WVTR was collected on days 1, 14 and 28 (weeks 1, 3, and 5). Each sample had 10 WVTR data points collected, resulting in 60 WVTR data points for each material at each timepoint. The average WVTR is reported. After each test, the samples were kept inside a ziplocked bag at room temperature and pressure.

5.7.2 Results

All treated mask samples had significantly higher WVTR compared the control during week 1 of testing, with the PEG and HA samples having greater transmission than the PEG Sham. The HA and PEG samples had a higher WVTR compared to the control during week 3, with the PEG Sham sample having lower transmission. Interestingly the PEG and PEG Sham samples had a higher transmission rate at week 5. While there were differences between samples and weeks all samples except for the PEG Sham had decreasing a WVTR over the study and all maintained high water vapor transmission as would be expected from a porous material. Figure 5.12 shows the WVTR results for each sample at day 1, 14, and 28.

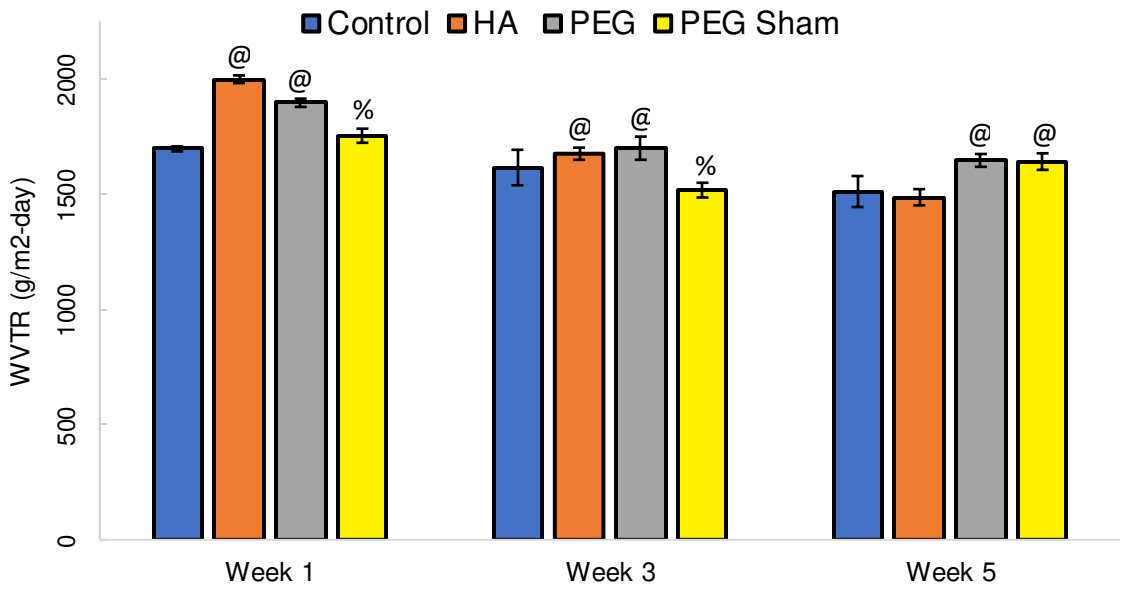

Figure 5.12: WVTR results for all timepoints for all treatment groups compared to that week's control sample. Columns sharing a symbol are not statistically different (p value < 0.05, n = 6) Column and error bars represent mean ± standard deviation.

5.7.3 Discussion

The WVTR of the HA samples reduced more compared to PEG and PEG Sham treatment and approached the transmission rate of the control samples over the course of the study. It should be noted that except for the PEG Sham all samples had a reduction in WVTR, but that the HA

samples had the greatest reduction. The most probable reason for this reduction in WVTR is the swelling of the HA microcomposite on the PP fibers caused a reduction of pore sizes of the material. Since the materials were stored in plastic between time points, they were unable to dry. This indicates that the HA treated samples retain water, but not to a degree that prevents breathability. In fact, all samples were either more breathable or not significantly less breathable than the control except the PEG Sham after 3 weeks. While the PEG Sham was lower after 3 weeks it was not so low as to cause concern. The WVTR results indicate that the treatment does not hinder the breathability of the PP fabric.

5.8 Cytotoxicity Assay

5.8.1 Methods

Samples were assessed for cytotoxicity using an LDH (Lactate Dehydrogenase) assay. Samples were rinsed using PBS (Phosphate-buffered saline) and sterilized using UV light for 15 mins. Smooth muscle cells were grown for 24 hours on the surface of each sample. After 24 hours of incubation with the cells, 50µL LDH reagent was added to 50µL of incubated cell solution and allowed to react for 30 minutes. Later 50µL stop solution was added to each well and the absorbance was measured at 600 nm using a plate reader (BMG Labtech FLUOstarOmega). A negative control was used to determine the maximum LDH release, in which the cells were lysed with 10% 50µL Triton-X100 solution. A positive control was used to determine the minimum LDH released from apoptosis, in which the cells were cultured on tissue culture polystyrene with no sample.

5.8.2 Results

All samples had significantly lower cytotoxicity expression than the negative control and were not significantly different from the positive control. Figure 5.13 shows the cytotoxicity test results.

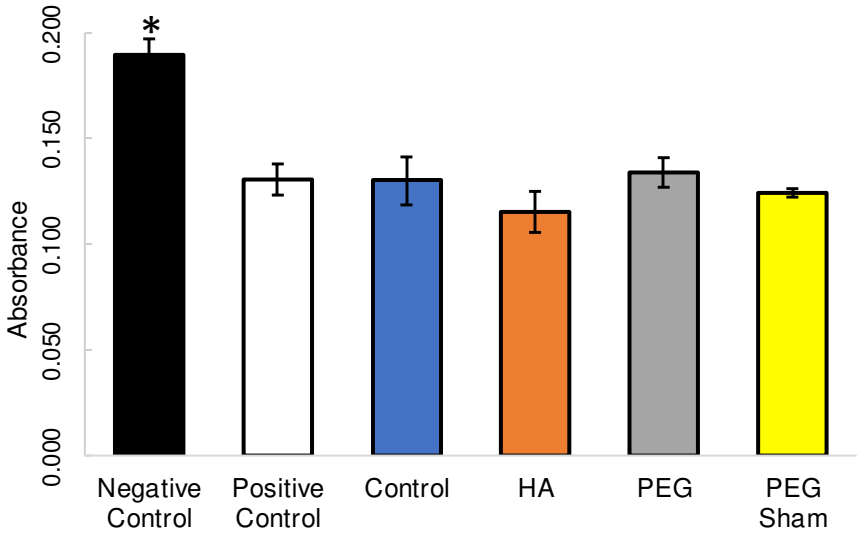

Figure 5.13: Cytotoxicity assay results for all treatment groups. All samples were significantly less cytotoxic than the negative control and no different than the positive control (p value < 0.05, n =3). Column and error bars represent mean ± standard deviation.

5.8.3 Discussion

As expected, each treatment group was not cytotoxic. While this was expected as previous studies of these treatments on other polyolefins were demonstrated to be non-cytotoxic, it was necessary to check each treatment considering this would be a skin contacting application.

5.9 Spike Protein ELISA

Traditionally enzyme-linked immunosorbent assays (ELISAs) are used to detect the presence of an antigen in a sample. Briefly a solution which may contain a certain antigen is introduced to a well plate and allowed to adhere to the surface, the rest of the surface is covered in a protein to which the antibody will not bind. Excess protein is washed away and the primary antibody with a

conjugated enzyme is added. This antibody has specific binding capacity for the antigen that the researcher wants to detect. Excess antibody is washed away and a substrate is added that causes a color change in the enzyme. This color change is analyzed with a spectrometer to determine the quantitative amount of antigen present[46].

While this study did not explore the specific binding of an antigen the ELISA was used to determine if the material treatment was able to bind the external spike protein found on the surface of the SARS-CoV-2 virion at higher rates than the untreated PP.

5.9.1 Methods

Prior to ELISA studies, all samples were sterilized using sterile PBS and incubated in protein solution (1 ug/ml) (Sinobiological, spike protein 40591-V08H SARS-CoV-2 (2019-nCoV) Spike S1-His Recombinant Protein) for 2 hours using a low attachment well plate. Protein solution was also incubated in empty wells as a positive control (the least adsorption possible). After this, the supernatants were collected and diluted 200-fold with assay buffer to obtain a protein solution in the standard curve range. The standard curve was obtained previously using the standards provided by the manufacturer (Sinobiological). The solutions' concentrations were then measured with an ELISA (Sinobiological, SARS-CoV-2 (2019-nCoV) Spike Protein ELISA Kit) with the following protocol: 100 ul of each diluted solution was added to the wells and incubated for 2 hrs. The wells were washed 4 times with wash buffer and 100 ul of detection antibody was added. After 1 hour of incubation, the antibody was aspirated, and the wells were washed 4 times. 100 ul of TMB (3,3′,5,5′-Tetramethylbenzidine) substrate solution was then added, followed by 20 mins incubation in dark environment. 100 ul of Stop Solution was then added and the optical density of each well was immediately measured at 450 nm. The concentrations were calculated using the standard curve and the values were subtracted from the positive control to obtain the amount of protein adsorbed on each surface. Data was analyzed using one-way ANOVA using GraphPad software.

5.9.2 Results

All samples had significantly higher adsorption of the spike protein compared to the control samples. Figure 5.14 shows the COV-Spike protein adsorption.

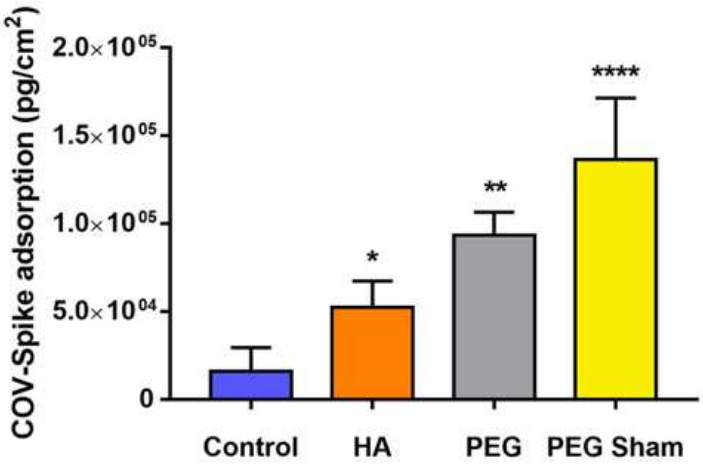

Figure 5.14: *Spike protein adsorption on nonwoven PP substrates. Asterisks indicates significance (p=0.05). Each sample was significantly different than all other samples as indicated by the different number of asterisks.*

5.9.3 Discussion

The significantly greater rates of spike protein adsorption indicate the HA and PEG treatments may be effective ways to treat nonwoven PP to further retain live SARS-COV-2. By preventing the live virus from detaching from a facemask or other PPE material that has SARS-COV-2, surface transmission of the virus may be greatly reduced. Interestingly the most effective method at adsorbing the spike protein was the PEG sham treatment. This indicates that the addition of active oxygen groups on the surface may be the most ideal way to trap SARS-COV-2 on the surface of PP, however the other treatment groups were also effective in increasing adsorption.

5.10 Chapter Conclusions

The treatment of nonwoven polypropylene with HA, PEG, and PEG sham all increased the adsorption of SARS-CoV-2 spike protein indicating they may help reduce COVID-19 transmission. Most interesting is that the PEG Sham treatment was most effective indicating that oxygen plasma treatment alone may be effective. However, further studies are warranted first would be to investigate irreversible adsorption of SAR-CoV-2 spike proteins followed by live virus studies to determine if these treatments are not only effective at trapping SAR-CoV-2 but also to determine if they are potentially viricidal. These further investigations could shed light on whether a low-cost process such as oxygen plasma treatment could significantly enhance PPE against COVID-19.

5.11 References

1. Jordà, Ò., Singh, S. R. & Taylor, A. M. Longer-Run Economic Consequences of Pandemics. *Rev. Econ. Stat.* **104**, 166–175 (2022).

2. Ma, C., Rogers, J. & Zhou, S. Modern Pandemics: Recession and Recovery. *J. Eur. Econ. Assoc.* jvad019 (2023) doi:10.1093/jeea/jvad019.

3. Bernstein, A. S. *et al.* The costs and benefits of primary prevention of zoonotic pandemics. *Sci. Adv.* **8**, eabl4183 (2022).

4. Di Marco, M. *et al.* Sustainable development must account for pandemic risk. *Proc. Natl. Acad. Sci.* **117**, 3888–3892 (2020).

5. Tripathi, A., Dhakal, H. C., Adhikari, K., Chandra Timsina, R. & Wahl, L. M. Estimating the risk of pandemic avian influenza. *J. Biol. Dyn.* **15**, 327–341 (2021).

6. CDC. Coronavirus Disease 2019 (COVID-19). *Centers for Disease Control and Prevention* https://www.cdc.gov/coronavirus/2019-ncov/index.html (2020).

7. CDC. Coronavirus Disease 2019 (COVID-19) PPE. *Centers for Disease Control and Prevention* https://www.cdc.gov/coronavirus/2019-ncov/hcp/using-ppe.html (2020).

8. Reddy, S. C., Valderrama, A. L. & Kuhar, D. T. Improving the Use of Personal Protective Equipment: Applying Lessons Learned. *Clin. Infect. Dis.* **69**, S165–S170 (2019).

9. Fischer, W. A., Weber, D. J. & Wohl, D. A. Personal Protective Equipment: Protecting Health Care Providers in an Ebola Outbreak. *Clin. Ther.* **37**, 2402–2410 (2015).

10. Kilinc, F. S. A Review of Isolation Gowns in Healthcare: Fabric and Gown Properties. *J. Eng. Fibers Fabr.* **10**, 180–190 (2015).

11. Vozzola, E., Overcash, M. & Griffing, E. Environmental considerations in the selection of isolation gowns: A life cycle assessment of reusable and disposable alternatives. *Am. J. Infect. Control* **46**, 881–886 (2018).

12. N95 Masks Explained | Honeywell. https://www.honeywell.com/content/honeywell/us/en/newsroom/news/2020/03/n95-masks-explained.html.

13. Lam, T.-N. *et al.* Multi-Scale Microstructure Investigation for a PM2.5 Air-Filter Efficiency Study of Non-Woven Polypropylene. *Quantum Beam Sci.* **3**, 20 (2019).

14. van Doremalen, N. *et al.* Aerosol and Surface Stability of SARS-CoV-2 as Compared with SARS-CoV-1. *N. Engl. J. Med.* **382**, 1564–1567 (2020).

15. Bui, H., Harris, K., Li, E., Prawel, D. & James, S. The Development and Fabrication of Vapor Crosslinked Hyaluronan-Polyethylene Interpenetrating Polymer Network as a Biomaterial. *ACS Appl. Mater. Interfaces* **11**, (2019).

16. Zhang, M., King, R., Hanes, M. & James, S. P. A novel ultra high molecular weight polyethylene–hyaluronan microcomposite for use in total joint replacements. I. Synthesis and physical/chemical characterization. *J. Biomed. Mater. Res. A* **78A**, 86–96 (2006).

17. Li, P. *et al.* Exogenous and endogenous hyaluronic acid reduces HIV infection of CD4+ T cells. *Immunol. Cell Biol.* **92**, 770–780 (2014).

18. Bui, H. T., Friederich, A. R., Li, E., Prawel, D. A. & James, S. P. Hyaluronan enhancement of expanded polytetrafluoroethylene cardiovascular grafts. *J. Biomater. Appl.* **33**, 52–63 (2018).

19. NIOSH guide to the selection and use of particulate respirators certified under 42 CFR 84. (2019) doi:10.26616/NIOSHPUB96101.

20. Polypropylene, UNIPOL Technology, Dow, Applications, Properties, Plastic, Polymer, Thermoplastic. *Am. J. Polym. Sci.* 11 (2016).

21. Rombaldoni, F. *et al.* Adhesion enhancement of electrospun nanofiber mats to polypropylene nonwoven fabric by low-temperature oxygen plasma treatment. *Surf. Coat. Technol.* **216**, 178–184 (2013).

22. Jaleh, B., Parvin, P., Wanichapichart, P., Saffar, A. P. & Reyhani, A. Induced super hydrophilicity due to surface modification of polypropylene membrane treated by O2 plasma. *Appl. Surf. Sci.* **257**, 1655–1659 (2010).

23. Juang, R.-S., Hou, W.-T., Huang, Y.-C., Tseng, Y.-C. & Huang, C. Surface hydrophilic modifications on polypropylene membranes by remote methane/oxygen mixture plasma discharges. *J. Taiwan Inst. Chem. Eng.* **65**, 420–426 (2016).

24. Abednejad, A. S., Amoabediny, G. & Ghaee, A. Surface modification of polypropylene membrane by polyethylene glycol graft polymerization. *Mater. Sci. Eng. C* **42**, 443–450 (2014).

25. Mason, M. *et al.* Attachment of hyaluronic acid to polypropylene, polystyrene, and polytetrafluoroethylene. *Biomaterials* **21**, 31–36 (2000).

26. Saxena, S., Ray, A. R. & Gupta, B. Chitosan immobilization on polyacrylic acid grafted polypropylene monofilament. *Carbohydr. Polym.* **82**, 1315–1322 (2010).

27. Gupta, B., Saxena, S. & Ray, A. Plasma induced graft polymerization of acrylic acid onto polypropylene monofilament. *J. Appl. Polym. Sci.* **107**, 324–330 (2008).

28. Zhu, N. *et al.* A Novel Coronavirus from Patients with Pneumonia in China, 2019. *N. Engl. J. Med.* **382**, 727–733 (2020).

29. Minaberry, Y., Chiappetta, D. A., Sosnik, A. & Jobbágy, M. Micro/Nanostructured Hyaluronic Acid Matrices with Tuned Swelling and Drug Release Properties. *Biomacromolecules* **14**, 1–9 (2013).

30. Shen, X., L. Shamshina, J., Berton, P., Gurau, G. & D. Rogers, R. Hydrogels based on cellulose and chitin: fabrication, properties, and applications. *Green Chem.* **18**, 53–75 (2016).

31. Guo, C. & Bailey, T. S. Highly distensible nanostructured elastic hydrogels from AB diblock and ABA triblock copolymer melt blends. *Soft Matter* **6**, 4807–4818 (2010).

32. Harrison, A. G., Lin, T. & Wang, P. Mechanisms of SARS-CoV-2 Transmission and Pathogenesis. *Trends Immunol.* **41**, 1100–1115 (2020).

33. Pandey, L. M. Surface engineering of personal protective equipments (PPEs) to prevent the contagious infections of SARS-CoV-2. *Surf. Eng.* **36**, 901–907 (2020).

34. Shajahan, A., Supekar, N. T., Gleinich, A. S. & Azadi, P. Deducing the N- and O-glycosylation profile of the spike protein of novel coronavirus SARS-CoV-2. *Glycobiology* **30**, 981–988 (2020).

35. Santos, M. C., Seabra, A. B., Pelegrino, M. T. & Haddad, P. S. Synthesis, characterization and cytotoxicity of glutathione- and PEG-glutathione-superparamagnetic iron oxide nanoparticles for nitric oxide delivery. *Appl. Surf. Sci.* **367**, 26–35 (2016).

36. Reznickova, A. *et al.* PEGylated gold nanoparticles: Stability, cytotoxicity and antibacterial activity. *Colloids Surf. Physicochem. Eng. Asp.* **560**, 26–34 (2019).

37. Jiang, G., Sun, J. & Ding, F. PEG-g-chitosan thermosensitive hydrogel for implant drug delivery: cytotoxicity, in vivo degradation and drug release. *J. Biomater. Sci. Polym. Ed.* **25**, 241–256 (2014).

38. Liu, G. *et al.* Cytotoxicity study of polyethylene glycol derivatives. *RSC Adv.* **7**, 18252–18259 (2017).

39. Prawel, D. A. *et al.* Hemocompatibility and Hemodynamics of Novel Hyaluronan–Polyethylene Materials for Flexible Heart Valve Leaflets. *Cardiovasc. Eng. Technol.* **5**, 70–81 (2014).

40. James, S., Oldinski, R., Zhang, M. & Schwartz, H. UHMWPE–Hyaluronan Microcomposite Biomaterials. in *UHMWPE Biomaterials Handbook* 412–433 (2016). doi:10.1016/B978-0-323-35401-1.00023-5.

41. Gangwish, J. *et al.* Treatment of nonwoven polypropylene to increase adsorption of SARS-CoV-2 spike protein. *Mater. Adv.* (2022) doi:10.1039/D2MA00614F.

42. Mirabella, F. M. *Internal reflection spectroscopy: theory and applications*. (Marcel Dekker, 1993).

43. Qian, H. *et al.* Indoor transmission of SARS-CoV-2. *Indoor Air* **31**, 639–645 (2021).

44. Klompas, M., Baker, M. A. & Rhee, C. Airborne Transmission of SARS-CoV-2: Theoretical Considerations and Available Evidence. *JAMA* **324**, 441–442 (2020).

45. Tang, S. *et al.* Aerosol transmission of SARS-CoV-2? Evidence, prevention and control. *Environ. Int.* **144**, 106039 (2020).

46. Berg, J. M. *Biochemistry Eighth edition by Berg, Jeremy M., Tymoczko, John L., Gatto, Gregory J., Stry e (2015) Hardcover*. (W. H. Freeman, 2015).

APPENDIX A: PROTOCOLS

A.1 HA-CTA Complexation

Objective

Hydrophobic modification of hyaluronan for reaction in anhydrous solvents

Materials and Equipment

- Sodium hyaluronan (NaHA)
- Cetyltrimethylammonium bromide (CTAB)
- Fresh Deionized water (DI H_2O)
- 1000 ml beaker or flask
- 500 ml beaker or flask
- Magnetic stir bars
- Stir plates
- Freezer mill/Cryogrinder
- Liquid nitrogen
- Hyaluronan-cetyl trimethylammonium complex (HA-CTA)
- Vacuum oven
- Vapor trap
- Vacuum pump
- Thermal gloves
- Safety glasses
- Buckner funnel
- Filter paper
- Erlenmeyer flasks

Procedure

1. Prepare a 0.30% w/v solution of sodium hyaluronan in DI H_2O. Minimize large clumps when adding NaHA.
   a. Example: 1.5g NaHA in 500 ml DI H_2O
   b. Stir the reaction at room temperature until the NaHA is completely dissolved. This can take several hours depending on the molecular weight of the NaHA. Stir for 15 hours to 3 days. Parafilm the beaker.
   c. When fully dissolved, the solution is clear.
   d. To get the NaHA into solution, turn the stir bar RPMs high enough to get a vortex on the top part of the stir bar for at least 5 mins. Then, turn the RPMs down to a low setting to form a little vortex.
   e. Record the following in lab notebook:

- Date, Time, Mass of NaHA (g) used, Volume of DI H_2O (mL) used, Dissolve Time (from start of mixing to when CTAB is added), Manufacturer, Lot Number, Part Number, and when the bottle of NaHA was opened.

2. Prepare a 1.00% w/v solution of CTAB in DI H_2O.
   a. Example: 1.69 g CTAB in 169 ml DI H_2O
   b. Stir the reaction at 40°C until the CTAB is completely dissolved. When dissolved, the solution will be clear. This takes 10-15 mins.
   c. Record the following in lab notebook:
      - Date, Time, Mass CTAB (g) used, Volume DI H_2O (mL) used, Dissolve time, Manufacturer, Lot Number, Part Number, and when bottle of CTAB was opened.
3. Slowly add the CTAB solution to the NaHA solution while under magnetic stirring. Parafilm the beaker. The mixture will become increasingly opaque as the CTAB solution is added. When the reaction is complete, a white precipitate forms and the supernatant is clear. Varying the addition rate affects the size of the precipitate (a slower addition rate produces a smaller precipitate). Stir for 15 hours – 36 hours.
   a. Record the following in lab notebook:
      - Date, and Time of addition.
4. The precipitate is HA-CTA. Collect and wash the HA-CTA to remove excess CTAB by vacuum filtration using a Buchner funnel. Use a vapor trap on the oven.
   a. Set up a Buckner funnel to two Erlenmeyer flasks. (pic)
   b. Place filter paper on the funnel and wet it using DI H_2O.
   c. Pour the HA-CTA/DI H_2O solution into the Buchner funnel slowly to prevent HA-CTA from getting under the filter paper.
   d. Rinse the HA-CTA with 500 ml DI H_2O.
   e. Use a spatula to scrape the HA-CTA into an Erlenmeyer flask with 300 ml DI H_2O.
   f. Cover the Erlenmeyer flask with a serum stopper and shake it for 30 seconds.
   g. Pour the contents of the Erlenmeyer flask in the Buchner funnel and vacuum off the water.
   h. A second time, rinse the HA-CTA with 500 ml DI H_2O.
   i. A second time, use a spatula to scrape the HA-CTA into an Erlenmeyer flask with 300 ml DI H_2O.
   j. Cover the Erlenmeyer flask with a serum stopper and shake it for 30 seconds.
   k. Pour the contents of the Erlenmeyer flask in the Buchner funnel and vacuum off the water.
   l. A third time, rinse the HA-CTA with 500 ml DI H_2O.
   m. A third time, use a spatula to scrape the HA-CTA into an Erlenmeyer flask with 300 ml DI H_2O.
   n. Cover the Erlenmeyer flask with a serum stopper and shake it for 30 seconds.
   o. Pour the contents of the Erlenmeyer flask in the Buchner funnel and vacuum off the water.
   p. A fourth time, rinse the HA-CTA with 500 ml DI H_2O.
   q. A fifth time, rinse the HA-CTA with 500 ml DI H_2O.
   r. Move the HA-CTA to the center of the filter paper, and carefully place the filter paper inside a petri dish. Spread the HA-CTA out.
   s. Place the petri dish and filter paper in a vacuum oven to dry at 50°C for 3 days. Occasionally wipe the water off the inside of the oven door. Be sure to watch vapor traps to make sure they don't fill and are functioning correctly. <<note: combine with 5 below>>
   t. Record the following in lab notebook:
      - Date, Process Start Time, Process End Time, and Oven in Time.

5. Dry HA-CTA in a vacuum oven (-25 in Hg, 50°C) for 3 days or until no change in weight is observed. A yield of about 2.5 g HA-CTA is expected for a starting NaHA weight of 1.5 g.
6. Grind the dried HA-CTA to a powder using a freezer mill/cryogrinder.
    a. Wear thermal gloves and safety glasses.
    b. Slowly fill the cryogrinder with liquid nitrogen to the fill line. This typically requires about 5L of liquid nitrogen and will cool the cryogrinder down. Close the top cover and let the cryogrinder sit until vapor stops coming out of the rear vent.
    c. Weigh the HA-CTA and record the weight.
    d. Place the bottom cap on a cryogrinder tube, and place half of the HA-CTA into the tube with a magnet.
    e. Place the top on the cryogrinder tube, with the slotted end towards the outside so that it can be removed using the "tool".
    f. Insert the cryogrinder tube into the cryogrinder so that the cap slot is aligned with the end of the tube chamber.
    g. Use a low impact frequency for a total of 12 mins.
    h. Collect the HA-CTA powder in a 50 ml centrifuge tube.
    i. Repeat the previous steps to cryogrind the remaining half of the HA-CTA.
    j. Periodically check the liquid nitrogen level and add more if needed.
    k. Clean cryogrinder tubes with 2% Liquinox and DI H_2O. **Do not use solvents, including acetone**. Clean metal caps and magnet with 2% Liquinox, DI H_2O, and acetone.
    l. Record the following in lab notebook:
        - Date, Process Start Time, Grind Time, Process End Time, and Oven in Time
7. Dry the ground HA-CTA in a vacuum oven (-25 mm Hg, 50°C) for 24 hours or until no change in weight is observed.
8. When dry, HA-CTA should be stored in a desiccator.

A.2 HA-CTA Silylation

Objective

Hydrophobic modification of hyaluronan for reaction in anhydrous solvents

Materials & Equipment

- Hyaluronan-cetyl trimethylammonium complex (HA-CTA)
- Dimethyl sulfoxide ≥99.9% ReagentPlus (DMSO) – Part # 276855
- Hexamethyldisilazane ≥99.9% ReagentPlus (HMDS ≥ 99.9% ReagentPlus) – Part # 44019
- Xylenes dried over sieves (250 ml)
- 500 ml Round Bottom Flask (RBF) – 2x
- Graduated cylinders (25 mL, 100 mL)
- Crystalizing dish
- Separatory funnel -125 mL
- Serum stoppers
- Copper wire
- Needle nose pliers
- Keck clips
- Condenser
- Dry Nitrogen (N_2) gas
- Magnetic stir bars
- Stir plates
- Vacuum oven
- Vapor trap
- Vacuum pump

Before beginning the procedure, ensure that the HA-CTA has been sitting in the oven at 50° C the night before to dry the reactant as much as possible.

Procedure

Glassware preparation

Acid Bath Cleaning Method for Glassware:

Before beginning, remember to take proper safety precautions. Cover yourself with the appropriate PPE (lab coat, face shield, acid resistant gloves in addition to rubber latex gloves, closed toed shoes, etc.) in order to avoid contact with the acid that you will be using. Tuck lab coat into the acid resistant gloves for optimal coverage. If the acid resistant gloves are loose around the wrist, use rubber bands to create a tighter fit.

1. Begin by turning on the faucet and allow for water to flow constantly.
2. Bring the acid bath over to the sink and remove the lid.
    a. This can be accomplished by pushing in the red clip on the cap of the bucket while simultaneously rotating the cap counterclockwise until the cap detaches from the threads of the bucket.

3. Take each piece of glassware needed for silylation and ensure that it is submerged in the acid bath, all the while taking note of any splashing or bubbling that could potentially cause bodily harm. This is especially important in regard to RBF's as they tend to sputter if they are submerged too quickly, so it is always best to do this step slowly.
    a. Make note of which hand is being used to transfer the glassware from the counter next to the sink (dry hand) and which hand is submerging the glassware in the acid bath (wet hand).
    b. It is important to keep the wet hand over the bucket in order to minimize dripping or spilling.
4. Once all glassware has been placed in the acid bath, liberally rinse the acid-resistant gloves with running water. Make sure to take time on this step, washing between folds in the rubber and between fingers where acid could potentially remain.
5. Once rinsed thoroughly, dry with paper towels.
6. After rinsing the gloves, cap the bucket. Then move the securely closed acid bath with all glassware back to the holding area at the north end of the lab.
    a. While transferring the acid bath, do so gently. The glassware is fragile, and oftentimes placed in awkward positions in the bath itself to ensure the best submersion possible.
7. Remove rubber bands and acid resistant gloves and set atop the acid bath bucket.
8. Allow for the glassware to sit for at least 24 hours in acid bath.
9. Before removal, once again make sure that all safety precautions are being taken before working with the acid bath and that all PPE guidelines are being followed accordingly.
10. Once again, allow for both tap and DI H_2O to run constantly in the sink before bringing the acid bath over.
11. Begin by removing each piece of glassware while remembering to maintain a wet acid hand and a water/rinse hand.
    a. Once again, the acid hand should be held over the bucket to reduce the chance of drips/spills.
12. Each piece of glassware should be rinsed thoroughly first with tap water, and then finally with DI water.
13. Once all pieces of glassware have been rinsed, place them in the oven until dry.
14. The capping and transfer process of the acid bath does not change from the previous process.
    a. Always take care to move slowly and surely with the bath and be on the lookout for any missed drips on the floor.

Silylation of Glassware:

1. Once the glassware is dry, remove it from the oven and allow for it to cool to room temp.
2. When cool, reserve one 25 mL graduated cylinder for 5 mL of HMDS, the rest of the cooled glassware can be placed in the oven.
3. Add 5 ml HMDS to the 25 mL graduated cylinder
4. Place the 25 mL graduated cylinder containing the 5 mL of HMDS in the oven with the rest of the glassware.
5. Turn off the main (blue) vacuum pump and disconnect the outlet tubing.
6. Attach the solvent resistant welch vacuum pump on top of the vacuum pump with the red tubing
7. Pull vacuum to -20 in.Hg, close the vacuum pump valve and shut off the pump itself. At this point, both the atmosphere and vacuum valves should be closed.
8. Turn the heat knob to 150°C and turn on the heat switch on the vacuum oven. At this point the glassware will be left in the oven for 1.5 hours

9. Wait 30 minutes and check the temperature of the oven by looking at the internal thermometer.
10. After 1.5 hours vent the chamber 5 times.
    a. Open the oven to atmosphere letting the pressure reach 0 in.Hg
    b. Close the oven to atmosphere and use the welch pump to pull vacuum to -20 in.Hg
11. Repeat these steps 3 times.
12. Remove the red tubing and reattach the main vacuum pump.
13. Turn on the main pump and leave the glassware under vacuum for the duration of the silylation reaction except when retrieving glassware for use.

Add DMSO

Note: DMSO is light sensitive. Be sure to minimize exposure to hood light and outside light.

1. Use a pre–silylated 100 ml graduated cylinder and a 500 ml RBF.
2. Place a stir bar and the cryoground HA-CTA powder into a 500 ml single neck RBF.
    a. Be sure a sample for FTIR was taken.
3. Cap the RBF and a graduated cylinder with rubber stoppers and copper wire. The copper wire should be tight and pinch into the rubber.
4. Turn on the dry nitrogen and adjust to a low flow rate.
5. Vent the RBF and graduated cylinder with dry N_2. Depending on the nitrogen flow, venting five times for five seconds each time is recommended.
6. Add 50 ml of DMSO for every 1.5g of starting HA-CTA to the RBF via a cannula and dry N_2. Maintain positive pressure in the graduated cylinder and RBF. Mark the number of punctures in tally form on the bottle.
7. Swell the HA-CTA in the DMSO at room temperature. (about 4-12 hours).
8. Lower the RBF into a 50°C oil bath and continue to stir until the starting material is fully dissolved (4-24 hrs). DMSO/HA-CTA solution should gel preventing the stir bar from turning once the HA-CTA is “dissolved”
    a. Make sure the thermocouple light on the hot plate is turned on.
9. Record the following in lab notebook:
    a. Date, Time, Manufacturer, Lot number, Part number, date the bottle of DMSO was opened, and time the heat was turned on.

Add HMDS

1. Silylate a 25 ml graduated cylinder.
2. Cap a graduated cylinder with a rubber stopper and copper wire. The copper wire should be tight and pinch into the rubber.
3. Vent the graduated cylinder with dry N_2before adding HMDS. Depending on the nitrogen flow, venting five times for five seconds each time is recommended.
4. Add 25 ml of HMDS ≥dd 25 mReagentPlus for every 1.5g of starting HA-CTA to the RBF via a cannula and dry N_2while maintaining positive pressure in the graduated cylinder and RBF. Increase the temperature of the oil bath to 75°C for 24 hrs. Vigorous stirring is important to mix the HMDS and DMSO layers. Mark the number of punctures in tally form on the bottle. Solution should go from gel to liquid within 10-15 minutes
    a. Make sure the thermocouple light on the hot plate is turned on.
5. Turn the heat to 60 °C after 24 hrs and allow to stir for an additional 48 hrs. (72 hours total)

6. Periodically check stirring and hot plate temperature. Stirring is important for mixing the DMSO and HMDS to increase the degree of silylation.
7. Record the following in lab notebook:
    a. Date, Time, Manufacturer, Lot Number, Part Number, and when the bottle of HMDS was opened.

Separating and washing silyl HA-CTA

1. Cool the reaction to room temperature.
2. Silylate a separatory funnel and a crystallizing dish.
3. Pour the reaction mixture into a 250 ml separatory funnel (125 ml works as well), and let the two phases separate for at least 60 minutes.
4. The **upper** layer contains HMDS and silylated HA-CTA.
5. The bottom layer is DMSO.
6. Let the DMSO drain into an Erlenmeyer flask, and dispose of the DMSO into a hazardous waste bottle **only after you have washed (see below) SHACTA** to avoid disposing SHACTA into hazardous waste .
7. Let the upper layer drain into the second vapor silylated RBF. This RBF now contains the silyl HA-CTA.
8. Close the separatory funnel stopper and add 10 ml of **dry** xylenes. Cap the funnel and swirl the xylenes to rinse the funnel. Collect the xylenes into the RBF containing the silyl HA-CTA. The purpose of this rinse step is to increase the yield of silyl HA-CTA.
9. Wash the silyl HA-CTA using a rotavap. (This helps remove residual DMSO from the final Silyl HA product).
10. Fill the bowl of the rotavap with DI H_2O.
11. Heat the DI H_2O to 60-70°C. If the water heats to 75°C, cool it down to prevent degradation of the silyl HA-CTA.
12. Apply vacuum grease to the two stopcocks, to the top surface of the cold finger, and to the inside surface of the RBF condenser as needed (see how to grease a stopcock by Mike).
13. Place the cold finger inside the outer condensing column.
14. Place the rubber gasket flat against the rotavap arm as seen in Figure XX.
15. Screw the grey clamp partially on as seen in Figure XX.
16. Hold the edge of the coldfinger flat against the gasket and screw the grey piece until snug.
17. Attach the RBF condenser using a keck clip.
18. Fill the inner cold finger with ice.
19. Check vacuum tubing connection between the coldfinger and pump.
    a. Follow pump protocols taped to front of fume hood along with below.
        i. Make sure the exhaust port of the pump is not blocked by the back wall of the fume hood (or anything else).
        ii. Run the pump for a few (2-3) minutes before connecting it to the rotovap until it has warmed up.
        iii. Once finished rotovapping, let the pump run for three minutes disconnected from the system to make sure no vapors remain in the pump.
20. Lower the rotavap arm using the lever so that the RBF containing silyl HA-CTA is partially submerged in water but still able to rotate.
21. Turn the vacuum pump strength to low, and turn the pump on. Wait for the vacuum to pull through the system.
22. Set the rotation speed to 60RPM.

23. Slowly increase the strength of the vacuum until vapor is pulled into the cold finger. Be careful to avoid boiling the solution because this could decrease the yield of silyl HA-CTA by pulling it into the cold finger.
24. When the silyl HA-CTA is mostly dry, turn the rotation off, turn the vacuum pump strength down, and turn the vacuum pump off.
    a. At this point, the silyl HA-CTA should be thick like honey, or thicker.
25. Raise the rotavap arm using the lever.
26. Release the vacuum from the system using the upper stopcock, and let air back into the tubing by opening and closing the stopcock a few times.
27. Gently twist and pull the RBF containing silyl HA-CTA off of the rotavap.
28. Add 40 ml of **dry** xylenes to the RBF, cover with a serum stopper, and dissolve the silyl HA-CTA by swirling the flask.
29. When dissolved, uncap the RBF and attach it to the rotavap using a keck clip.
30. Wash the dry xylenes as in the previous steps.
31. Add dry xylenes 4 more times and wash as described, for a total of 5 washes with xylenes (in addition to the first wash in HMDS).
    a. The sample should be allowed to crystallize on washes 2 and 4 and the time recorded for the sample to dissolve back into xylenes recorded.
32. On the last wash, leave a few milliliters (~5 ml) of xylenes in the flask.
33. Pour the silyl HA-CTA/xylenes into a silylated crystallizing dish.
34. Add 5 ml more xylenes to the RBF to dissolve any remaining silyl HA-CTA, and pour it into the same crystallizing dish.
35.

36. Dry Silyl HA overnight at room temp.
    a. Cover with aluminum foil that has holes in it. Puncture the aluminum **before** covering the silyl HA in order to avoid contamination.
37. Dry the silyl HA-CTA at 50°C using a vapor trap until no weight change is observed. Save a sample for NMR analysis. A yield of 2.5-3.0 g of silyl HA-CTA is expected when starting with 1.5 g NaHA.Dry Silyl HA overnight at room temp.
    a. Cover with aluminum foil that has holes in it. Puncture the aluminum **before** covering the silyl HA in order to avoid contamination.
38. Record the following in lab notebook:
    a. Date, Time, Oven in Time, Oven out Time, and Final Weight.
39. Record all information in the Silyl HA Tracker in the BREL drive.

Note

- Cannula transfers should be done with at least two people. Never try a cannula transfer alone.

A.3 SHACTA Treatment of LLDPE

Objective

Linear low-density polyethylene (LLDPE) will be integrated with silylated hyaluronan-cetyltrimethylammonium complex (SHACTA) by swelling the LLDPE in a solution of SHACTA and xylenes followed by vapor cross-linking. The volumes and masses given in this procedure are specific for 2 cm x 3 cm LLDPE samples.

Materials & Equipment

- One 250 mL (or 500 mL) round-bottom flask *(Vapor Silylation)*
- Small crystallizing dish *(Vapor Silylation)*
- 100 mL graduated cylinder *(Vapor Silylation)*
- 25 mL graduated cylinder *(Vapor Silylation)*
- 100 mL glass jars with caps *(Vapor Silylation)(<u>One for each film being treated</u>)*
- 125 ml Erlenmeyer flask *(Vapor Silylation)*
- Two 60 ml beakers *(Vapor Silylation) (<u>One for each film being treated</u>)*
- Two Glass funnels *(Vapor Silylation)*
- One 600 ml beaker *(Vapor silylation) (Optional for transfer of SHACTA/xylene solution)*
- Large crystallizing dish
- Dowlex 2045G LLDPE films
- Fiskars Rotary Fabric Cutter
- Xylenes on activated sieves
- Solvent vacuum oven
- Teflon stoppers
- Teflon stir bars
- SHACTA
- Hot plate with thermal probe
- Heating block
- Infrared thermometer
- Metal binder clips
- Teflon scaffolds
- Needle-nosed tweezers
- Toluene 2,4-diisocyanate (TDI)
- P1000 Micropipette and tip
- Half-moon Teflon blocks
- NaCl
- Ethanol
- Small jars

<u>Notes before starting</u>
Untreated LLDPE films can be cleaned in bulk and stored.
TDI is extremely toxic, handle with extreme care.
All xylenes used should be dried on activated molecular sieves (except for xylenes used in first step “Preparing LLDPE films”)

Procedure

Preparing LLDPE Films

1. Use Fiskars rotary fabric cutter to cut out LLDPE films approximately the size of the Teflon scaffolds.
2. Put LLDPE films in a jar, pour in enough acetone to submerge the films, and rinse.
3. Soak the films in xylenes for 12 hours at room temperature. Xylenes do not have to be distilled.
4. If treatment is planned for the next day, prepare the following glassware (wash and silylate):
    1. A slow-draining fritted funnel for every 2 samples.
    2. Round-bottom flask (RBF) large enough for 40 mL of solution per 2 samples. E.g., For 4 samples, the RBF needs to hold at least 80 mL of solution.
    3. 100 mL graduated cylinder
    4. One medium glass jar (that can be capped) for every 2 samples.
5. Pull films from xylenes, rinse with acetone.
6. Line a large crystallizing dish with a large kimwipe.
7. Place clean films into lined crystallizing dish. Ensure they do not touch the glass.
8. Dry films in solvent vacuum oven for at least 3 hours. Store in a labeled jar.

Silylation of Glassware

1. Once the glassware is dry, remove it from the oven and allow for it to cool to room temp.
2. When cool, reserve one 25 mL graduated cylinder for 5 mL of HMDS, the rest of the cooled glassware can be placed in the oven.
3. Add 5 ml HMDS to the 25 mL graduated cylinder.
4. Place the 25 mL graduated cylinder containing the 5 mL of HMDS in the oven with the rest of the glassware.
5. Turn off the main (blue) vacuum pump and disconnect the outlet tubing.
6. Attach the solvent resistant welch vacuum pump on top of the vacuum pump with the red tubing.
7. Pull vacuum to -20 inHg, close the vacuum pump valve and shut off the pump itself. At this point, both the atmosphere and vacuum valves should be closed.
8. Turn the heat knob to 150°C and turn on the heat switch on the vacuum oven. At this point the glassware will be left in the oven for 1.5 hours
9. Wait 30 minutes and check the temperature of the oven by looking at the internal thermometer.
10. After 1.5 hours vent the chamber 5 times.
    1. Open the oven to atmosphere letting the pressure reach 0 inHg
    2. Close the oven to atmosphere and use the welch pump to pull vacuum to -20 inHg
11. Repeat these steps 3 times.
12. Remove the red tubing and reattach the main vacuum pump.
13. Turn on the main pump and leave the glassware under vacuum for the duration of the silylation reaction except when retrieving glassware for use.

Swelling in SHACTA and Xylenes Solution

1. Prepare a 1% (w/v) solution of SHACTA and xylenes, 60 mL for every sample.
   Example 1 – 1 gram of SHACTA in 100 ml dry xylenes
   Example 2 – 0.5 grams of SHACTA in 50 ml dry xylenes

a. Measure out the SHACTA into the silylated RBF.
b. Collect a Teflon stir bar, Teflon stopper, RBF with SHACTA, silylated graduated cylinder, and dried xylenes.
c. Add the appropriate volume of xylenes for a 1% (w/v) SHACTA xylenes solution.
d. Stir at 50°C until all the SHACTA is dissolved.
2. Warm heating block to 55°C. Setting on block should be around 63°C causing the average measured by the infrared thermometer to be 55 °C from top and bottom of tape on aluminum mantle.
3. Place medium glass jars in the block.
4. Clip one LLDPE film to one scaffold with two binder clips.
5. Gently blow samples with nitrogen to get rid of any dust.
6. Use an infrared thermometer to confirm the heating block has reached 50°C.
7. Place the samples into the glass jars, one construct per jar.
8. Measure out 60-65 mL of SHACTA solution into each jar.
9. Cap jars and swell for two hours.
10. Preheat vacuum oven to 50 °C.

Rotavap can be set up during this time.

Film Elevator Prep

1. Ensure batteries are fully charged.
2. Determine rate of withdrawal and check “Rate of Elevation vs Dial setting” PDF
3. Reset screw to 11/32 inch (drop from seat at about 6/32”)
4. Turn on Elevator briefly to ensure motor is functioning and gears are locked in and turning.

11. Disconnect the solvent vacuum from the pump and connect it to the blue vacuum pump.
12. Remove gasket from oven and place film elevator inside along with Teflon block and 60 ml beakers, replace gasket.
13. After swelling is complete (two hours) use needle-nosed tweezers to extract the samples from the jars
14. Place hooks back on one binder clip
15. Hang films from elevator aluminum rod.
16. Pour the SHACTA solution into the beakers.
17. Place films into beakers with SHACTA solution with Teflon block underneath
18. Keep air flowing out of the oven while the house vacuum continually pumps it down to maintain a pressure at -15 in. Hg while films are lifted from solution.
19. When draining is complete hang films over beaker or place in clean crystalizing dish with kimwipe.
20. Recover SHACTA from solution with rotavap and collect in a silylated small crystallizing dish.

<u>Vapor Cross-Linking</u>

1. Prepare a 10% (v/v) toluene diisocyanate (TDI) solution in xylenes, 10 mL per sample.
   Note: TDI is extremely volatile and toxic, use with great care.
   a. Collect a P1000 micropipette (set at the correct volume for TDI), its tip, TDI, a kimwipe, distilled xylenes, a silylated graduated cylinder, a 125 mL Erlenmeyer flask with a stir bar, and a Teflon stopper.
   b. Measure out the correct volume of TDI with the micropipette into the Erlenmeyer.
   c. Measure out the correct volume of xylenes into the Erlenmeyer.
   d. Place stopper in the Erlenmeyer and stir for 15 minutes.
2. Keep the pipette tip that contacted TDI in the fume hood.

3. Warm the heating block up to 60°C. (Set at 68 °C)
    a. Note the heating block heats unevenly and should have an average of 60 °C the bottom will be about 8-10°low and the top 8-10° high.
4. Place a half-moon shaped Teflon block in each glass jar (1 per sample) with the flat side up and warm them in the heating block.
5. Secure both ends of each LLDPE sample to its own, individual, Teflon scaffold.
6. Use the infrared thermometer to confirm that the heating block has reached 60°C.
7. Collect the TDI solution, graduated cylinder from step 1 (rinsed with acetone), caps for each jar, and LLDPE samples.
8. Pour 10 mL of the TDI solution into each jar. Do not pour directly onto the Teflon block. Warm the solutions up in the heating block for 2-3 minutes.
9. Place the samples on top of the Teflon blocks. Make sure the samples do not touch the Teflon block. (i.e. the order from bottom up should be half-moon Teflon block, Teflon scaffold, sample).
10. Cap tightly, cross link for one hour in the glove bag.
11. Remove samples from Teflon scaffolds and dry in the solvent vacuum oven on a kimwipe-lined crystallizing dish.

<u>Hydrolysis</u>

1. Prepare a 1:1 solution of 0.2M NaCl to ethanol, about 150 mL per sample.
    1. Ex 2.34g NaCl in 200 ml DI water then add 200 ml ethanol.
        2. 0.2 (mols NaCl) *58.44 (g/mol NaCl)*0.2 (l DI water) = 2.34 g NaCl
            1. Note 0.2 M solution is for NaCl in DI water and the final solution is 0.25 M
2. Run sonicator for 30 minutes to de-gas.
3. Place each sample into a small glass jar. Fill each jar with roughly 50 mL of hydrolyzing solution and sonicate for 60 minutes. Keep the temperature between 30°C and 40°C.
4. Repeat for 3 total cycles, 60 minutes each. Switch the solution out each time.
5. Prepare a 0.2 M NaCl solution, about 50 mL per sample.
6. Use tweezers to pull the samples out of the NaCl ethanol solution and rinse with DI water.
7. Place samples in new small jars.
8. Fill the jars with roughly 50 mL of the 0.2M NaCl solution.
9. Sonicate for 60 minutes. Keep the temperature under 40°C.
10. Prepare a 3:2 solution of water: ethanol, 50 mL per sample.
11. Use tweezers to pull the samples out of the 0.2M NaCl solution and rinse with DI water.
12. Place samples in new small jars.
13. Fill the jars with water: ethanol solution, cover with watch glasses, and let sit for at least 2 hours.
14. Rinse samples with DI water and put them in new small jars.
15. Sonicate for 30 minutes in DI water.
16. Dry in the water oven on a kimwipe-lined crystallizing dish.

A.4 Melt Pressing Radiopaque Powders into LLDPE

Objective

Embed known radiopacifiers into LLDPE to render the material radiopaque.

Materials & Equipment

- Heat or melt press (the Carver model C manual heat press in the SAMDCore laboratory was used for tis work)
- Analytical balance
- 6 cm x 6 cm sheets of LLDPE (Clean)
- Kapton sheets
- Radiopacifiers (tungsten, bismuth trioxide, barium sulfate)

Procedure

Preparing LLDPE films

9. Cut 6 cm x 6 cm LLDPE films.
10. Put LLDPE films in a jar, pour in enough xylenes to submerge the films.
11. Soak the films in xylenes for 12 hours at room temperature.
12. Pull films from xylenes, rinse with acetone.
13. Line a large crystallizing dish with a large kimwipe.
14. Place clean films into lined crystallizing dish.
15. Dry films in solvent vacuum oven for at least 3 hours.

Melt pressing radiopacifiers into LLDPE films

Always use thermal gloves when using the melt press or handling materials from the melt press!

1. Turn on heat press to 150 °C and allow it to heat completely.
    a. Aluminum plates should be removed before heating and should be cooled between each press. Note they do not need to be room temperature but should be cool enough to touch and handle before each press.
2. Weigh two 6 cm x 6 cm LLDPE films.
3. Record the mass of the two films.
4. Calculate the amount of radiopacifier needed for the weight percent desired.
    a. Ex. For a 70% tungsten film with the LLDPE films (both) weighing one gram, 0.700 grams of tungsten would be needed.
    b. This assumes 100% of radiopacifier is embedded, however when adding the radiopacifier some is generally lost so 10-20% above the calculated mass is recommended.
5. Place one film on a Kapton sheet and tare the balance to zero.
6. Sprinkle radiopacifier onto the LLDPE sheet.
7. Record the mass of the radiopacifier added.

8. Place the second LLDPE sheet on top of the first LLDPE sheet and radiopacifier.
    a. This should be a “sandwich”. LLDPE – Radiopacifier – LLDPE
9. Place a second sheet of Kapton over the LLDPE-radiopacifier sandwich.
10. Place the LLDPE-radiopacifier sandwich between the Kapton sheets in between the aluminum plates.
    a. From top to bottom the layers should be aluminum plate – Kapton – LLDPE – radiopacifier – LLDPE – Kapton – aluminum plate.
11. Place the entire construct into the melt press and apply pressure to no more than 100 PSI for 3 minutes.
    a. Between 50 – 100 PSI is ideal as this LLDPE needs to melt, but does not need significant pressure to embed the radiopacifiers.
12. After 3 minutes remove the plates from the heat press and remove the Kapton – LLDPE – radiopacifier – LLDPE – Kapton sandwich from the plates and allow it to cool for at least 3 minutes
13. Weigh the final radiopacified LLDPE film.
14. Determine the mass percent of the radiopacifier.
    a. Ex. Original LLDPE weighed 1.000 gram and the final construct weighs 1.682 grams. (1.682 – 1.000)/(1.000) * 100 = 68.2 % tungsten (w/w).
15. If melt pressing multiple samples wait for aluminum plates to cool until they can be handled without thermal gloves.
    a. This is because LLDPE begins melting around 100 °C and will cause repeatability issues if the Kapton – LLDPE – radiopacifier – LLDPE – Kapton is placed on already hot plates.

A.5 Toluidine Blue O Staining Assay

Objective

TBO (toluidine blue O) assay is used to identify acidic tissue molecules. On HA-LLDPE treated samples, TBO binds to the carboxyl groups in HA staining them blue/purple, differentiating them from the cross-linker and the LLDPE film.

Materials & Equipment

- Scintillation vial & cap
- Small stir bar
- TBO
- Urea
- X-Acto knife
- Needle

Notes before starting

TBO stained items can be cleaned with ethanol or 2% Liquinox.
Use stir bars that already appear to be stained blue if possible.

Procedure

Prepping HA-LLDPE Samples

1. Hydrate samples in DI H_2O for at least 24 hours prior to staining
2. Dry samples with a Kim Tech wipe prior to placing in TBO assay to avoid diluting the solution.

Making 10mL 0.1% TBO Stain in 8M Urea

3. Measure 10mL DI H_2O and add to cleaned scintillation vial with stir bar.
4. Add 4.8g urea to scintillation vial.
5. Stir at room temperature for 30 minutes.
6. Add 0.01g TBO to aqueous urea solution allowing it to dissolve completely

Staining Samples

7. Place sample on needle by puncturing an edge*
8. Submerge sample in TBO solution for 20 minutes at room temperature.
9. Rinse excess TBO using DI H_2O, leaving behind bound TBO.
10. Dip stained sample in fresh DI H_2O and agitate until excess dye in leached out
11. Dry sample on Kim Tech wipe.
12. Place sample in vial and allow to dry in drying oven.
13. Take photos of samples from each treatment group .

A.6 Whole Blood Clotting Protocol

Objective

To determine if the material treatment has reduced acute whole blood clotting.

Materials & Equipment

- Petri dishes (for pipetting blood onto the samples, one for each treatment group)
- 24 well plates (for freeing hemoglobin)
- 96 well plates (for plate reading)
- DI water
    - DI water is used to release free hemoglobin from red blood cells that were not trapped in a blood clot, after clotting time has elapsed.
- Timer
- 20 µl and 1000 µl pipettes and pipette tips
- Vacuum tubes which have not been coated in anticoagulant.
- Plate Reader (Dr. Popat's Lab)

Safety Considerations

Work carefully and avoid contact with blood at all times.
Remember to take the Blood-borne Pathogens (BBP) Precautions and Training offered by CSU.

Note: Blood must be drawn on site so that it can be immediately transferred onto samples/ well plates!!! You must make an appointment to have the phlebotomist come to the lab.

Preparation

- Determine how much blood and how many samples needed prior to the study. Samples will be run in quadruplicate for two different time points (15 min and 30 min). Total samples needed per treatment group are 8. Each sample will have 5 μl of whole blood pipetted onto the surface. A 1:200 Blood to DI water ratio will be used for data analysis.
- Treatment groups are as follows
- TCPS
- Untreated LLDPE
- Melt Press Control LLDPE (HA treated)
- 70% Tungsten LLDPE (HA Treated)
- 40% Bismuth Trioxide (HA Treated)
    - Determining Number of Samples and Total Volume of Blood for 5 treatment groups.
        - 8 samples x 5 μl of blood= 40 μl of blood per treated group
        - 40 μl of blood x 5 groups= 200 μl total blood for treatment

    - 200μl+ 25μl of blood for t_0 (5μl for 5 wells) = 225 μl total blood for the study
- One blood vacuum tube holds approximately 6 ml of blood.
- Make sure to label the 24-well plate according to the time points and materials which will be used. Only one 96 well plate is needed for plate reading. At least 3 wells should be blanks.
- Soak samples at least 2 hours prior to the study to swell the hyaluronan.
- For 8 mm samples, be sure to use carbon tape to seal them on center of the 24 well plate
    - and have them hydrated for at least 2 hours prior to the test. Samples should be removed from DI water, blotted dry, and taped to well plate immediately prior to blood draw. The well plate should be covered to prevent HA from drying out.
- Pipette 1000 µl and 200 ul of DI water into each To and blank well, respectively
- Cover all well plates while waiting for the phlebotomist

Procedure

1. Have phlebotomist draw blood into vacuum tubes which have not been coated with anticoagulant. The first will be thrown away as it contains the skin plug and locally activated platelets. The second will be used for the study.

2. Pipette 5 µl of blood into each T_0 well of the 24-well plate. These should have 1000 µl of DI water in them. Gently agitate on the Titer plate shaker for 30 seconds at 100 RPM. Let wells sit to allow the free hemoglobin that was not trapped in the blood clot to be released into the water for 5 minutes.

3. Transfer 5 µl of whole blood onto each of the T_{15} samples. Start the timer as the first drop is placed on the samples. Ensure the blood is in the center of the materials. Be sure to change pipette tip each time to avoid cross contamination. DO NOT reuse pipette tips.

4. Repeat step 3 for T_{30} samples.

5. As each time point arrives, transfer 1000 µl of DI water (in the same order in which blood was transferred) to the corresponding wells on the 24-well plate.

6. Gently agitate on the Titer plate shaker for 30 s at speed 1. Let sit for five minutes to allow the free hemoglobin that was not trapped in the blood clot to be released into the water.

7. After 5 minutes, pipette 200 μl of the blood +DI solution into the 96-well plate. Be sure to change pipette tip to avoid cross contamination.

8. Analyze results using the plate reader at 540 nm wavelength. Open CLOTTING method on the plate reader in Popat's Lab.

A.7 Platelet Activation

Objective

To expose a material to human platelet cells for later evaluation of how those cells interact with the material surface.

Materials & Equipment

- Plate Shaker
- 1000 µl pipettor and tips
- 24 well plates
- Phosphate buffer saline (PBS)
- Sterile tweezers for transferring samples
- EDTA coated Vacutainer tube

Safety Considerations

Work carefully and avoid contact with blood at all times.
Remember to take the Blood-borne Pathogens (BBP) Precautions and Training offered by CSU.

Process Considerations

- If using aluminum or styrene pucks to submerge samples, be sure to sand the puck well enough to remove rough edges that can active platelets.
- Be gentle, work diligently and slowly to prevent activation of platelet.
- Avoid bubbles when pipetting blood and plasma.

Procedure

1. Be sure to sterilize samples and keep them hydrated in sterile DI water.
2. Collect blood from the phlebotomist and store them in EDTA coated tubes to prevent coagulation. Each tube can hold approximately 2 ml of plasma.
3. Using a centrifuge, spin blood at 150 g for 15 minutes and let it rest for another 15 minutes
4. There should be two visible layers of solution in the centrifuged blood tube: platelet rich plasma (PRP) on top, and blood cells (bottom). The buffy coat is located in the middle, but this is not always noticeable with the naked eye.
5. Pool PRP into one tube.
    a. Draw amount smaller than 1 ml each teach time can prevent liquid entering and sucking blood.
    b. Draw only 2/3 of plasma layer to prevent the risk of drawing blood and the buffy coat.
    c. This step can be time consuming. One in a while, rock the plasma/blood tube back and forth gently to prevent platelet aggregation.
    d. If the blood is mixed accidentally, centrifuge the tube for 5 minutes.

6. Aspirate DI water from the wells containing samples, and use tweezers to transfer the samples into the plasma containing wells. Ensure there is no water left on the sample (but hydrated) to avoid dilution of plasma.
7. Pipet 1 ml of PRP into each well of the 24 well plate.
    a. Avoid pipetting PRP onto the sample.
8. Put well plate on a shaker storing in the cell culturing incubator (37 C, 5% C02), and shake at 100 RPM for 2 hours.
9. Either aspirate the plasma. Avoid aspirating directly on the sample that could suck platelets.
10. Rinse the samples twice with PBS. Avoid pipetting directly at the sample to prevent adhered platelets from washing away.
11. Move onto SEM fixing (morphology analysis)

A.8 SEM Fixing

Objective

To fix platelets activated on the material for SEM evaluation.

Materials & Equipment

- Petri dishes (small)
- 10 ml pipettor and tips
- Sodium cacodylate
- Sucrose
- Glutaraldehyde 25% in DI Water
- Hexamethyldisilazane (HMDS), if used (see step 4.e.i. below)
- DI water
- Ethanol
- Beakers (to make the buffer and fixative solutions)

Safety Considerations

Work carefully and avoid contact with blood at all times.
Remember to take the Blood-borne Pathogens (BBP) Precautions and Training offered by CSU.

Process Considerations

- The complete fixing process takes about two hours. If crunched for time, the samples can be incubated in the buffer solution overnight -- Preparation step (c) and Procedure steps (1-3) can be accomplished in a little less than one hour.
- Make fixing solution and buffer solution simultaneously to save time. Both solutions are made through the same process.
- 10 ml of each solution in step 1 of the procedure is usually enough.

Preparation of Fixative and Buffer

- 3% glutaraldehyde in 0.1 M sodium cacodylate and 0.1 M Sucrose
- To make 10 ml buffer and 10 ml of fixative simultaneously:
    a. Put 18.8 ml of DI water into appropriate beaker.
    b. Add 0.68 g of sucrose and 0.43 g of sodium cacodylate to DI water, and swish until everything is fully dissolved.
    c. Remove 10 ml of this solution and add to a Petri dish (step 1 below). **This is the buffer solution**.
    d. Add 1.2 ml of glutaraldehyde to the remaining solution. Swish gently and add to a Petri dish (step 1 below). **This is the fixative solution**.

Procedure

1. Prepare the fixative and buffer solutions per steps (c) and (d) above, resulting in each of these solutions in a unique Petri dish. Prepare additional Petri dishes, each containing one of: 35% ethanol, 50% ethanol, 70% ethanol, 100% ethanol, and HMDS.
2. Transfer samples to the fixative solution and sit for 45 minutes. Be gentle when transferring samples to prevent cell/platelet displacement.
3. Transfer samples to the buffer solution and let sit for 10 minutes. If crunched on time, the samples can be incubated in the buffer solution overnight.
4. After incubating in buffer solution, move the samples into the following solutions for the designated times:
    a. 10 min- 35% ethanol
    b. 10 min- 50% ethanol
    c. 10 min- 70% ethanol
    d. 10 min- 100% ethanol
    e. 10 min – HMDS
        i. HMDS is used for critical drying, but this step can be removed if HMDS can damage or alter the samples. For example, HMDS may react with hyaluronan and swell silicones.
5. If skipping step 4e, allow air dry of ethanol residue and store them in the desiccator prior to SEM imaging.

A.9 Freeze Fracturing

Objective

To create a brittle fracture in LLDPE.

Materials & Equipment

- Tongs
- Hammer
- Styrofoam Container
- X-acto knife
- Liquid Nitrogen

Safety Considerations

Liquid nitrogen should be handled carefully and with proper PPE.

Process Considerations

- Freeze films in order to create a clean-cut perpendicular to the films surface, primarily for SEM imaging.
- Films need to be fractured immediately (within 1-2 seconds) after pulling from liquid nitrogen to ensure a clean cut.

Preparation of Liquid Nitrogen

- Collect liquid nitrogen, one Dewar full (approximately 2-3 liters) is usually enough.
- Clear off a workspace (specifically a cutting board) and place Styrofoam container (or any container appropriate for containing liquid nitrogen) on top of the workspace.
- Pour liquid nitrogen into the container and wait until rapid boiling has subsided (should only take around five minutes).

Procedure

- Dry all films that are planned to be freeze fractured.
- Take one film and lightly fold to prepare an edge to be fractured.
- Using tongs, and while having all proper protective equipment on, slowly place the film inside the liquid nitrogen bath for 30 - 45 seconds.
- Once frozen, quickly remove the film from the bath, place on cutting board, and use the hammer to fracture the film along the fold made earlier.
- The film should be held in the tongs throughout this process.
- You should be hitting the film firmly to induce fractur

- Look for the fracture made along the fold line, if no fracture was made, repeat steps 3 and 4 to create the fracture.
- If the fracture is apparent, use X-Acto knife in order to make to similar sized triangles on either side of the fracture.
- During this step, it is crucial to always note where the fracture is: indicate this by making a small incision in the opposing corner from the fracture side.
- Utilize Figure 1 to avoid any confusion.
- Repeat this process (steps 3 – 6) for each film.
- Put each pair of triangles in their own clean, labelled vials.

Figures

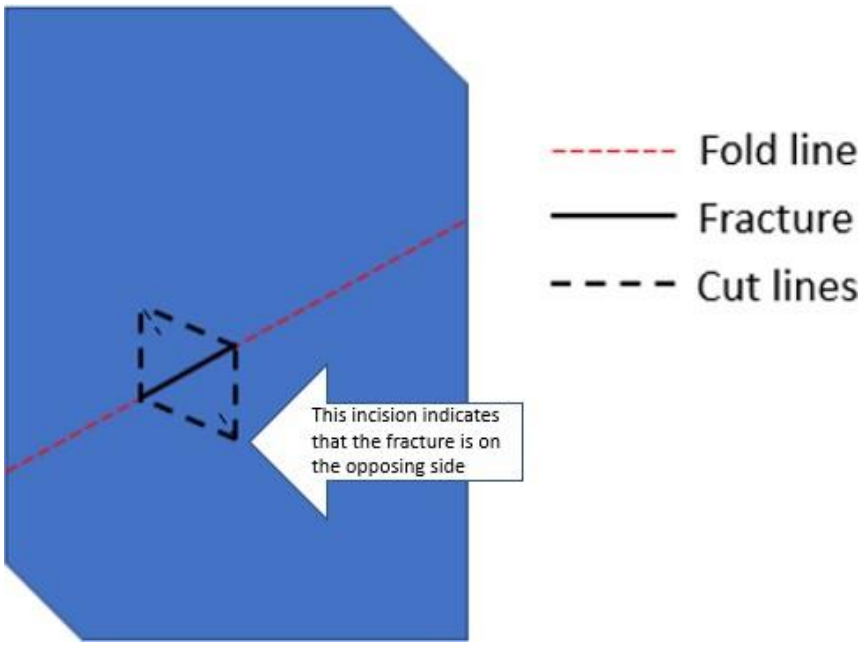

Figure 1. *Graphic visualizing an example freeze fracturing protocol.*

APPENDIX B: TENSILE EVALUATION

B.1 Evaluation of non-ASTM Tensile Testing Protocol

Purpose

The purpose of this study was to validate that LLDPE samples pulled to failure following the ASTM D882-18 standard would produce statistically similar results to LLDPE samples pulled to failure using different sample dimensions, percent strain rates, and a different tensiometer.

It should be noted that some mechanical properties of polyethylene are known to be strain rate dependent[1–4]. However, this viscoelastic behavior is generally observed in experiments which examine order of magnitude changes in strain rate. This study had much smaller strain rate variation (an approximately 50% change) and thus it was expected that the tensile parameters being evaluated would not be significantly different.

The tensile parameters evaluated were Young's modulus, yield stress, yield strain, elongation at break, ultimate tensile strength, and toughness.

Cause for study

The tensiometer primarily available for this research was an Instron 4443. This tensiometer does not have the extension necessary to pull LLDPE samples to failure when starting with the two-inch grip separation that is recommended by ASTM D882-18. Beyond instrument availability it is difficult and expensive to produce large radiopaque and HA treated samples for failure analysis.

Another tensiometer, an Instron 5596, with the extension required to pull large samples to failure had limited availability. Thus, untreated, or virgin 2045G LLDPE films were pulled to failure per the ASTM standard using the Instron 5596 and compared to virgin 2045G LLDPE films pulled to failure outside the ASTM standard on the Instron 4443.

Hypothesis

The LLDPE materials will not have significantly different Young's modulus, yield stress, yield strain, elongation at break, ultimate tensile strength, and toughness when pulled to failure with different dimensions on different Instron's with different load cells.

Methods

Tensile testing was performed per ASTM standard D882-18 on an Instron 5596 with a 10 kN load cell. Apart from sample storage, the ASTM standard was followed and sample dimensions were: gauge length: 25.4 mm (2 inch grip separation), width: 6 mm, thickness 80 µm. Samples were taken from blown LLDPE films using an ASTM standard punch. Samples were stored at room temperature and humidity because there was no controlled temperature and humidity chamber available. Five samples were pulled to failure in both the machine direction (MD) and transverse direction (TD) at both 50 mm/min and 500 mm/min. These tests established a baseline for the 2045G LLDPE blown films. Samples with smaller dimensions (gauge length: 12 mm, width: 3.16 mm, thickness 80 µm) again taken with a standard punch were pulled to failure in both the MD and TD at both 50 mm/min and 500 mm/min. Young's modulus, yield stress, yield strain, elongation at break, ultimate tensile strength, and toughness were calculated and compared across the different strain rates and instruments. One key item to note is the modulus data at 500 mm/min on the Instron 4443 is highly suspect because only 3 or 4 data paints are linear and can be used to calculate the Young's modulus. This is because the small sample combined with a high strain rate meant the fastest data collection rate the instrument can provide yielded very few

data points in the initial linear region. Because of this samples were tested on both instruments at lower strain rate (50 mm/min) as recommended by the ASTM standard to examine the moduli, but not other tensile characteristics.

Data was evaluated for normality and equal variances. If data was not normal Grubb's test was performed to determine if an outlier prevented normality and if so that outlier was removed. No more than one data point was ever removed. Finally, data was compared with an ANOVA and post hoc Tukey's test to determine significant differences (n=5 or n=4 if data prevented normality, $p < 0.05$)

Results

Figure 1 shows the moduli for all samples. Note that each sample was pulled at 50 and 500 mm/min to examine the moduli as the ASTM D882-18 recommends reducing strain rate for modulus calculations. There were no significant differences between any sample except the moduli of samples pulled at 500 mm/min on the 4443 Instron which were significantly lower than all other samples.

Figure 2 shows the yield stress for all samples tested. While the yield stress measured with the 5596 Instron was significantly lower than the 4443 Instron in the transverse direction the yield stresses were within 1 MPa.

Figure 3 shows the yield strain for all samples tested. Yield strain of samples tested on the 5596 were significantly lower than that of samples tested on the 4443 Instron in transverse direction. Again while the result is statistically significant, it only represents a shift of four percent strain. This shift does not indicate a large difference in material property. There was no difference between the 4443 and 5596 Instron's in the machine direction.

Figure 4 shows the elongation at break for all samples tested. There were no significant differences between samples.

Figure 5 shows the ultimate tensile strength for all samples tested. There were no significant differences between samples.

Figure 6 Toughness at break for LLDPE samples. There were no significant differences between samples.

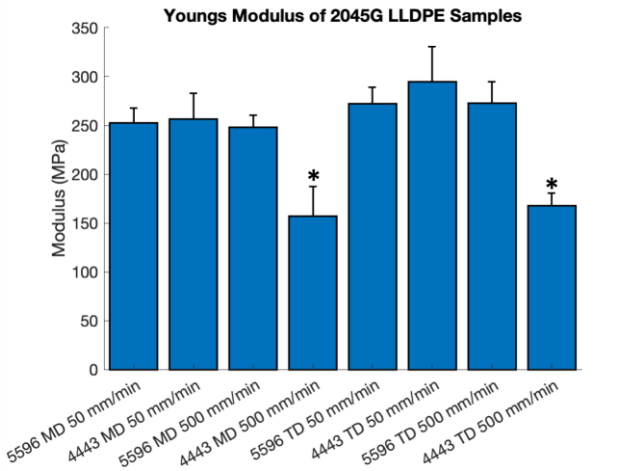

Figure 1: Young's Modulus for LLDPE samples. Error bars represent one standard deviation and asterisks indicate that the samples had significantly

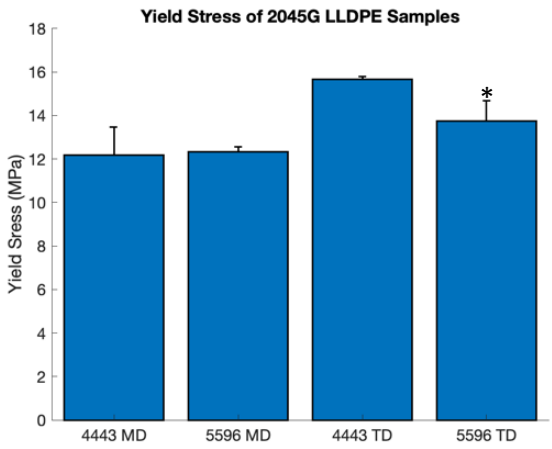

Figure 2: Yield stress for LLDPE samples. Error bars represent one standard deviation. Asterisks indicate that the samples had significantly lower

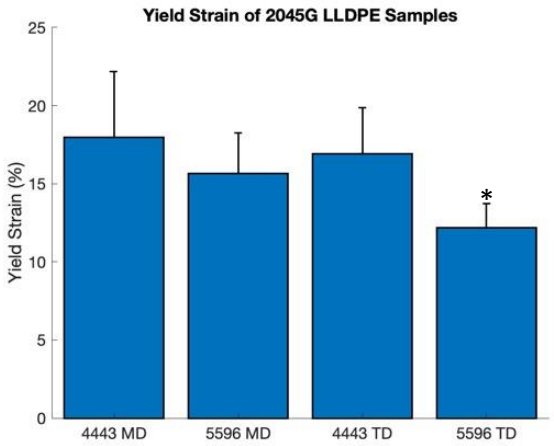

Figure 3: Yield strain for LLDPE samples. Error bars represent one standard deviation. Asterisks indicate that the samples had significantly lower yield strain than its respective counter sample ($p < 0.05$)

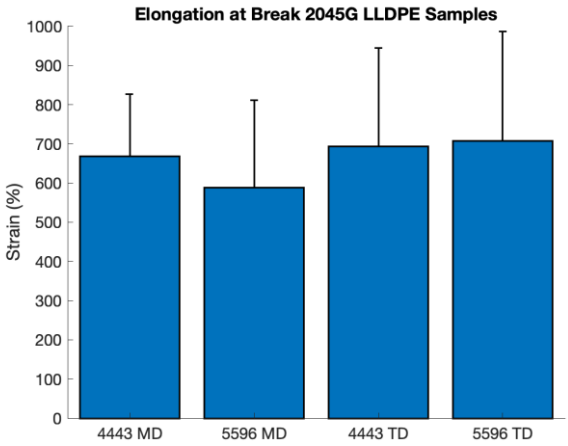

Figure 4: Elongation at break for LLDPE samples. Error bars represent one standard deviation. There were no significant differences between samples ($p < 0.05$).

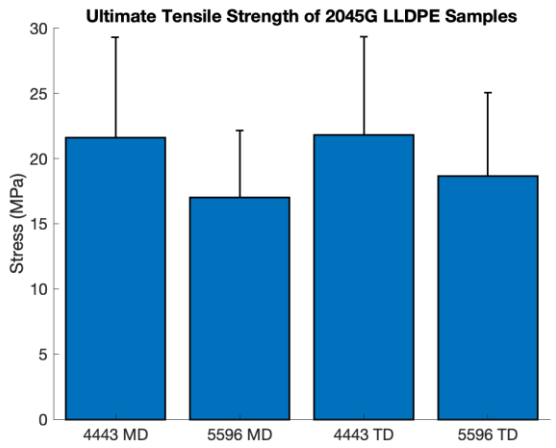

Figure 5: Ultimate tensile strength of LLDPE samples. There were no significant differences between samples Error bars represent one standard deviation. ($p < 0.05$).

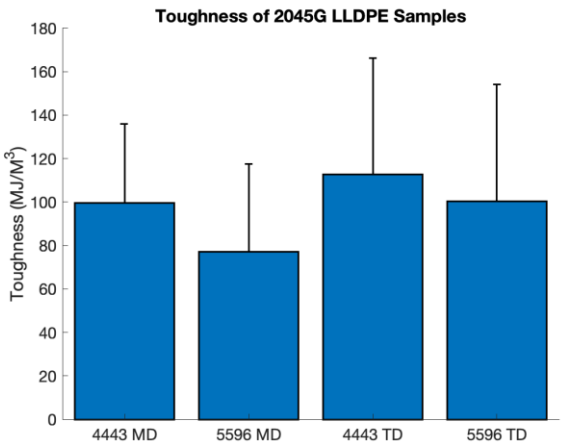

Figure 6: Toughness of LLDPE samples. There were no significant differences between samples Error bars represent one standard deviation. ($p < 0.05$).

Discussion

Moduli

The moduli were only different for the samples pulled at high strain rate on the 4443 indicating that to determine the modulus of LLDPE samples a lower rate of extension should be used on the 4443 Instron. This was not unexpected considering that there was not enough data to properly model the modulus on the 4443 the 500 mm/min strain rate.

Yield Stress

While the 5596 and 4443 Instron's had no difference in the results for the machine direction yield stresses, the 5596 Instron did have a slightly lower yield stress than the 4443 in the transverse direction. Though this is less than ideal the average yield strain difference was less than one

MPa indicating the instruments provided very similar results even though statistically different when using an alpha value of 0.05.

Yield Strain

The 5596 Instron had significantly lower yield strains than that of the 4443 Instron in the transverse direction, but not in the machine direction. While the difference in the transverse direction was statistically significant, it was only a shift of four percent strain. This slight difference is again not a cause for concern.

Elongation at Break

There were no significant differences between the elongation at break values between two instruments for indicating that the smaller dimensions do not affect the test results.

Ultimate Tensile Strength

There were no significant differences between the ultimate tensile strength between two instruments for indicating that the smaller dimensions do not affect the test results.

Toughness

There were no significant differences between the toughness between two instruments for indicating that the smaller dimensions do not affect the test results.

Summary

Both tensiometers yielded the statistically similar results except for the following: yield strain and yield stress in the transverse direction and modulus at the higher strain rate. This indicates a lower strain rate should be used for examining the modulus of samples when testing with the 4443 Instron and that yield strains reported may be slightly higher but did not vary more than 5%. While

this is less than ideal it is a reasonable concession considering the restrictions on available testing equipment and sample size. The following tensile analysis section will use the machine direction data as the machine direction data was never significantly different between instruments.

APPENDIX C: SEM PLATELET IMAGES AND ANALYSIS

C.1 SEM Images of Platelets on Radiopacified Samples

TCPS

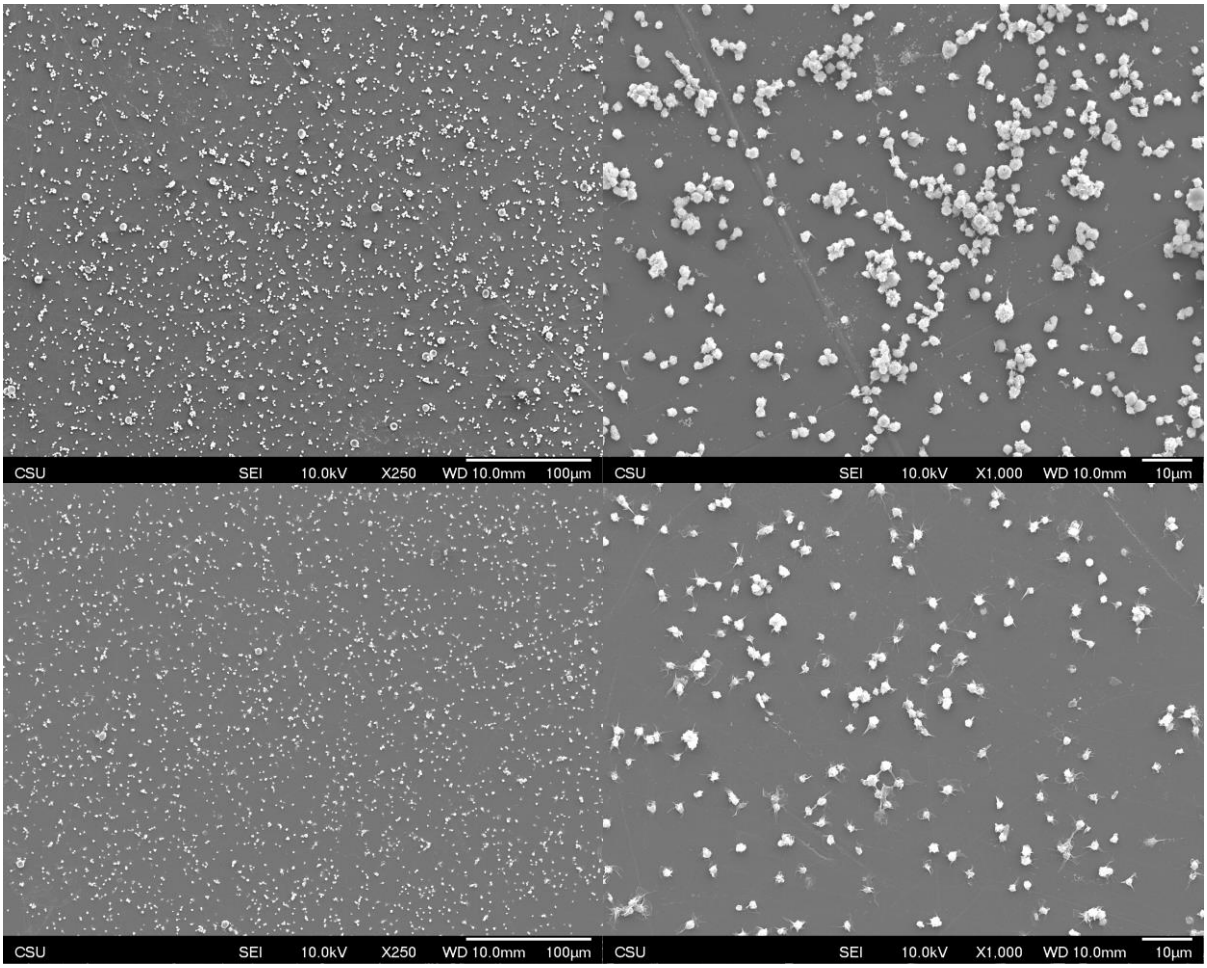

LLDPE

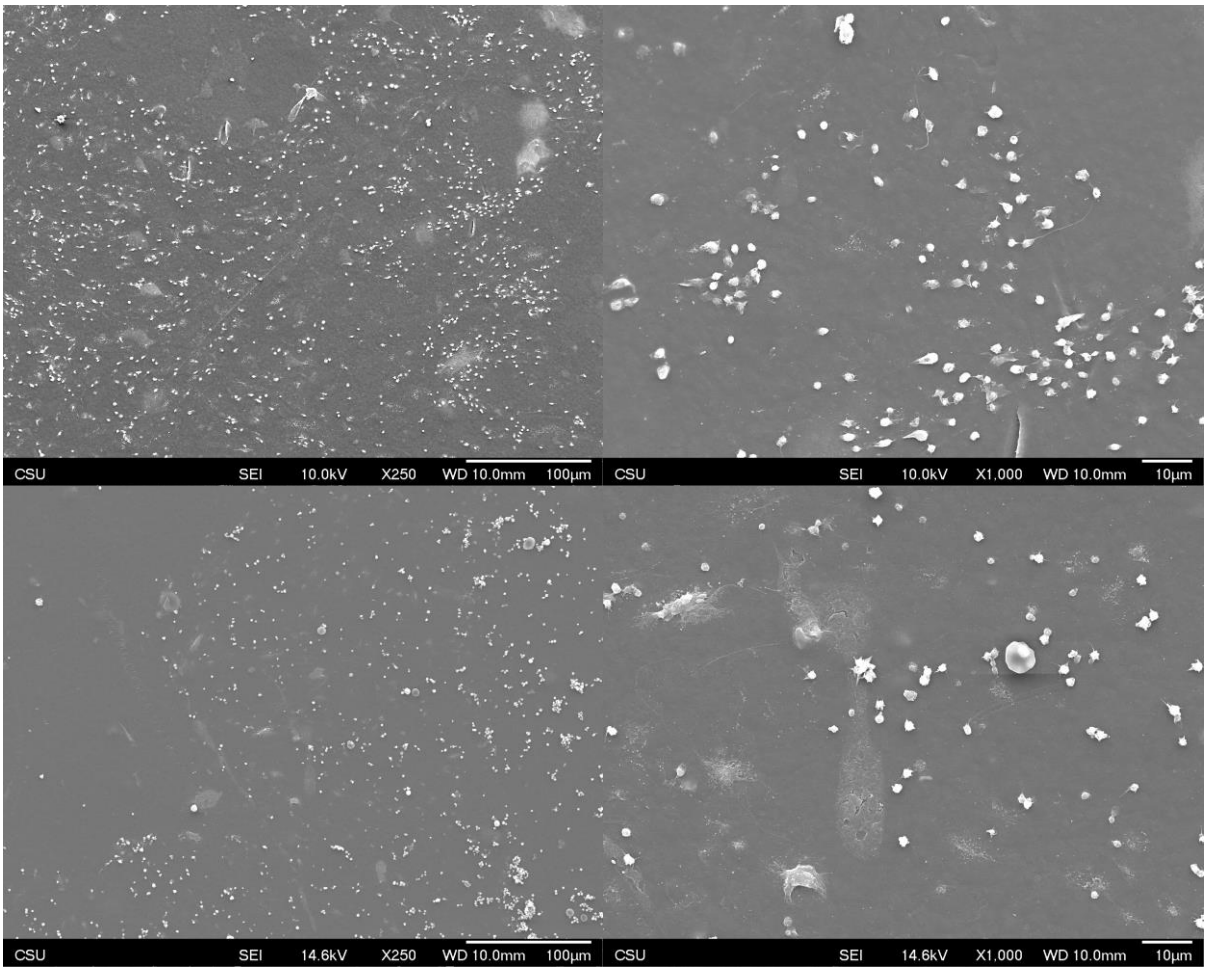
CSU SEI 10.0kV X250 WD 10.0mm 100µm
CSU SEI 10.0kV X1,000 WD 10.0mm 10µm
CSU SEI 14.6kV X250 WD 10.0mm 100µm
CSU SEI 14.6kV X1,000 WD 10.0mm 10µm

Tungsten

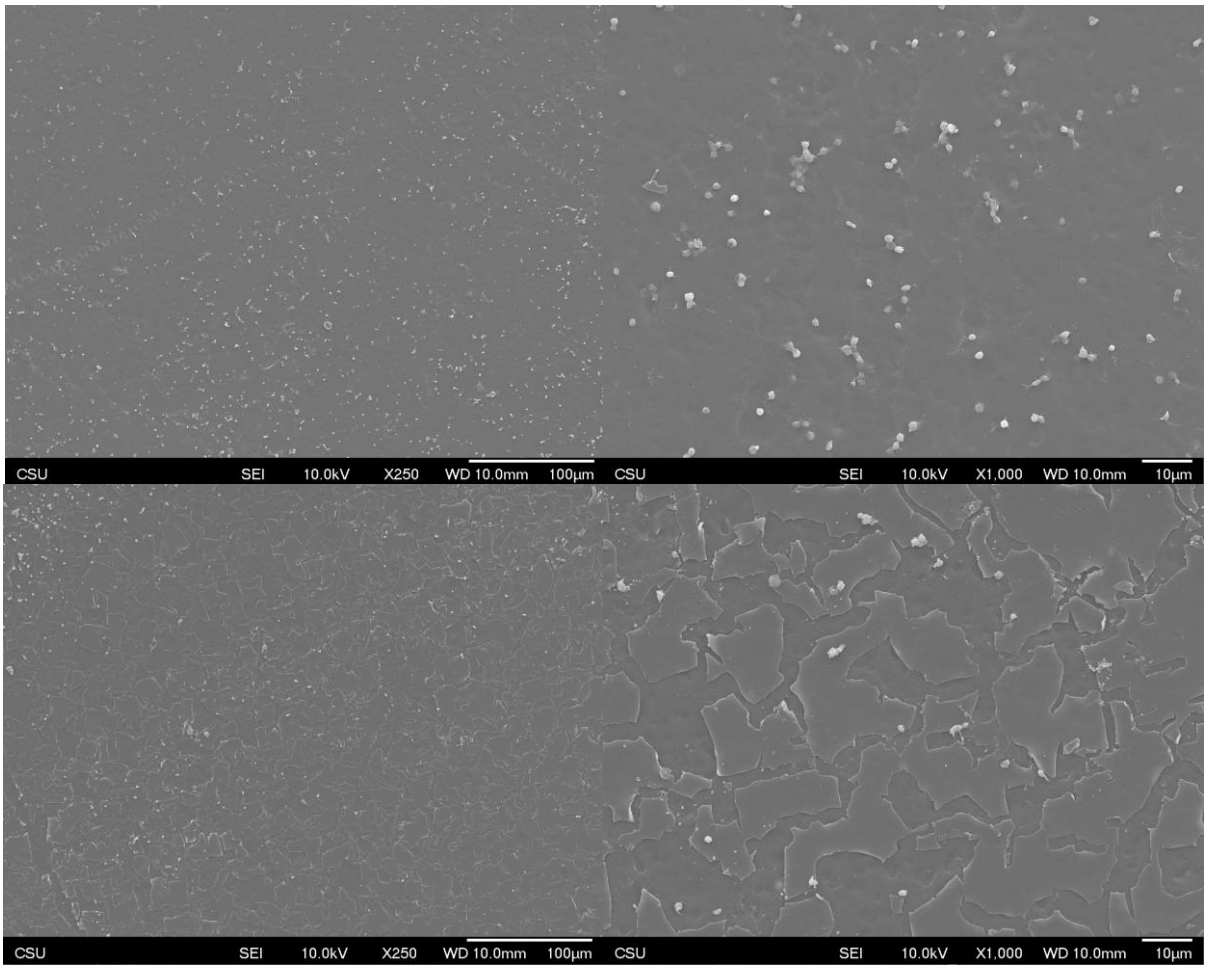
CSU SEI 10.0kV X250 WD 10.0mm 100µm
CSU SEI 10.0kV X1,000 WD 10.0mm 10µm
CSU SEI 10.0kV X250 WD 10.0mm 100µm
CSU SEI 10.0kV X1,000 WD 10.0mm 10µm

Bismuth

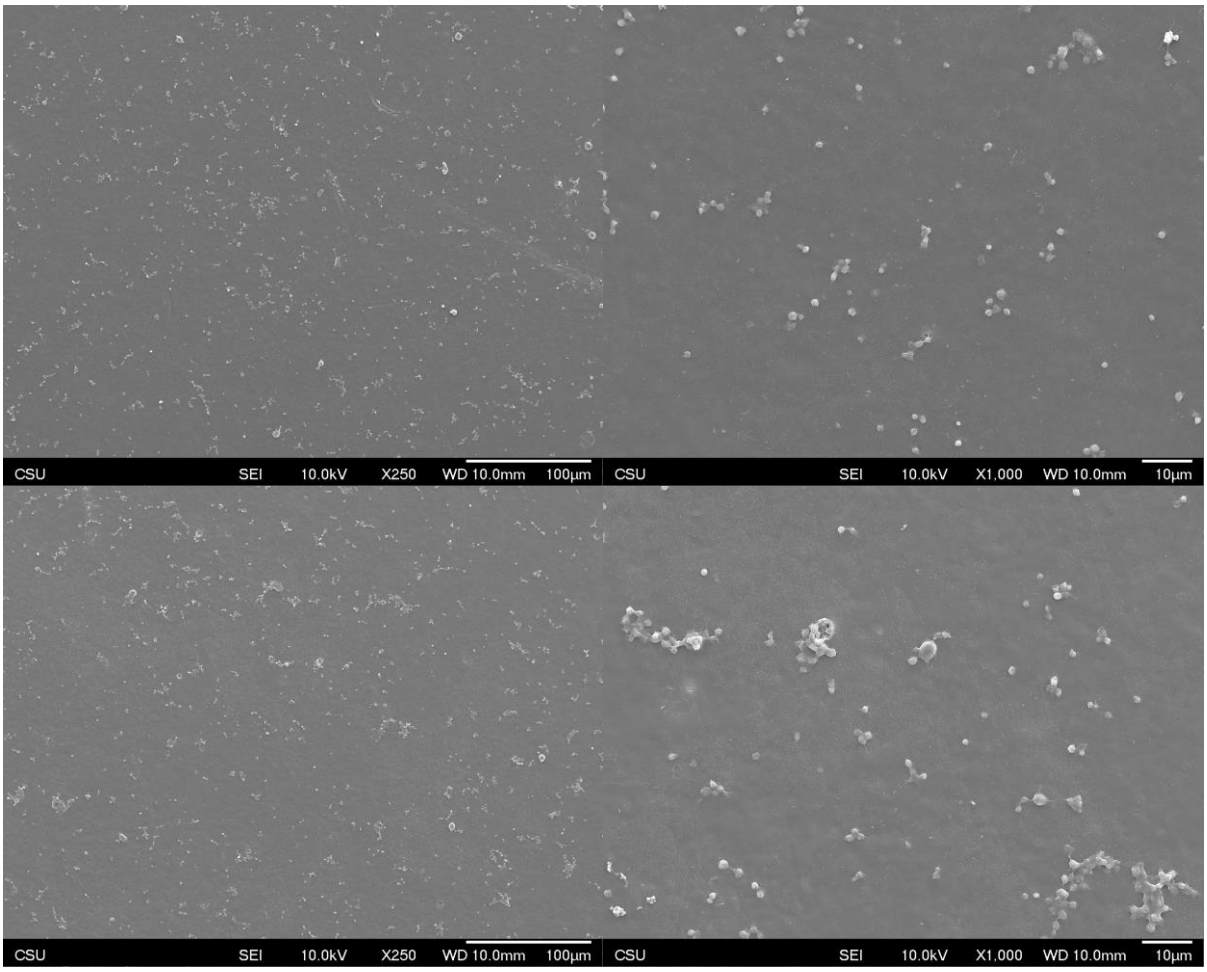
CSU SEI 10.0kV X250 WD 10.0mm 100µm
CSU SEI 10.0kV X1,000 WD 10.0mm 10µm
CSU SEI 10.0kV X250 WD 10.0mm 100µm
CSU SEI 10.0kV X1,000 WD 10.0mm 10µm

Melt Press Control

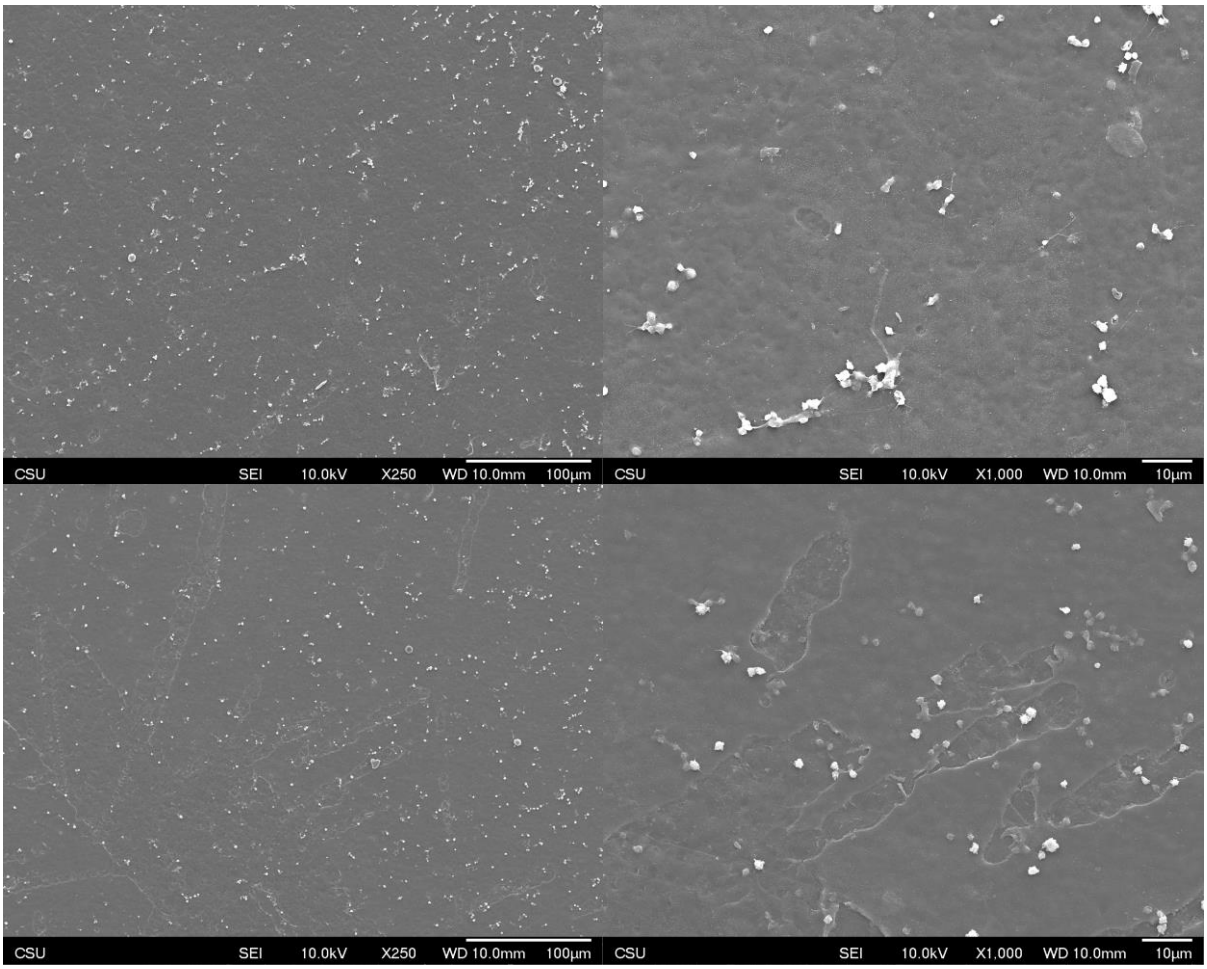

C.2 Platelet Data by Observer

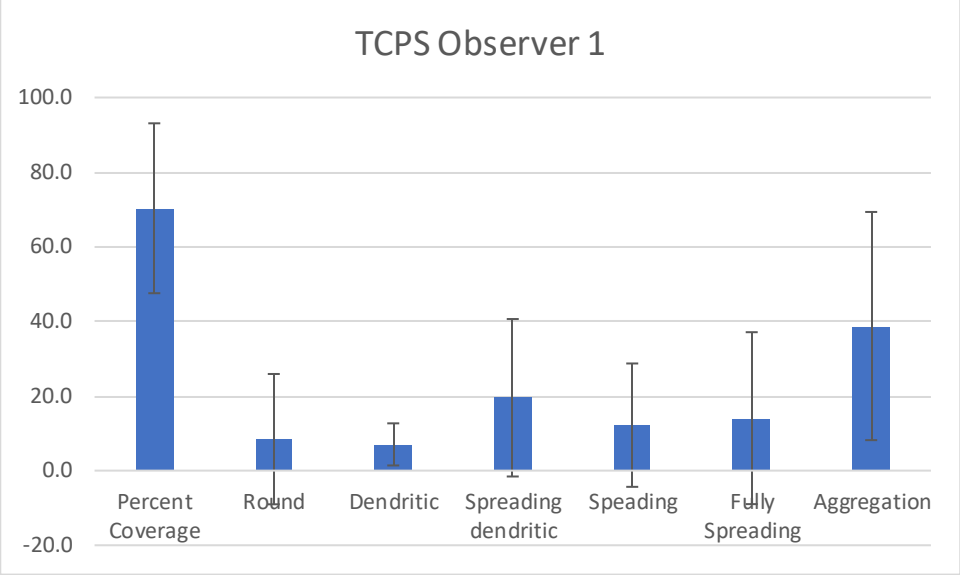

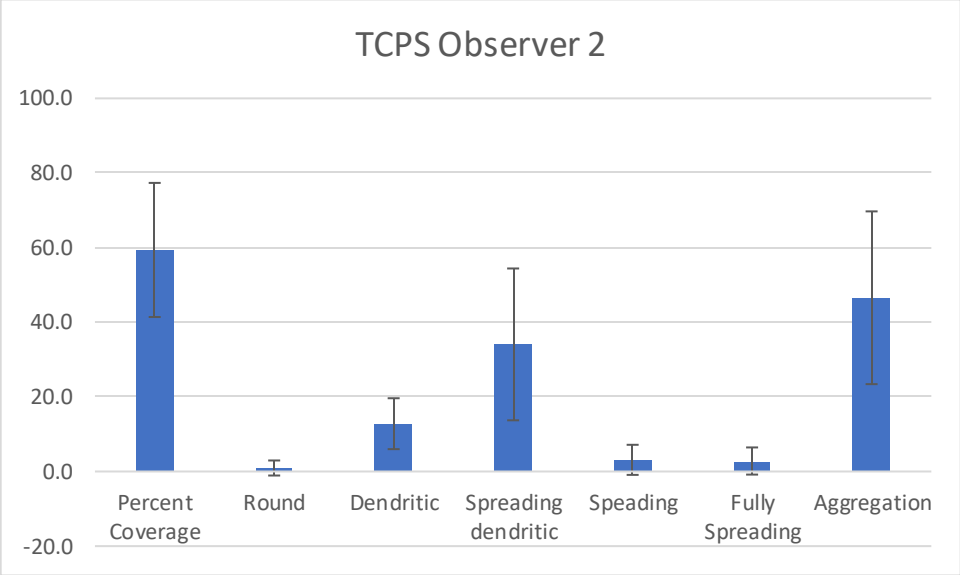

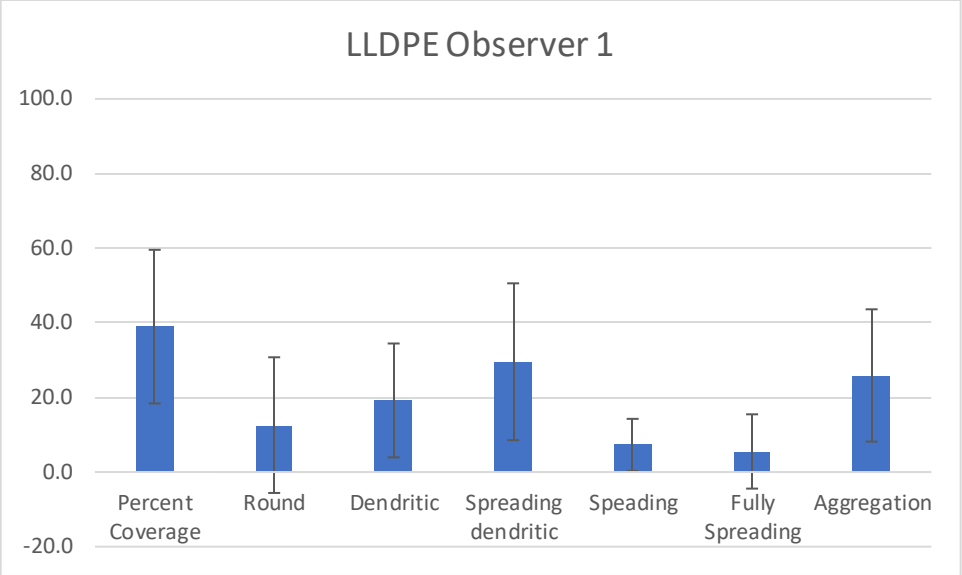
LLDPE Observer 1
100.0
80.0
60.0
40.0
20.0
0.0
-20.0
Percent Coverage
Round
Dendritic
Spreading dendritic
Speading
Fully Spreading
Aggregation

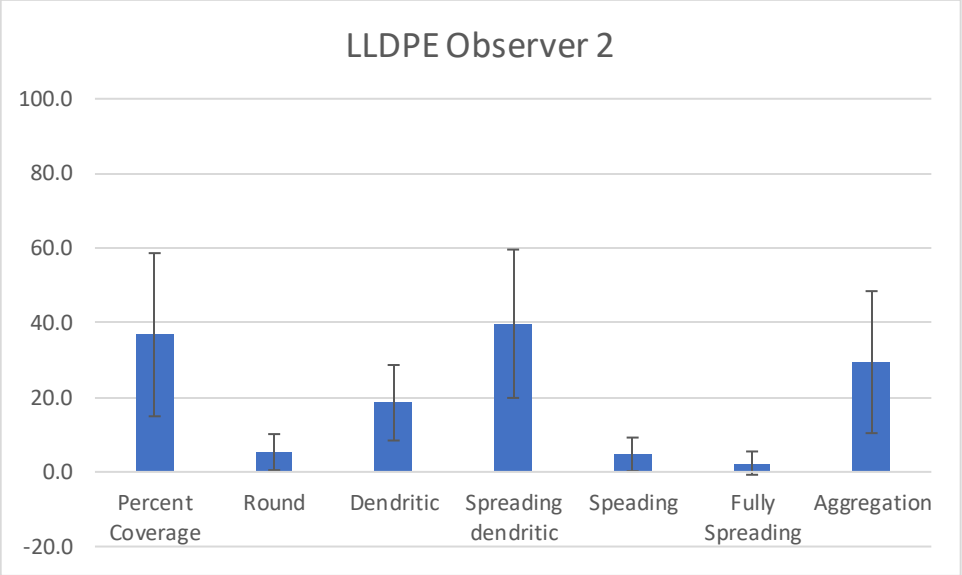
LLDPE Observer 2
100.0
80.0
60.0
40.0
20.0
0.0
-20.0
Percent Coverage
Round
Dendritic
Spreading dendritic
Speading
Fully Spreading
Aggregation

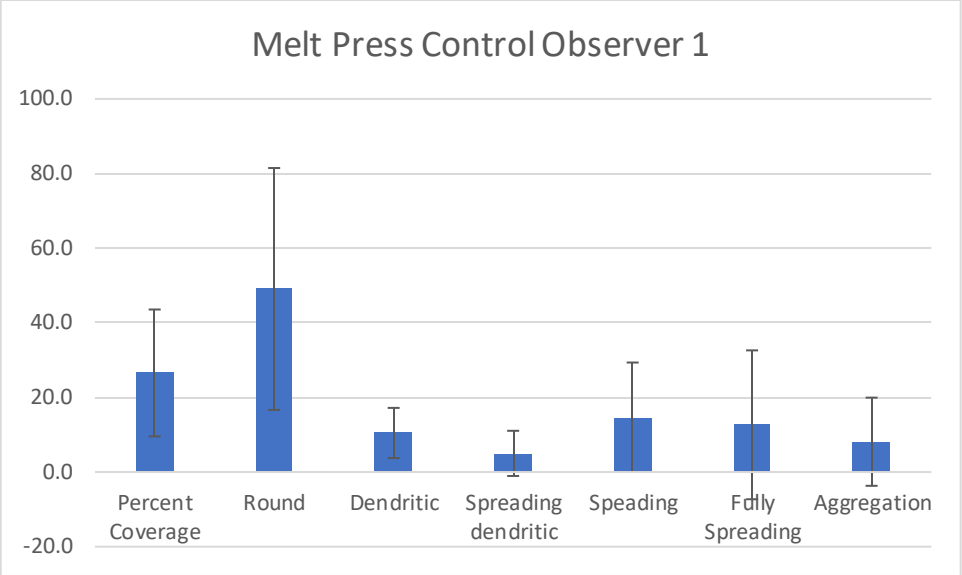
Melt Press Control Observer 1
100.0
80.0
60.0
40.0
20.0
0.0
-20.0
Percent Coverage
Round
Dendritic
Spreading dendritic
Speading
Fully Spreading
Aggregation

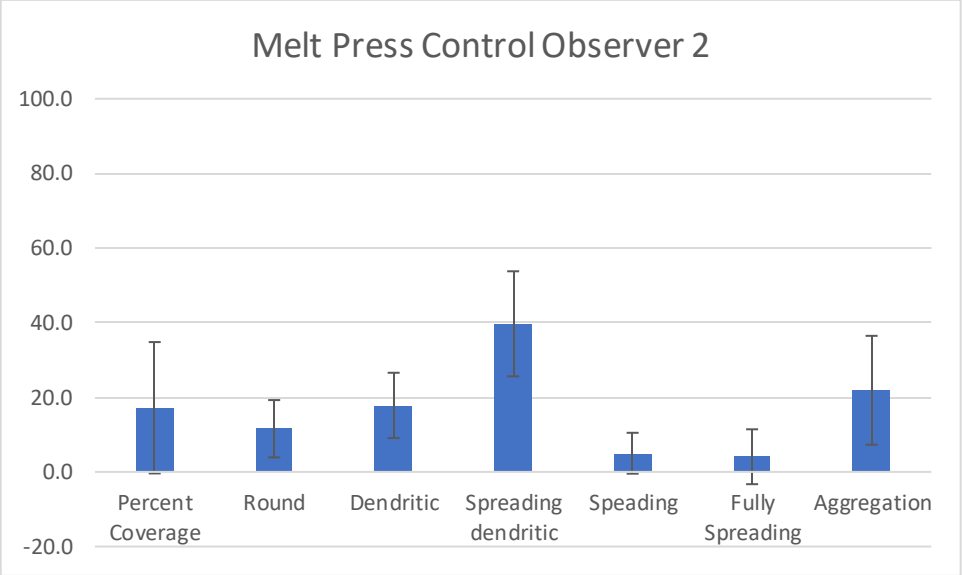
Melt Press Control Observer 2
100.0
80.0
60.0
40.0
20.0
0.0
-20.0
Percent Coverage
Round
Dendritic
Spreading dendritic
Speading
Fully Spreading
Aggregation

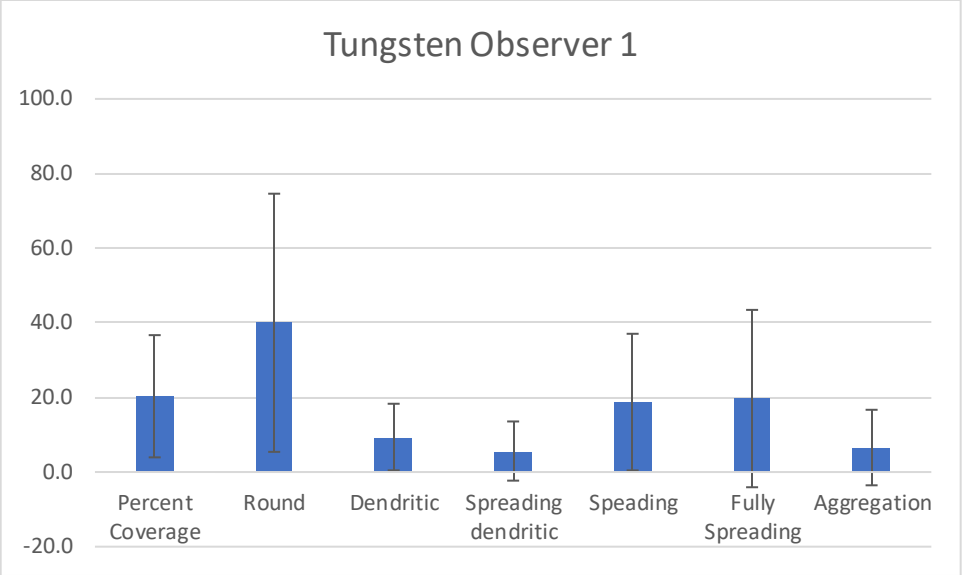
Tungsten Observer 1
100.0
80.0
60.0
40.0
20.0
0.0
-20.0
Percent Coverage
Round
Dendritic
Spreading dendritic
Speading
Fully Spreading
Aggregation

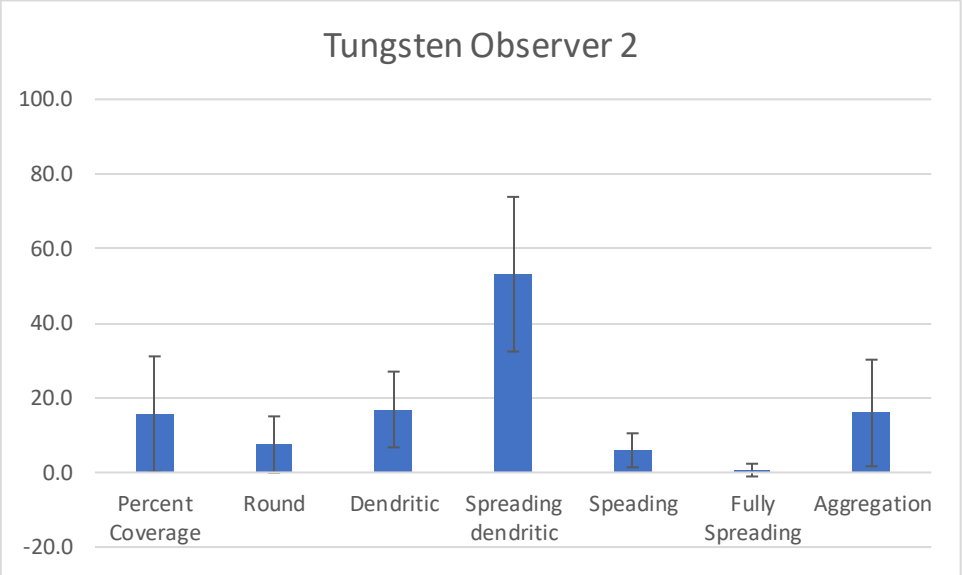
Tungsten Observer 2
100.0
80.0
60.0
40.0
20.0
0.0
-20.0
Percent Coverage
Round
Dendritic
Spreading dendritic
Speading
Fully Spreading
Aggregation

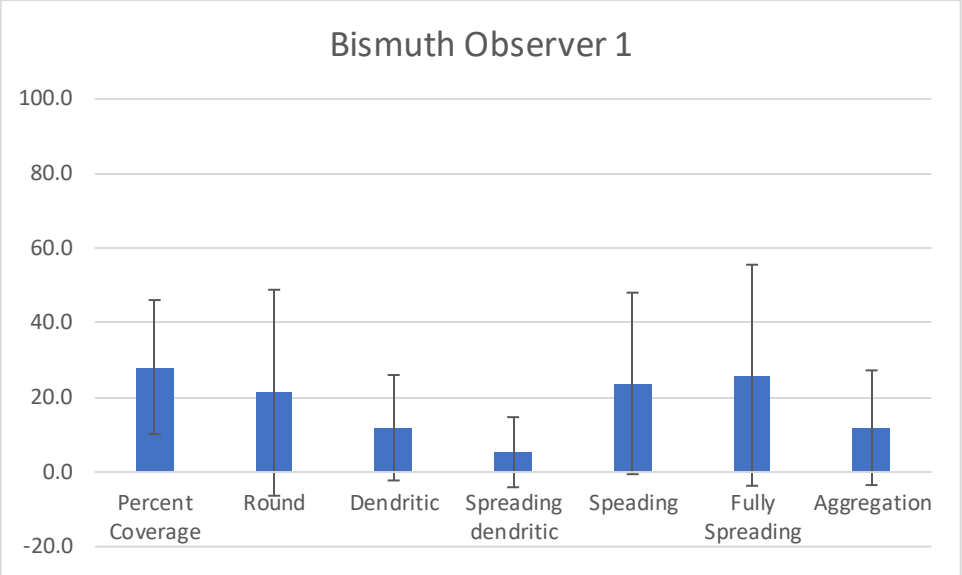
Bismuth Observer 1
100.0
80.0
60.0
40.0
20.0
0.0
-20.0
Percent Coverage
Round
Dendritic
Spreading dendritic
Speading
Fully Spreading
Aggregation

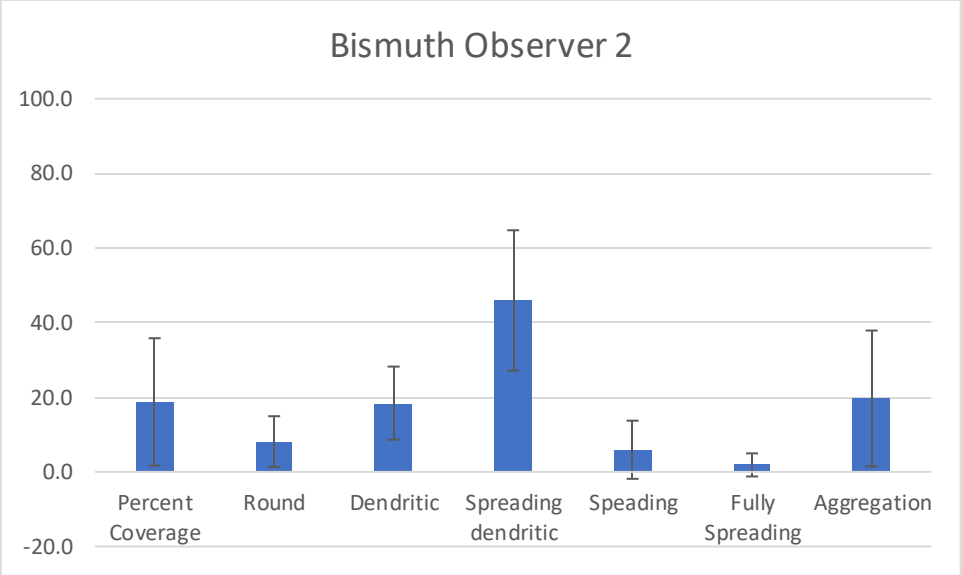
Bismuth Observer 2
100.0
80.0
60.0
40.0
20.0
0.0
-20.0
Percent Coverage
Round
Dendritic
Spreading dendritic
Speading
Fully Spreading
Aggregation

C.3 Notes on Surface Morphology of Melt Pressed LLDPE from SEM images

Samples that had been melt pressed (bismuth, tungsten, and the melt pressed control samples) had some notable changes in surface morphology that were not seen on any non melt pressed LLDPE samples.

Both bismuth and tungsten samples shown below had pockmarking on the surface. Though it is not known what caused this damaged it was speculated that it could be from the radiopacifying agents heating up faster than the LLDPE causing the powder to burn through the LLDPE. Another theory is that removing the Kapton sheets when the samples were either cooler or warmer caused exposed bismuth or tungsten to stick to the Kapton creating a hole or pockmark.

Tungsten sample with surface damage

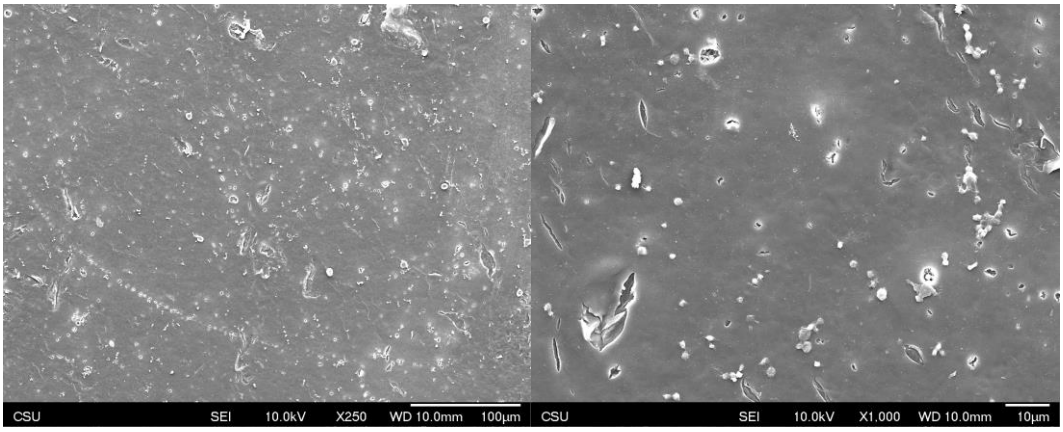

Bismuth sample with surface damage

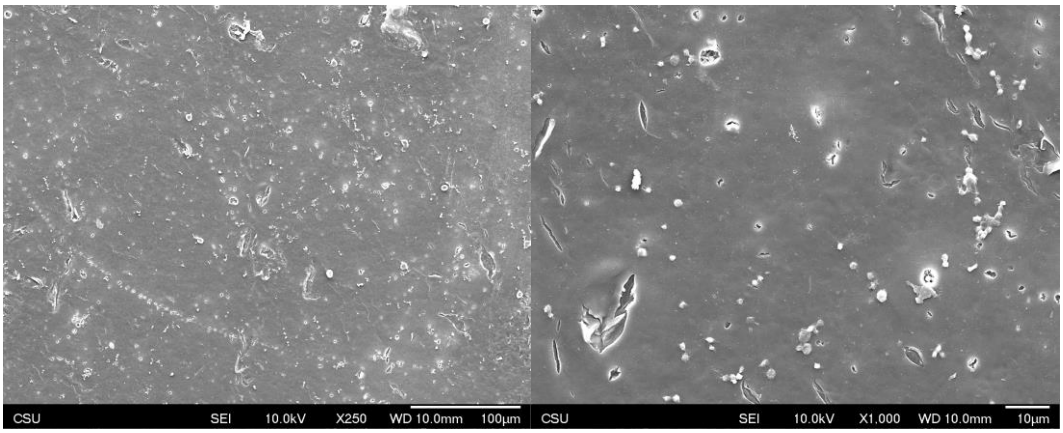

While the bismuth and tungsten samples had pockmarking both the tungsten and melt press control samples had surface structures that were not seen on other samples. Again no cause was determined but it was thought this may be from removal of the Kapton sheet after melt pressing. It is interesting that this morphology was not seen on the bismuth samples however which were also melt pressed.

Melt pressed control with surface structure

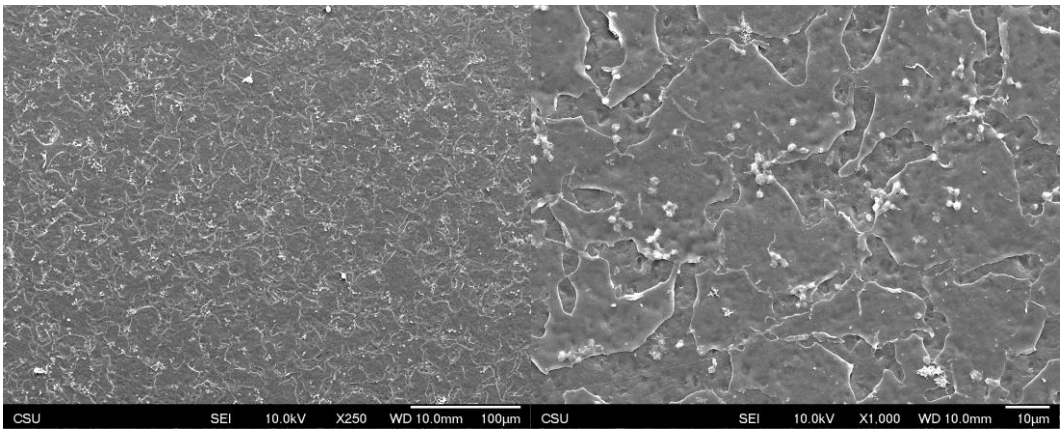

Tungsten sample with surface structure

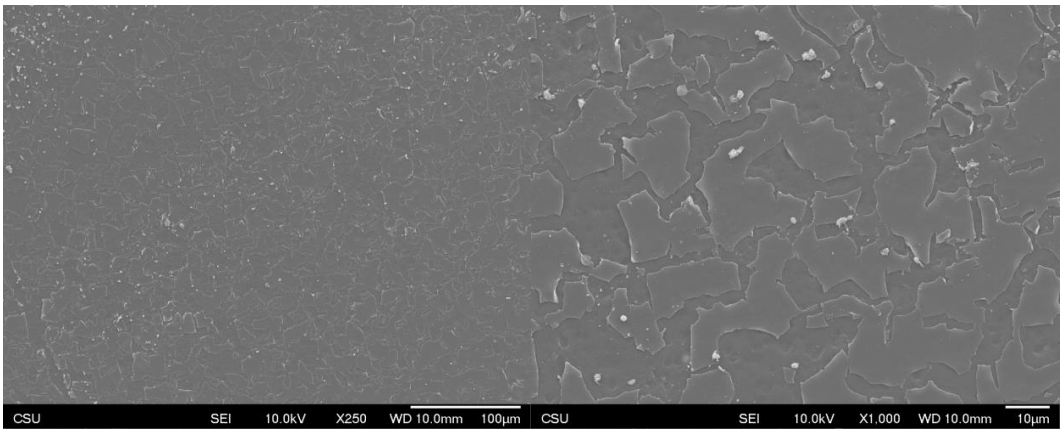

LIST OF ABBREVIATIONS

AS – Aortic Stenosis

AR – Aortic Regurgitation

CDC – Centers for Disease Control

CT – Computed Tomography

CTAB – Cetyltrimethylammonium bromide

DI – Deionized Water

DMSO – Dimethyl Sulfoxide

EDS – Energy-dispersive X-ray spectroscopy

ELISA – Enzyme-Linked Immunosorbent Assay

EOA – Effective Orifice Area

HA – Hyaluronan or Hyaluronic Acid

HACTA – Hyaluronic Acid Complexed with Cetyltrimethylammonium

HMDS – Hexamethyldisilazane

IPN – Interpenetrating Polymer Network

LDH – Lactate dehydrogenase

LLDPE – Linear Dow Density Polyethylene

MW – Molecular Weight

NIOSH - The National Institute for Occupational Safety

PBS – phosphate buffered saline

PE – Polyethylene

PEG – Polyethylene glycol

PET - Polyethylene Terephthalate

PP – Polypropylene

PPE – Personal Protective Equipment

ΔP – Pressure Gradient

RF – Regurgitant Fraction

RH – Relative Humidity

SAVR – Surgical Aortic Valve Replacement

SHACTA – Silylated Hyaluronic Acid Complexed with Cetyltrimethylammonium

TAVR – Transcatheter Aortic Valve Replacement

TBO – Toluidine Blue O

TCPS – Tissue Culture Polystyrene

TDI – Toluene Diisocyanate

WVTR – Water Vapor Transmission Rate

XPS – X-ray Photoelectron Spectroscopy